Molecular interactions between gastric stem cells and their niche upon *Helicobacter pylori* infection

D i s s e r t a t i o n

zur Erlangung des akademischen Grades

d o c t o r r e r u m n a t u r a l i u m

(Dr. rer. nat.)

im Fach Biologie

eingereicht an der

Lebenswissenschaftlichen Fakultät

der Humboldt-Universität zu Berlin

von

Marta Jablonska, M. Sc.

Präsidentin der Humboldt-Universität zu Berlin

Prof. Dr.-Ing. Dr. Sabine Kunst

Dekan der Lebenswissenschaftlichen Fakultät

Prof. Dr. Bernhard Grimm

Gutachter/innen:

1. Prof. Dr. Bertram Wiedenmann
2. Prof. Dr. Achim Leutz
3. Prof. Dr. Thomas F. Meyer

Tag der mündlichen Prüfung: 25.06.2020

Table of contents

Abstract

Infection with *Helicobacter pylori* (*H. pylori*) leads to alterations of the topology and cellular composition of the gastric epithelium. These changes usually involve epithelial hyperproliferation and impaired differentiation, and may further develop into the gastric pathologies such as hyperplasia, atrophy and metaplasia, which are precursor lesions of gastric cancer. Although much is known about the organization of the epithelium during homeostasis, the molecular mechanisms regulating differentiation and turnover upon infection remain largely unknown. Recent studies have put stem cells in the gland base into focus and it has been demonstrated that these cells give rise to the whole gastric unit within one to two weeks and thus are the main drivers of gland repopulation. Additionally, recent studies have shown that stromal cells located in close proximity to the epithelial stem cell are creating the niche for this compartment and provide crucial factors that regulate stem cell turnover and fate decisions. Therefore, this thesis focuses on of Myh11+ myofibroblasts that are located beneath and between the epithelial gland cells and represent a central component of epithelial microenvironment and their responses to *H. pylori* infection.

I found that during homeostasis, the myofibroblasts generate a BMP gradient along the gland axis with strong expression of Bmp2 in the upper part, whereas the base is surrounded by cells producing BMP inhibitors. Based on functional analysis with 3D organoid models, the BMP gradient occurs to be a main factor responsible for rapid differentiation of stem cells into pit surface mucous cells. Moreover, experiments led me to identify an auto-paracrine feed-forward BMP2 loop in epithelial cells, which further stabilizes BMP signaling once it is activated and induces terminal differentiation. Data presented in this study demonstrated a reduction of BMP signaling in *H. pylori*-infected myofibroblasts. Furthermore, infection with *H. pylori* resulted in loss of not only stromal, but also epithelial Bmp2 expression. This observation was accompanied with increase of Interferon γ (IFNγ), which indicated a link between both pathways. Consistently, stimulation of organoids with IFNγ impairs BMP signaling and the BMP2 feed-forward loop, and thereby blocks terminal differentiation.

Together, this study shows that the fate of a cell migrating into the surface of the gastric gland is determined by an induction of BMP signaling and stabilized by an auto-paracrine BMP signaling enhancement. Reduction of this signaling by IFNγ revealed a mechanism which contributes to altered cellular differentiation and development of premalignant epithelial alterations in the context of *H. pylori* infection.

Zusammenfassung

Infektionen mit *H. pylori* führen zu Veränderungen im Aufbau und der zellulären Zusammensetzung des Magenepithels. Diese Veränderungen sind normalerweise mit einer epithelialen Hyperproliferation und einer beeinträchtigten Differenzierung verbunden und können sich weiter zu pathologischen Veränderungen wie der Hyperplasie, Atrophie und Metaplasie entwickeln, die Vorläuferläsionen von Magenkrebs darstellen. Obwohl viel über die Organisation des Epithels während der Homöostase bekannt ist, sind die molekularen Mechanismen, die die Differenzierung und den veränderten Zellumsatz im Kontext der Infektion regulieren, immer noch unbekannt. Aktuelle Studien haben Stammzellen in der Drüsenbasis in den Fokus gerückt, und es wurde gezeigt, dass diese Zellen innerhalb von ein bis zwei Wochen die Magendrüsen neu besiedeln und somit den Zellumsatz im Epithel entscheidend beeinflussen. Darüber hinaus haben neuere Studien gezeigt, dass Stromazellen, die sich in unmittelbarer Nähe der epithelialen Stammzelle befinden, die funktionelle Nische für dieses Kompartiment bilden und wichtige Faktoren für die Regulierung des Stammzellumsatzes und Differenzierung darstellen. Daher konzentriere ich mich bei dieser Arbeit auf die Rolle der Myh11+ Myofibroblasten, die sich sowohl unter als auch zwischen den Epitheldrüsenzellen befinden und eine zentrale Komponente der epithelialen Mikroumgebung bilden; besonderes Interesse wird dabei auf die Reaktion dieser Zellen im Verlauf einer Infektion mit *H. pylori* gelegt.

Ich fand heraus, dass die Myofibroblasten in der Homöostase einen BMP-Gradienten entlang der Drüsenachse mit erhöhter Expression von Bmp2 im oberen Teil erzeugen, während die Drüsenbasis von Zellen umgeben ist, die Bmp-Inhibitoren produzieren. Basierend auf der Funktionsanalyse mit 3D-Organoidmodellen ist der Bmp-Signalweg ein zentraler Faktor für die rasche Differenzierung von Stammzellen in faveoläre mukusproduzierende Zellen. Darüber hinaus wurde ein auto- bzw. parakriner Signalweg gefunden, der zur Bildung von Bmp2 in Epithelzellen führt. Damit wird die Bmp-Signalübertragung nach ihrer Aktivierung weiter stabilisiert, wodurch eine terminale Differenzierung induziert wird. Meine Untersuchungen Daten zeigten eine Verringerung des BMP-Signalwegs in *H. pylori*-infizierten Myofibroblasten. Darüber hinaus führte eine Infektion mit *H. pylori* nicht nur zum Verlust der stromalen, sondern auch der

epithelialen Bmp2-Expression. Diese Beobachtung ging mit einer Zunahme von Interferon γ (IFNγ) einher, was auf eine Verbindung zwischen beiden Signalwegen hinwies. Tatsächlich zeigten anschließende Experimente mit Organoiden, dass IFNγ den Bmp-Signalweg hemmt und dadurch die terminale Differenzierung blockiert.

Zusammenfassend zeigen meine Untersuchungen, dass das Schicksal einer Zelle, die zur Oberfläche der Magendrüse wandert, eine Induktion des BMP-Signalwegs erfährt, der durch auto-parakrine BMP-Signalverstärkung zusätzlich stabilisiert wird. Die Reduktion dieses Signals durch IFNγ deutet auf einen Mechanismus hin, der Veränderungen in der zellulären Differenzierung und die Entwicklung von prämalignen epithelialen Läsionen im Verlauf einer *H. pylori*-Infektion bewirkt.

1 Introduction

1.1 THE STOMACH

1.1.1 ANATOMY AND FUNCTION

The stomach as well as the rest of gastrointestinal track is of endodermal origin (Zorn and Wells 2009) and develops from the dilated part of the foregut during the fourth week of gestation. One week later, one side of the stomach grows faster than the other to create the greater curvature, which gives the stomach its characteristic shape. Three weeks later, the organ rotates by 90° positioning itself in its final position (Chaudhry, Liman, and Peterson 2019).

Developed human stomach is located between esophagus and duodenum and consists of four main regions: the cardia, fundus, corpus and antrum (Figure 1.1.a). The ingested food gets to the stomach through cardia, which is located between esophagus and fundus and acts as valve closing the top of the stomach. However, multilayer histopathology of esophagogastric junction has shown that cardia contains features characteristic for both esophagus and stomach, so it is controversial to assign it to any of these organs (Lenglinger et al. 2012). The superior portion of the stomach is called fundus and is located on the left side of the cardia and has a dome-like shape (Chaudhry, Liman, and Peterson 2019). Following the fundus, there is the main and the largest portion of stomach called ‘the body’ or ‘corpus’ (San Roman and Shivdasani 2011). The most distal part of the stomach is the antrum, that includes the pylorus, which connects stomach with duodenum (Chaudhry, Liman, and Peterson 2019). Since in my work involves mouse models to investigate stomach changes upon *Helicobacter pylori* (*H. pylori*) infection, it is important to highlight the difference in the anatomy of murine compared to human stomach. The fundus region is absent in mice, but instead characteristic upper curvature is occupied by the not glandular forestomach (Figure 1.1.b) (Kim and Shivdasani 2016). This part of the stomach is able to store well chewed food for one to three hours or longer and supply it for further digestion once the animal needs it, which is probably an adaptation to the murine lifestyle (Gartner and Pfaff 1979).

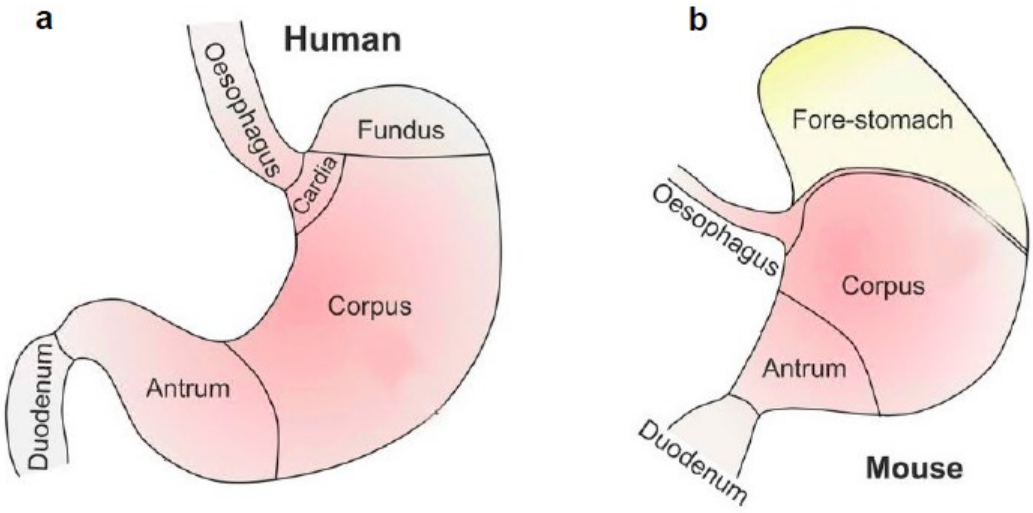

Figure 1.1. Stomach regions in human and mouse.
Representative schemes of stomach regions for human (a) and mouse (b) showing that both species possess corpus and antrum part of the stomach, but mouse has fore-stomach in characteristic upper curvature occupied by fundus in humans. Figure modified from (Burkitt et al. 2017)

As a part of the gastrointestinal tract, the stomach is involved into the process of digestion. While absorption is mainly taking place in the small intestine, the main role of the stomach is to contribute to the process of digestion by providing a reservoir as well as by acid secretion and enzyme secretion (O'Connor and O'Morain 2014).

Functionally, the stomach may be divided into a reservoir and a pump part. The first one acts in fundus and upper parts of corpus and is characterized by the ability to increase its volume significantly, while internal pressure stays on the same level (Cooke 1975). Therefore, stomach acts as a holding chamber and doses small portions of food for digestion and absorption into the small intestine. The lower portions of stomach, including antrum and lower corpus, contract in a rhythmic fashion and use peristatic waves to mechanically digest the food. The waves originate in gastric wall as an electric signal, which further induces tonic contractions and peristatic waves in proximal stomach propagating to the pylorus. In the lowest point of antrum, the waves increase their intensity until they finally reach the pyloric sphincter. Here, sufficiently liquefied chyme is dosed further into small intestine (Chaudhry, Liman, and Peterson 2019). Additionally, the stomach takes part in chemical digestion by producing pepsinogen and hydrochloric acid (HCl), which also create acidic environment lethal for many bacteria. Although main absorption is taking place in small intestine, stomach is also capable to

absorb amino acids, ethanol, caffeine and by production of intrinsic factor it is relevant for the absorption of vitamin B12 that itself takes place in the distal part of the small intestine (Chaudhry, Liman, and Peterson 2019).

1.1.2 MICROSCOPIC ANATOMY

The wall in all gastrointestinal organs, including stomach, is built by four layers: serosa or adventitia, muscularis externa, submucosa and mucosa (Figure 1.2.a). In the stomach, serosa is a smooth tissue membrane, located outermost of the stomach, and which is known to reduce the friction from muscle movement. Next, muscularis externa is built by smooth muscle fibers and consists of, unlike other gastrointestinal organs, three layers: longitudinal, circular and additional oblique layer, which enables mechanical digestion (Pangtey, Kaul, and Mishra 2017). Dense connective tissue called 'submucosa' is located right next to muscularis externa. It contains blood vessels, lymphatic vessels and nerves, which supports the mucosa (Hsu and Lui 2019). Finally, the most inner layer of the stomach wall is the mucosa. The mucosa is divided into three sections: a muscle layer named muscularis mucosae, connective tissue layer called lamina propria and the epithelial glands. The main function of the muscularis mucosae and lamina propria is to stabilize the epithelium, not only as a scaffold but also by providing signals and factors (Aoki et al. 2016; Sigal et al. 2017; Stzepourginski et al. 2017). It may be crucial, because epithelial cells are the source of mucus, pepsinogen and HCl, which are relevant for proper digestion (Chaudhry, Liman, and Peterson 2019).

The glandular epithelium is composed of a single layer of epithelial cells specialized into different cell types. A closer insight into the cells distribution within glands allows to distinguish two different gland types that are usually assigned to the main parts of the stomach, the antrum and the corpus (which includes not only corpus but also fundus part of the stomach) (Saenz and Mills 2018). The cellular composition of corpus glands consists of surface pit or foveolar cells, parietal cells, mucous neck cells, chief cells, endocrine cells and undifferentiated isthmus cells that serve as multipotent stem cell. Antral glands are composed of surface pit or foveolar cells, endocrine cells, progenitor cells as well as isthmus stem cells and deep glandular cells, which include mucous neck cells, chief cells and basal stem cells (Figure 1.2.b) (Willet and Mills 2016). Similar to the

anatomical specificity, there are also differences at the cellular level between human and mouse. Mouse antrum does not consist any parietal cells, whereas half of the human antrum glands does have some parietal cells (Choi et al. 2014). In addition, in human stomach these cells express gastric intrinsic factor, whereas in mouse it is expressed in chief cells (Levine, Nakane, and Allen 1980).

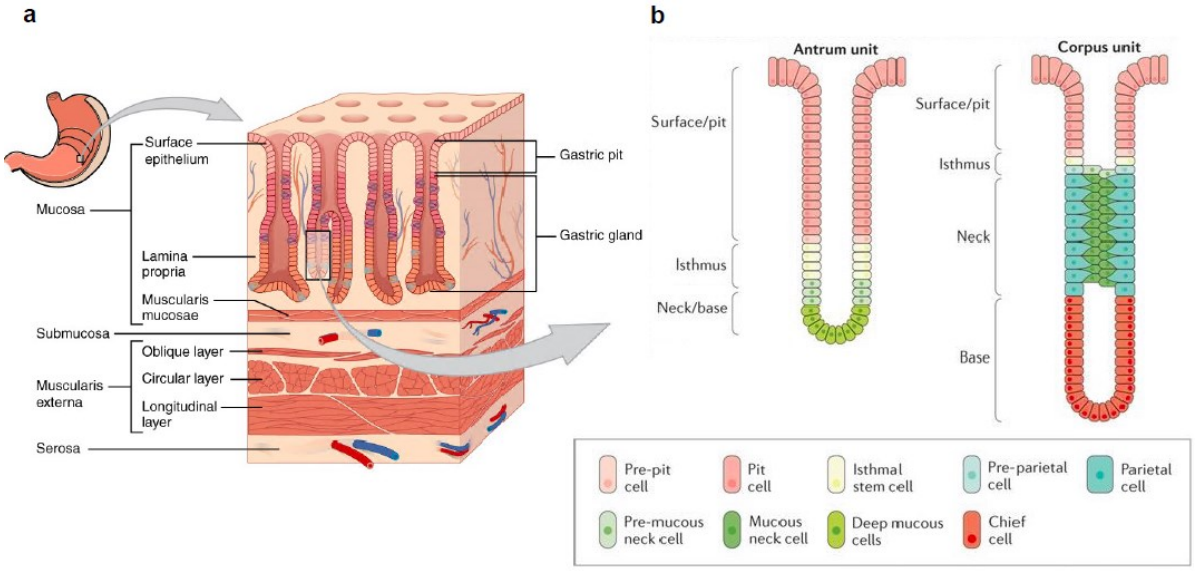

Figure 1.2. Gastric cell types in antral and corpus gland.
Representative schemes of stomach wall (a) showing four main layers of stomach and epithelial mucosa in antral and corpus gland unit (b) showing different cell types specification. Figure modified from (Saenz and Mills 2018).

To understand changes in tissue structure upon *H. pylori* infection, it is crucial to gain better insight into different cell types and comprehend gland architecture in homeostasis. Surface mucus cells or foveolar cells are, as the name indicates, the most surface pit cells in gastric glands, which secrete mucus that protect stomach from gastric acid (Kantani-Matsumoto and Kataoka 1987). These cells are produced in the basal parts of the gland and migrate to the top during differentiation into pit cells. Once the cells reach the surface, terminal differentiation takes place, cells are culminated into necrosis or apoptosis and phagocytosed or extruded into gastric lumen (Ootani et al. 2003). Surface mucus cells may be distinguished by MUC5AC secretory mucin marker (Choi et al. 2014). Next, in the middle of the gland, gastric acid producing parietal cell are located (Yao and Forte 2003). To rapidly produce sufficient quantities of HCl, these cells are rich in mitochondria generating large amounts of adenosine triphosphate (ATP), which may

be further used by H+-K+-ATPase pump in hydrogen/potassium ions exchanged (Kopic, Murek, and Geibel 2010). As mentioned before, in humans, parietal cells are also the source of gastric intrinsic factor, which is required for the absorption of vitamin B12 (Merchant 2018). A characteristic marker for parietal cells is the β-subunit H+-K+-ATPase enzyme (ATP4b) (Zhao et al. 2010). Following the parietal cells, small triangular mucous neck cells, which secrete an acidic fluid containing mucin proteins, can be distinguished (Hanby et al. 1999). In the corpus gland, these cells are interdigitated between the parietal cell, but in the antrum unit they are located near the base of the glands (Mills and Shivdasani 2011). Mucous neck cells may be identified by expression of mucin 6 (Muc6) (Kang et al. 2005), but also by staining with lectin Griffonia Simplicifolia II (GS II) (Falk, Roth, and Gordon 1994). In the trans-differentiation process mucous neck cells migrate towards the base of the gland and convert into chief cells (Goldenring, Nam, and Mills 2011). Chief cells release pepsinogen, which reacts with acid produced by parietal cells and gets activated into the digestive enzyme pepsin (Stange et al. 2013). In addition, enteroendocrine cells are distributed scattered throughout the gland (Choi et al. 2014). These cells secrete many hormones supporting the digestion process like gastrin (GAST), which stimulates secretion of gastric acid (Prosapio and Jialal 2019), somatostatin which acts as a paracrine regulator of acid secretion (Makhlouf and Schubert 1990) or chromogranin A (CHGA), which promotes formation of several bioactive peptides (D'Amico M et al. 2014). Finally, in the base or isthmus of the gland, epithelial stem cells are located (Matsuo et al. 2017). These pluripotent, long-lived and self-renewing cells give rise to all the differentiated epithelial cells during the constant gland regeneration (Leushacke et al. 2013). However, antral and corpus stem cells populations are different. In the antrum, located at the gland base, leucine-rich repeat-containing G-protein coupled receptor 5 (Lgr5) positive stem cells are able to repopulate the gland throughout their life span, but lineage tracing demonstrated relatively low proliferation rate of these cells (Barker et al. 2010). Moreover, recent report has showed that upon *H. pylori* infection, Lgr5+ stem cells acts not only as stem cells, but also as differentiated cells expressing antimicrobial genes (Sigal et al. 2019). In addition, in lower isthmus of antrum glands, highly proliferative axis inhibition protein 2 (Axin2) positive stem cells have been found, which are able to repopulate the whole gland within one week (Sigal et al. 2017). Moreover, many others markers have been reported

as antrum stem cells, including: Sox2, Lrig1, Mist1, eR1, Cckbr for isthmus region and Cxcr4 for both basal and isthmus part (Hata, Hayakawa, and Koike 2018).

In contrast, Lgr5+ and Axin2+ stem cells in the corpus do not fully trace the gland (Sigal et al. 2017; Barker et al. 2010). Lineage tracing studies have identified Sox2+ cells situated in highly proliferative isthmus but also in the base of corpus gland, as potential stem cells (Arnold, Sarkar, et al. 2011). However, scattered location of this marker raised doubts whether all or only a subset of this population has stem cell properties. Further research associate Troy (Stange et al. 2013), Mist1 (Hayakawa et al. 2015) and Lrig1 (Choi et al. 2018) expressing cells with the corpus stem cell markers, but always in both isthmus and base gland location, suggesting that stem cells in the corpus are not only highly-proliferating isthmus cells but may also arise from differentiated chief cells (Nam et al. 2010). On the other side, recent study has reported that corpus stem cells populations in the isthmus and in the base are independently maintaining their gland compartments with the barrier created by parietal cells (Han et al. 2019).

1.1.3 ORGANOIDS CULTURE

The complex gland structure built by many different cell types, which depend on many different signaling pathways, encouraged scientists to create a culture model, which may mimic *in vivo* cell composition and enable to understand the mechanisms underlying gland homeostasis in gastric tissue. A model termed “organoids model” has been developed as cultured cells under appropriate culture conditions form structures, which resemble the features of organs they are derived from. Identification of Lgr5+ stem cells in the small intestine was a crucial point in developing organoids, which allowed infinite propagation of stem cells originating from different tissues (Sato et al. 2009). Initially the model was obtained for small intestine, but within a short time it was extended to mouse (Barker and Clevers 2010) and human stomach divided into culture from antrum and corpus tissue (Schlaermann et al. 2016; Bartfeld et al. 2015). Technically the method is based on Matrigel, which at temperature below 4°C is a liquid but at 37°C it becomes a solidified, jelly drop. Moreover, Matrigel contains critical components of extracellular matrix like collagen type IV and lamin-I (Hughes, Postovit, and Lajoie 2010) produced by the sarcoma Engelbreth-Holm-Swarm cell line (Kleinman

et al. 1982), which enables embedding of epithelial glands in extracellular matrix that supports their growth. In addition, cultured cells require defined factors supplied with the medium, which mimic stem cell niche and thus provide signals for infinitive culture (Sato et al. 2009). In these conditions, embedded glands organized itself in structures similar to glands in the tissue consisting not only stem cells but also differentiated and dead cells, which, like in the stomach, are shed into the lumen (Sato et al. 2011). Furthermore, organoids culture can be stimulated with other factors which may mimic any desired niche or condition making it a perfect model to study gastric gland responses and adaptations *in vitro* (Co et al. 2019; Kessler et al. 2015; Broda, McCracken, and Wells 2019).

1.2 HELICOBACTER PYLORI

1.2.1 BACTERIA AND ITS ADAPTATION

H. pylori belongs to the class *Epsilonproteobacteria*, order *Campylobacterales*, family *Helicobacteraceae* and genus *Helicobacter* (Owen 1998). The genus *Helicobacter* was part of *Campylobacter* genus but in 1989 became an independent category with *H. pylori* as a representative (Solnick and Vandamme 2001; Vandamme et al. 1991). Today *Helicobacter* genus includes 35 species, which are gram-negative bacteria and many of them are characterized by resistance to mammalian stomach acid due to urease production and by high motility due to unipolar flagella (Dunn, Cohen, and Blaser 1997; Hua, Zheng, and Bow 1999). *H. pylori* remains the most prominent bacterium in this genus and colonizes over 50% of human populations, which makes it one of the most widespread infection in the world (Pounder and Ng 1995). However, there is a strong diversity in infection rates between developing countries in Africa, Asia and South America, where prevalence of bacteria reaches even more than 70% and industrial countries in Europe, North America and Australia where infection is estimated to be under 40% (Figure 1.3.) (Hooi et al. 2017).

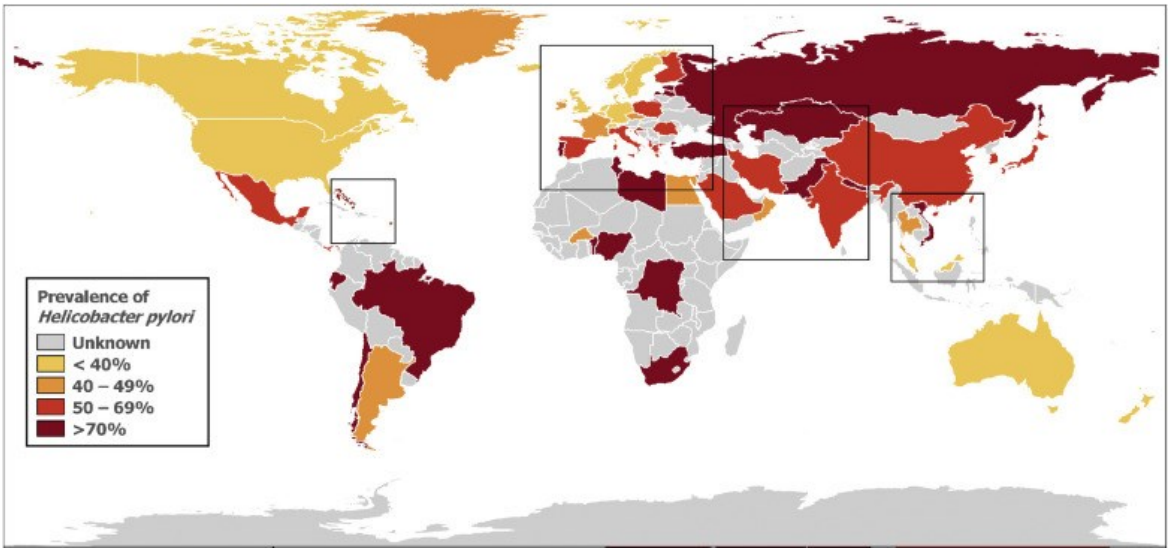

Figure 1.3. Worldwide epidemiology of H. pylori.
Global H. pylori prevalence of map showing large variation among regions. Figure adapted from (Hooi et al. 2017).

Such a big variety may have a cause in transmission route, which is related with water, food, animals (Kusters, van Vliet, and Kuipers 2006) and most of all with oral and fecal person-to-person contact, but the exact way of transmission still remains unclear (Dominici et al. 1999; Escobar and Kawakami 2004; Schwarz et al. 2008). Furthermore, scientific data suggest that infection depends on socioeconomic status, hygiene and living standards (Malaty et al. 1996), mainly occurs during early childhood and without antibiotics treatment it may persist over time (Suerbaum and Michetti 2002).

To become one of the most widespread infection in the world and persist in gastric acid, which creates barrier to pathogens (Tennant et al. 2008), *H. pylori* evolved by adapting to its environment. A functional chemotaxis machinery helps bacteria to sense a pH gradient in the mucus and break through to less acidic epithelial cell layer underneath (Schreiber et al. 2004). High motility is possible due to presence of 3-5 unipolar flagella on the side of the bacterium (Kim et al. 1999) as well as because of peptidoglycan crosslinking relaxation, which promotes its helical shape (Sycuro et al. 2010). However, *H. pylori* not only escapes from the acidic environment but also produces urease to convert urea into carbon dioxide and ammonia and thus neutralize acetic area around the bacteria (Meyer-Rosberg et al. 1996). Except adaptations associated with acidic environment, bacteria evolved other virulence factors, which help in colonization and the establishment of inflammation. One of them are outer membrane proteins (OMP)

separating further into Helicobacter outer porins (Hop) and Hop-related proteins (Hor) groups (Alm et al. 2000). This paralogous family including 33 members is involved in processes like importing nutrients and translating signals from the environment, but also plays a crucial role in adhesion to gastric epithelium by adhesins (Odenbreit et al. 1999) and in cytotoxin-associated gene A (CagA) translocation into cells by type IV secretion system (T4SS) (Ishijima et al. 2011). Moreover, occurrence of various OMP has extremely variable rates across different hosts and over time even within individual, which indicates their function in adaptation to the host or gastric niche (Odenbreit et al. 2009). Another *H. pylori* adaptation is expression of vacuolating toxin A (VacA). This toxin is able to form anion-selective channel in the host cell membrane resulting in large vacuolization and apoptosis of host cells (Yahiro et al. 2015). Recent reports suggest even that VacA supports bacteria to escape from phagosomes (Zheng and Jones 2003). However, the most prominent virulence factor is the cytotoxin-associated gene pathogenicity island (CagPAI). Strains carrying CagPAI induce stronger inflammatory response and greater risk of peptic ulcers and gastric cancer occurrence than strains lacking the island (Boonyanugomol et al. 2013). CagPAI encodes T4SS which acts like a molecular syringe and injects ADP-glycero-β-D-manno-heptose (ADP heptose), an lipopolysaccharides (LPS) intermediate produced in gram-negative bacteria (Pfannkuch et al. 2019; Stein et al. 2017). The injection results in activation of alpha kinase 1 (ALPK1) in the host cells, which causes TRAF-interacting protein with forkhead-associated domain (TIFA) phosphorylation and formation of TIFA large complex (TIFAsomes) (Zimmermann et al. 2017). These ADP-ALPK1-TIFA axis mediates NF-κB activation, interleukin 8 (IL-8) secretion and evokes innate immune response (Gall et al. 2017; Zimmermann et al. 2017). Most importantly, CagPAI encodes for first discovered bacterial oncoprotein CagA that is translocated into the cells by T4SS (Hatakeyama 2014). Once protein reaches the host cytosol it gets phosphorylated by tyrosine kinase (TK), which is a domain of epidermal growth factor receptor (EGFR), activates Src homology region 2 domain-containing phosphatase-2 (Shp2) protooncogene and causes alterations in cell proliferation and morphological changes (Hatakeyama 2004). In addition, independently of tyrosine phosphorylation, C-terminal region of CagA is involved in gene transcription alternation in host cells (Baldwin et al. 2007). Moreover, CagA has been shown to induce gastric cancer when overexpressed in mice (Ohnishi et

al. 2008) and has been linked to human gastric cancer in epidemiological studies (Parsonnet et al. 1997).

1.2.2 GASTRIC PATHOLOGIES

Spiral-shaped bacteria present in mammalian stomach and peptic ulcers caused by infectious agents have been observed in the early twentieth century (Salomon 1896; Balfour 1906; Doenges 1939). However, the first *H. pylori* cultivation was established 80 years later by Barry Marshall and Robin Warren (Marshall and Warren 1984), who not only isolated the bacteria but also revealed the connection between the bacteria and chronic gastritis (Marshall et al. 1985). These finding led to further exploration of *H. pylori* associations with gastrointestinal diseases and thus contribute to the creation of Correa's cascade (Correa et al. 1975; Correa and Piazuelo 2012), which shows *H. pylori*-induced gastric precancerous process (Figure 1.4.). Finally, in 1994 World Health Organization (WHO) classified this gastric-specific pathogen as a class I carcinogen (IARC 1994). However, it is important to highlight that although in all *H. pylori* infected individuals gastritis will develop, only in 10% of them it progresses to gastric ulcers and in another 1 to 3% results in gastric cancer or mucosa associated lymphoid tissue (MALT) lymphoma (Wroblewski, Peek, and Wilson 2010).

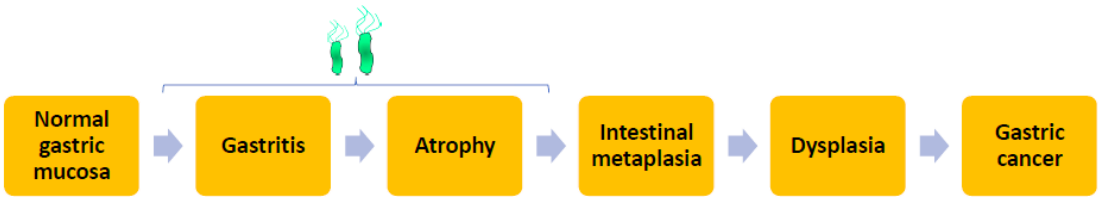

Figure 1.4. Correa's cascade.
H. pylori infection of the normal gastric mucosa causes gastritis, followed by atrophy, intestinal metaplasia, dysplasia and gastric cancer. Bacteria is only present until intestinal metaplasia develops. Figure modified from (Correa and Piazuelo 2012).

H. pylori infection induces inflammation through many different pathways in circulating immune cells, which increase production of inflammatory molecules like IL-1, IL-6, IL-8, tumor necrosis factor alpha (TNFα) and interferon gamma (IFNγ) but also in gastric epithelial cells, which first have contact with bacteria (McGee and Mobley 2000; Sayi et al. 2009). This inflammatory environment leads to gastritis and development of peptic ulcers disease in 10-20% infected patients (Crabtree et al. 1991). Chronic inflammation

induces gastric gland alteration such as increased stem cell compartment, proliferation of these cells and their pit-/neck-progenitors resulting in gland hyperplasia (Mills et al. 2002; Sigal et al. 2015). Following gastritis, atrophy can occur, which is characterized by loss of acid producing parietal cells and chief cells (Kimura et al. 1996). The exact mechanism of parietal cell loss remains unknown, but it has been associated with a functional T4SS (Neu et al. 2002). Parietal and chief cells can be replaced by goblet, Paneth and enterocyte-like cells (Correa 1992) and MUC5AC and MUC6 producing mucous cells can be substituted by MUC2 cells (Reis et al. 1999). This switch from gastric epithelial cells to cells typical for intestine is named intestinal metaplasia (Correa 1992) and occurs in 25,7% of *H. pylori* infected patients with the 47.4% prevalence in those with gastric ulcers (Eidt and Stolte 1994). Simultaneously, spasmolytic polypeptide-expressing metaplasia (SPEM) may develop (Schmidt et al. 1999). It describes the trans-differentiation of basal chief cells into Muc6 and trefoil factor 2 (Tff2) expressing cells that are characterized by decrease of the zymogen and increase of mucous granule secretion (Leushacke et al. 2017; Mills and Sansom 2015). Next, neoplastic dysplasia appears, characterized by enlarged nuclei, cell polarity loss and gland morphology disruption (Rugge et al. 2000). Eventually, in 1% of the patients, as the last step of this series of events, intestinal type adenocarcinoma develops, mainly in the antrum region (Correa and Piazuelo 2012). This type of cancer consists of malignant epithelial cells with glandular differentiation able to infiltrate muscularis mucosae, submucosa and muscularis propria (Ban and Shimizu 2009). Interestingly, *H. pylori* which is able to induce the Correa's cascade is cleared in intestinal metaplasia regions, probably due to presence of Paneth cells secreting different bactericidal substances (Fukuda et al. 1995).

1.3 BMP SIGNALING

1.3.1 BONE MORPHOGENETIC PROTEINS

Bone morphogenetic proteins (BMPs) belong to large Transforming Growth Factor-β (TGFβ) superfamily of regulatory proteins. Although they are part of the same protein family and have a high sequence homology, BMP and TGFβ often play opposite roles in the cell regulation (Rider and Mulloy 2010). BMP was first discovered in 1965 as an inductor of ectopic bone formation (Urist 1965). However, it took 23 years to

characterize and clone the first BMPs and start their biochemical studies (Wozney et al. 1988). Currently, BMP family includes over 20 different ligands and based on nucleotide and amino acid similarity or phylogenetic analysis main BMP ligands may be divided into subgroups: BMP2/4, BMP5/6/7/8, BMP9/BMP10, and BMP12/13/14 (GDF5/6/7) (Mueller and Nickel 2012). They have been reported to induce formation of cartilage and bone (Bandyopadhyay et al. 2006), determinate ectodermal cell fate (Munoz-Sanjuan and Brivanlou 2002), direct neuronal development (Christiansen, Coles, and Wilkinson 2000), inhibit limb formation (Niswander and Martin 1993), regulate heart remodeling (Duan et al. 2017) and to be involved in many others processes. Moreover, the European Medicines Agency (EMA) approved recombinant human (rh) BMP2 for treatment of lumbar spine fusion and for acute tibial fractures (Arrabal et al. 2013) and rhBMP7 for the treatment of recalcitrant long bone non-unions (Einhorn 2003).The American Food and Drug Administration (FDA) approved rhBMP2 for the treatment of open tibial fractures (Arrabal et al. 2013). In addition, BMPs up-regulation has been identified in thyroid carcinoma (Meng et al. 2017), blood (Shi and Pan 2016), breast (Alarmo et al. 2008) and melanoma cancer (Rothhammer et al. 2005), but at the same time BMPs down-regulation has been reported for bladder (Kuzaka et al. 2015) and prostate cancer (Horvath et al. 2004). Proteins from this family have been identified as key regulators in such a variety of processes in all organ systems that they gained the “body morphogenetic proteins” name (Wagner et al. 2010).

1.3.2 BMP PATHWAY

BMPs are secreted as dimeric pro-protein complex, which is cleaved by extracellular protein like Furin to form a mature protein (Harrison, Al-Musawi, and Walton 2011). In the canonical pathway active BMPs create a homo- or heterocomplex, bind to the cell surface receptors and generate heterotetrameric complex with type I and type II serine/threonine kinase receptors (Figure 1.5.) (Heldin, Miyazono, and ten Dijke 1997). For BMP family there are three known type I receptors: 1A BMP receptor (BMPR-1A or ALK3), 1B BMP receptor (BMPR-1B or ALK6) and t1A activin receptor (ActR-1A or ALK2) and three type II receptors: 2 BMP receptor (BMPR-2), 2 activin receptor (ActR-2A), and 2B activin receptor (ActR-2B) (de Caestecker 2004). The binding mechanism may vary

depending on ligand complex, for example BMP2/4 dimer binds to type I receptors and recruits type II receptors, whereas BMP6/7 bind the other way around, which results in activation of different pathways (Nohe et al. 2002). Once the heterotetrameric complex is formed, BMP type II receptor transphosphorylates type I receptor at a motif rich in glycine-serine (GS domain). This actives the type I receptor, which immediately phosphorylates receptor-regulated Smads including Smad1, Smad5 and Smad8 (Horbelt, Denkis, and Knaus 2012). Phosphorylated Smad1/5/8 complex associates with Smad4, which is a co-mediator, and translocates together into the nucleus where it acts as a transcription factor and regulates gene expression (Roelen et al. 2003). As a consequence of active BMP signaling up-regulation of target genes like Inhibitor of differentiation 1/2/3 (Id1/2/3/), Runt-related transcription factor (Runx) and Twist family BHLH transcription factor 1 (Twist1) is observed (Budna et al. 2017).

BMP pathway may be inhibited by Smad6/7 complex that is induced by the activation of BMP signaling itself leading to a negative feedback inhibition of the signaling pathway (Moustakas, Souchelnytskyi, and Heldin 2001). Moreover, BMP signaling can be blocked by endogenous BMP inhibitors which either bind to BMP ligands, such as Noggin (Groppe et al. 2002), Chordin (CHRD) (Piccolo et al. 1996) and Gremlin (GREM) (Kisonaite, Wang, and Hyvonen 2016), associate with receptors and blocks ligand binding such as BAMBI (Onichtchouk et al. 1999) and Endoglin (Scherner et al. 2007) or interact with both receptors and ligands as Follistatin (Iemura et al. 1998).

In addition, the Smad-independent non-canonical BMP signaling has been described as an activator of pathways such as mitogen activated protein kinase (MAPK) (Yang et al. 2015), phosphoinositide 3-kinase/protein kinase B (PI3K/Akt) (Chen et al. 2011), protein kinase C (P/kc) (Zhang 2009) and others pathways (Zhang 2017). Furthermore, it has been described that BMP pathway interacts with TGFβ signaling and although both are a part of one family, they acts as antagonists and inhibit each other effects in chondrocytes (Keller et al. 2011). Janus kinases/ signal transducer and activator of transcription (JAK/STAT) signaling has been associated with BMP4 as a co-mediator of non-canonical BMP signaling during megakaryopoiesis (Jeanpierre et al. 2008). Moreover, BMP has been also shown to interact with Wingless-Type MMTV Integration

Site Family (WNT) signaling and this cross-talk occurred to be both synergistic and antagonistic. For example, WNT has been reported to negatively regulate BMP ligands in the foregut (Stevens et al. 2017), but activate BMP2 expression in osteoblasts (Zhang et al. 2013). On the other side, BMP has been identified as suppressor as well as promotor of WNT signaling in colorectal cancer depending on SMAD4 and p53 status (Voorneveld et al. 2015). It is also not clear, which pathway is the main regulator, since it has been described that β-catenin acts downstream of BMPR1 but at the same time controls expression of Bmp4 (Soshnikova et al. 2003). Therefore, it has been suggested that BMP-WNT signaling interactions depend on the cellular context (Yang et al. 2016).

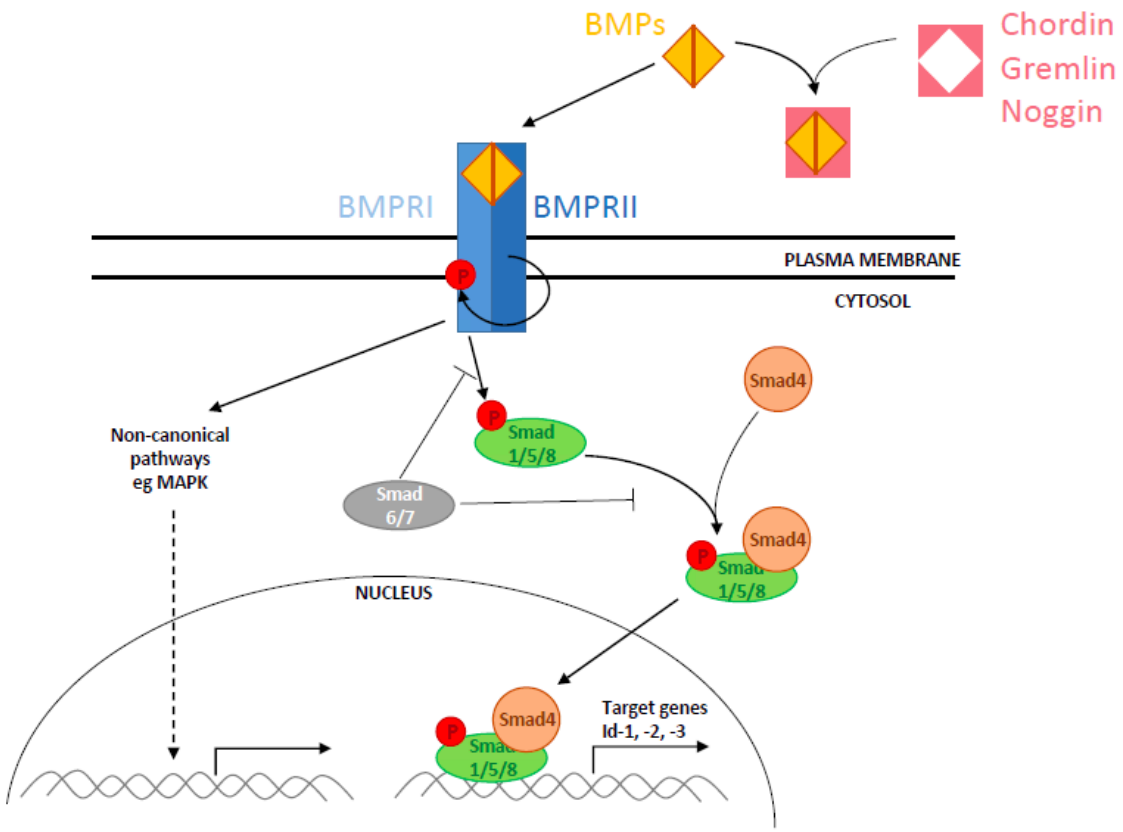

Figure 1.5. BMP pathway.
In canonical pathway BMP ligand dimer binds to BMP type I and II receptor complex and induces phosphorylation of BMP type I receptor, which further phosphorylates Smad1/5/8 and enables Smad4 association with pSmad1/5/8. This complex is translocated into the nucleus and regulates expression of target genes. In non-canonical pathway BMP ligands attachment to BMP receptors induces Smad-independent signaling. Figure modified from (Wang, Green, et al. 2014).

1.3.3 ROLE IN GASTROINTESTINAL TRACT

BMP pathway plays an important role also in gastrointestinal tract. It has been extensively investigated in the intestine, whereas its role in stomach is still unclear. In

the adult mouse intestine distribution of BMP ligands shows crypt-villus axis gradient with lowest activity at the bottom of the crypt, which increases to the top of the villus, whereas distribution of BMP inhibitor Noggin shows a reverse pattern (Qi et al. 2017; Haramis et al. 2004). Single-molecule RNA in situ hybridization (ISH) of BMP4 has revealed expression of this ligand mainly in mesenchymal cells surrounding villus and crypts (Haramis et al. 2004). Functionally, BMP signaling has been associated with suppression of intestinal proliferation and its inhibition leads to hyperproliferation and *de novo* crypt formation (Haramis et al. 2004). It has been reported that conditional knock-out (KO) of Bmpr1a in mesenchymal cells induces expansion of proliferating cells through WNT/β-catenin signaling (He et al. 2004). However, studies by Auclair and others (Auclair et al. 2007) as well as Qi and others (Qi et al. 2017) have shown that BMP regulates epithelial intestinal proliferation and stem cells compartment independently of WNT/β-catenin, directly through Smad4 regulation and a subset of WNT target genes is blocked via Smad4 independently of WNT signaling. In addition, Auclair and others described BMP signaling as an inducer of secretory cell differentiation (Auclair et al. 2007). Furthermore, Qi et al revealed an inhibitory influence of BMP on Lgr5+ intestinal stem cells (Qi et al. 2017). This observation has been supported by organoid experiments, which showed an expansion of Lgr5 cells upon BMP inhibitor LDN-193189 treatment (Tong et al. 2018). In contrast, BMP has been identified as a crucial protein required to establish colonic organoids from pluripotent stem cells, suggesting that BMP may also enhance cell growth and develop (Munera et al. 2017).

Studies performed in the stomach confirmed hyperproliferation and hyperplasia in transgenic mice with Bmpr1a KO (Maloum et al. 2011) or Noggin overexpression in parietal cells (Takabayashi et al. 2014). Surprisingly, epithelial hyperproliferation was also observed upon Bmpr1a KO not only in epithelial (Maloum et al. 2011) but also mesenchymal cells (Roy et al. 2016). Additionally, Bmpr1a KO was associated with loss of parietal cells (Takabayashi et al. 2014). Despite these findings, the distribution and the exact function of endogenous BMP signaling molecules has not been characterized in detail.

Compared to BMP signaling during homeostasis, the function of BMP signaling in gastrointestinal cancers appears to be more diverse. It has been shown that BMPs are

upregulated in cancer samples, including BMP2 (Park et al. 2008) and BMP7 (Aoki et al. 2011) in gastric cancer as well as BMP4 in colorectal cancer (Yokoyama et al. 2017). Inhibition of BMP signaling through BMPR1A by LDN-193189 inhibitor diminished tumor formation of colorectal cancer cell (Yokoyama et al. 2017) while expression of BMP inhibitor Noggin induces dysplasia and neoplasia in gastric epithelium (Todisco 2017). On the other hand, BMP2 has shown frequent downregulation in colon cancer (Vishnubalaji et al. 2016). Moreover, its re-expression leads to inhibition of growth and migration and increase of chemosensitivity in human colorectal cancer cell lines as well as tumor suppression in mice (Vishnubalaji et al. 2016). This effect was confirmed in gastric cancer cells where BMP2 inhibited proliferation and induced apoptosis (Zhang et al. 2012). Additionally, BMP10 has been shown to be down-regulated in gastric cancer samples, inhibited growth and migration in gastric cancer cells and its KO promoted metastasis in mice (Lei et al. 2016). Thus, dual-role of BMP signaling in cancer progression has been suggested, and it appears that it can act as both, suppressor and promotor of tumorigenesis (Bach, Park, and Lee 2018).

1.4 WNT SIGNALING

WNT signaling plays a crucial role in embryonic development, but it also regulates important cellular functions in adult tissues such as proliferation, differentiation, migration and apoptosis (Ring, Kim, and Kahn 2014; Nusse 2012). Canonical WNT pathway is induced by glycoproteins, which interact with cell surface receptor of the frizzled (FZD) family (MacDonald and He 2012) and low-density lipoprotein-related protein (LRP) co-receptors (Wehrli et al. 2000). Absence of WNT ligands results in phosphorylation of β-catenin by destruction complex. This leads to proteasomal degradation of β-catenin and initiates TCF/LEF and Groucho complex, which induces histone deacetylases (HDACs) to repress target genes. If WNT ligands bind to receptors, phosphorylation of LRP receptor occurs and leads to activation of disheveled (DVL) and axin proteins, which inactivate the destruction complex, inhibiting β-catenin degradation (Janda et al. 2012; Li et al. 2012). Stabilized β-catenin translocates into the nucleus, forms a complex with TCF/LEF and disturbs TCF/LEF-Groucho interactions (Potten, Wilson, and Booth 1997). This induces histone modifying co-activators and

results in the initiation of transcription of WNT target genes (MacDonald, Tamai, and He 2009). These genes are known to regulate cell morphogenesis and fate (van Amerongen and Nusse 2009).

In addition, non-canonical WNT pathway acts independent of β-catenin–TCF/LEF effectors and mainly regulates cell polarity and calcium mobilization (Veeman, Axelrod, and Moon 2003). Cell polarity is controlled by planar cell polarity (PCP) pathway (Axelrod 2009). The pathway is activated by FZD receptors inducing cascade of GTPase RAC1, Ras homolog gene family member A (RHOA) and c-Jun N-terminal kinase (JNK), which further leads to rearrangements in the gene expression and cytoskeleton (Simons and Mlodzik 2008). Calcium mobilization is regulated by WNT-Ca^{2+} pathway, which starts from WNT-FZD activation of heterotrimeric G proteins, followed by induction of phospholipase C (PLC) and finally Ca^{2+} release from intracellular stores (De 2011).

WNT signaling is essential for proliferation of intestinal and gastric organoids as well as for *in vivo* homeostasis of gastrointestinal epithelium (Schlaermann et al. 2016; Kuhnert et al. 2004; Pinto et al. 2003; Barker et al. 2010). Furthermore, in addition to WNT ligands, other molecules are known to enhance WNT signaling. R-spondins (RSPOs), which bind to Lgr4-6 receptors are able to enhance WNT signaling by preventing FZD ubiquitination and turnover (de Lau, Snel, and Clevers 2012). RSPO1 promotes crypt hyperplasia and is sufficient to culture intestinal organoids without WNT proteins, probably because intestinal cells produce themselves low doses of WNT molecules (Kim et al. 2005; Sato et al. 2009). Stromal-derived Rspo3 is expressed only in the stem cell niche and has been reported to induce proliferation of gastric stem cells by regulating WNT signaling, which leads to hyperplasia (Sigal et al. 2017). Moreover, it has been associated with *H. pylori* infection and increased anti-microbial gene expression (Sigal et al. 2019). In addition, withdrawn of WNT and RSPO from gastric organoids medium results in differentiation towards pit cells and increased amounts of parietal and ECL cells, suggesting its role in differentiation process (Bartfeld et al. 2015; Hayakawa et al. 2015).

1.5 INTERFERON γ

1.5.1 IFNγ PATHWAY

IFNγ is pleiotropic cytokine, which is released by host cells in response to infections. There are three types of interferons: type I, which consists of alpha and beta interferons, type II with IFNγ and type II with interferon lambda (Lazear, Schoggins, and Diamond 2019). The only member of type II class of interferons is encoded by different chromosomal locus, has an unrelated structure and interacts with other receptors than type I and III interferons (Gray and Goeddel 1982). Moreover, serologically IFNγ is acid-labile, whereas type I interferons are acid-stable (DeGrado, Wasserman, and Chowdhry 1982). IFNγ was described by Wheelock in 1965 as a product of leukocytes stimulated by phytohemagglutinin (Wheelock 1965). Followed this discovery other studies revealed that IFNγ is produced by CD4 T helper type 1 cells (Th1) and CD8 cytotoxic T lymphocyte (CTL) effector T-cells, natural killer (NK) and natural killer T (NKT) cells as well as antigen-presenting cell (APC) including macrophages, dendritic cells (DCs) and B-cells (Young 1996; Frucht et al. 2001; Harris et al. 2000). Biologically active IFNγ homodimer is binding to IFNγ Receptor (IFNGR) complex, which consists IFNGR1 (alpha) and IFNGR2 (beta) receptor chains assembled together prior to ligand attachment (Krause et al. 2002). IFNγ receptors are functional only as a heterodimer and cannot transduce signal individually (Pernis et al. 1995). Upon IFNγ binding, IFNGR complex changes its conformation and allows recruitment of JAK1 to IFNGR1 and JAK2 to IFNGR2 cytoplasmic domains. This is followed by JAK1/2 activation, which leads to second conformation change and allows STAT1 association with IFNγ-IFNGR complex (Blouin et al. 2016). Next, JAK1/2 phosphorylates STAT1, which translocates to the nucleus. In the nucleus pSTAT1 binds to the IFNγ activated site (GAS) and regulates transcription of IFNγ associated genes (Decker, Kovarik, and Meinke 1997).

In addition, IFNγ has been identified as a inductor of non-canonical pathways in the JAK/STAT independent process (Gil et al. 2001). This signaling may occur by activation of MAPKs such as PyK2, Erk1/2, and JNK (Takaoka et al. 1999), as well as the Src-family kinase Fyn (Uddin et al. 1997); c-Cbl, CrkL, CrkII and Vav adaptor proteins (Platanias et al. 1999), NF-κB transcription factor (Pfeffer 2011) and other pathways (Alsayed et al. 2000; Wei et al. 2017).

IFNγ acts as an inhibitor of microbial replication as well as regulates innate and adaptive immune responses (Billiau and Matthys 2009; Wheelock 1965). It has been reported as an effector cytokine of Th1 immunity and activator of macrophages towards "M1" phenotype, which induce expression of pro-inflammatory cytokines, production of reactive nitrogen and oxygen intermediates, promotion of T-cell responses and strong inflammatory activity (Cherwinski et al. 1987; Hoeksema et al. 2015; Wang et al. 2018). In addition, IFNγ improves antigen recognition in APC by regulation of class II major histocompatibility complex (MHC) as well as stimulates production of many other cytokines and factors, which help maintain inflammation (Romieu-Mourez et al. 2007; Dutta, Spence, and Lampson 2003; Zhu et al. 2019). However, IFNγ does not only interact with immune cells. It has been described as an antiproliferating, antiangiogenic and pro-apoptotic factor in neoplastic cells (Dighe et al. 1994; Beatty and Paterson 2001). Mechanism of these events still remains unclear but multiple down-stream signaling pathways, including PI3K/AKT and NF-κB signaling, have been reported to be involved (Zhang, Banik, and Ray 2007). Therefore, it has been suggested that effect of IFNγ may depend on tumor cells context, intensity of the signal and microenvironmental niche (Castro et al. 2018). Moreover, to avoid antiproliferative and pro-apoptotic IFNγ effect, tumor cells are losing responsive to this protein by losing the receptor of IFNγ or JAK/STAT component (Kaplan et al. 1998; Dighe et al. 1994). This tumor escape may activate alternative pathways like STAT3 which induces tumor progression and leads to protumorigenic effects (Evans et al. 2007). Opposite to its antiproliferative role, IFNγ has been reported to act as a stimulator of cells growth. In the murine pro B cells with blocked Stat1 function, IFNγ replaces the IL-3 pro-proliferating role (Asao and Fu 2000). Similar effect was observed in melanoma cells, where inhibition of Stat1 leads to induction of pro-proliferative IFNγ properties, suggesting that not IFNγ but Stat1 has anti-proliferative function (Kortylewski et al. 2004). Moreover, studies on hematopoietic stem cells (HSCs) has revealed that IFNγ promotes long-term repopulating HSCs proliferation and its *in vivo* KO results in lower proliferation rate (Baldridge et al. 2010). These results were further explored and indicated that IFNγ induces expansion of more differentiated multipotent progenitors of HSCs upon mice infection with *Ehrlichia muri* (MacNamara et al. 2011). Furthermore, it has been identified as an inhibitor of TGFβ and SMAD signaling (Ulloa, Doody, and Massague 1999) which are signals that drive

differentiation in the gastrointestinal epithelium. Thus, IFNγ is a major immune response regulator but may play diverse roles in tissue homeostasis, not only by regulating the immune system but also by directly interfering with epithelial stemness and differentiation.

1.5.2 ROLE OF IFNγ IN *H. PYLORI* INFECTION

IFNγ is an important cytokine within the inflammatory response to *H. pylori* infection. First, several studies have shown that mice lacking IFNγ have higher *H. pylori* colonization than wild-type mice, which indicates its protective role (Sayi et al. 2009; Sawai et al. 1999; Smythies et al. 2000). Antimicrobial activity of IFNγ has been associated directly with CagA expression in *H. pylori* (Zhao et al. 2011). Interestingly, a recent study has demonstrated how bacteria have developed mechanisms to overcome IFNγ-mediated antimicrobial clearance. *H. pylori* is inducing C-terminal tyrosine phosphorylation SHP2, directly through CagA, which except its tumor promoting properties, is a well-known inhibitor of IFNγ/STAT1 signaling (Wang, Chen, et al. 2014). These finding were further explained by CagA-SHP2 termination of EGFR activation, which led to down-regulation of MAPK as well as JAK/STAT signaling and results in suppression of antimicrobial human β-defensin 3 (hBD3) (Bauer et al. 2012). In addition, recent studies have shown that *H. pylori* is reducing cholesterol levels in gastric epithelial cells through cholesterol-a-glucosyltransferase (Cgt), which induces a degradation of IFNγ receptors, loss of IFNγ signaling and allows bacteria to escape inflammatory responses (Morey et al. 2018).

On the other side, by correlating IFNγ levels with gastric pathologies in mice infected with *H. pylori* IFNγ has been identified as a main factor driving gastric inflammation and infection-induced pre-neoplastic lesions (Sayi et al. 2009). IFNγ influence on gastric inflammation has been associated with induction of inflammatory mediators as MIP-2, iNOS, COX2 and interaction with NOD1 (Obonyo et al. 2002; Allison et al. 2013). Moreover, mice lacking IFNγ expression are not developing hyperplasia, atrophy and metaplasia upon *H. pylori* infection (Yamamoto et al. 2004). Lack of atrophy upon infection may be explained by apoptosis of corpus parietal cells showed upon IFNγ treatment in organoid model (Osaki et al. 2019). However, described anti-proliferative

properties of IFNγ did not clarify loss of hyperplasia upon infection in IFNγ-deficient mice. Thus, IFNγ influence on gastric epithelial cells organization does not seem so straightforward. Despite its inhibitory effect on parietal cells (Merchant 2018), it has been reported that IFNγ injections induce MUC6, TFF2 and pepsinogen II expression in murine fundic glands (Kang et al. 2005). Addition of IFNγ to bronchial epithelial cells suppresses MUC5AC expression, which is the marker of pit surface mucous producing cells in the stomach (Oyanagi et al. 2017). Moreover, administration of IFNγ to mice leads to amplification of quiescence and rare gastric progenitor cells subpopulation with multiple lineage potential (Qiao et al. 2007). Therefore, it has been hypothesized that *H. pylori* is developing IFNγ resistance via Cgt and SHP2 to avoid its bacterial clearance and at the same time is inducing IFNγ-mediated gastric inflammation, but its exact influence on gastric epithelial organization remains unclear (Wang, Chen, et al. 2014).

1.6 AIM OF THE STUDY

The epithelium in the stomach is organized into gland units that consist of multiple cell types. Although the epithelium has a high proliferative activity and turnover, the abundance and localization of different cell types within glands is quite stable (Saenz and Mills 2018). The high degree of organization of the gland is based on monoclonal unity, which means that each cell within the gland derives from the stem cell compartment located in the gland base. While stem cells divide, they drive a constant flow of cells upwards towards the gland lumen. Within this process, cells obtain their differentiation phenotype and ultimately, once they reach the surface after one or two weeks, they terminally differentiate and are eventually shed into the lumen (Hata, Hayakawa, and Koike 2018). However, the mechanisms that regulate the turnover kinetics and dictate differentiation within the gland remain poorly understood. In the context of an infection of the stomach with *H. pylori*, the epithelial turnover kinetics, the distribution of cells and differentiation processes are altered (Gao et al. 2000; Murakami et al. 2013; Sigal et al. 2015; Sigal et al. 2019). Such changes are also reflected in premalignant pathological lesions that are known to be driven by infection with *H. pylori*, such as hyperplasia (increased cell number) and atrophy (loss of differentiated cells) (Correa and Piazuelo 2012). Previous studies in our laboratory have revealed that the

stem cell identity is controlled by the stem cell niche, which is composed of cells that surround the stem cell compartment. It has been shown in particular that a subpopulation of myofibroblasts that are in close proximity to the stem cells produce RSPO3 which induces WNT signaling in stem cells (Sigal et al. 2017). The aim of the presented study is to explore in detail: (1) whether and how stomach myofibroblasts control epithelial turnover and differentiation, (2) how their expression profile is altered upon infection with *H. pylori* and (3) whether such changes could be responsible for the epithelial pathologies observed upon infection.

2 Materials and methods

2.1 MATERIALS

2.1.1 MOUSE STRAINS

Table 2.1. Mouse strains used in the study.

Mouse strain	Description	Reference
C57BL/6	Standard wild type mouse	Charles River Laboratory
IfnγRKO	KO of IFN-γ receptor gene	(Huang et al. 1993)
Lgr5CreErt2/Rosa26-tdTomato	Cre recombinase expression under Lgr5 promotor, which upon activation by tamoxifen induces conditional Rosa26-tdTomato lineage tracing. Mice were generated by breeding of Lgr5–eGFP–IRES-CreErt2 to Rosa26-tdTomato mice.	Lgr5–eGFP–IRES-CreErt2 mice - (Barker et al. 2007); Rosa26tdTomato mice - (Yan et al. 2012)
Myh11CreErt2/Rosa26-mTmG	Cre recombinase expression under Myh11 promotor, which upon activation by tamoxifen induces conditional Rosa26-mTmG lineage (GFP fluorescence). Mice were generated by breeding of Myh11CreErt2 to Rosa26-mTmG mice.	Myh11CreErt2 mice - (Herring et al. 2014); Rosa26-mTmG mice - (Muzumdar et al. 2007)
Myh11CreErt2/Rosa26-tdTomato	Cre recombinase expression under Myh11 promotor, which upon activation by tamoxifen induces conditional Rosa26-tdTomato lineage (Red fluorescence). Mice were generated by breeding of Myh11CreErt2 to Rosa26-tdTomato mice.	Myh11CreErt2 mice - (Herring et al. 2014); Rosa26tdTomato mice - (Yan et al. 2012)

2.1.2 BACTERIAL STRAINS

Table 2.2. Bacterial strains used in the study.

Strain	Description	Departmental collection number	Antibiotics resistance	Reference
H. pylori pre-mouse SS1 (preMSS1, PMSS1*)*	no mutation; wildtype	P504	Vancomycin	(Arnold, Lee, et al. 2011)
H. pylori PMSS1ΔcagE	isogenic mutant lacking the CagE gene	P551	Vancomycin and Chloramphenicol	(Arnold, Lee, et al. 2011)

2.1.3 PRIMARY CELL CULTURE REAGENTS

Table 2.3. Commercially available primary cell culture reagents and supplements.

Reagent	Final concentration	Supplier	Catalog number
Advanced/DMEM F12	-	Invitrogen	12634-010
B27 (50x)	1x	Invitrogen	17504044
Bovine collagen type I	15µg/ml	Gibco	A1064401
FCS	-	Biochrom	S 0415
fibroblast growth factor (FGF)-10	100ng/ml	Peprotech	100-26
Gastrin	10nM	Sigma Aldrich	G9145
GlutaMax (100x)	1x	Invitrogen	35050-038
HBSS no calcium, no magnesium	-	Gibco	14170088
Hepes	0.01 M	Invitrogen	15630-056
Liberase TL	1U/ml	Sigma Aldrich	05401020001
Matrigel, growth factor reduced, phenol red-free	-	BD	356231
mouse Noggin	100ng/ml	Peprotech	250-38-1000
murine epidermal growth factor (mEGF)	50ng/ml	Invitrogen	PMG8043
N2 (100x)	1x	Invitrogen	17502048
Nicotinamid (NAC)	10mM	Sigma Aldrich	N0636
Penicillin/Streptomycin (Pen/Strep)	100 U/ml	Invitrogen	15140-122
Sodium hypochlorite	-	Roth	9062.3
4OH-Tamoxifen	800nM	Sigma Aldrich	H7904
TrypLE	-	Gibco	12604021
Y-27632 dihydrochloride monohydrate (ROCK-inhibitor)	7,5µM in H2O	Sigma Aldrich	Y0503

Table 2.4. Primary cell culture supplements and media produced in house.

Reagents	Preparation	Cell line
ADF++	Advanced DMEM/F12 with 0.01M Hepes and 1x GlutaMax	-
MSC	Advanced DMEM/F12 with 10% FCS	-
RSPO1 conditioned medium	DMEM + 10 % FCS; selection by zeocin treatment (300 µg/ml; Invitrogen; #250-01) for 5 days. Conditioned media was collected after 5 and 10 days, centrifuged (300 x g, 15 min) and sterile filtrated (0.22 µm filter).	293T HA-RSPO1-FC kindly provided by Prof. Hans Clevers, Hubrecht Institute, Utrecht, Netherlands
WNT3A conditioned medium	DMEM + 10 % FCS; selection by zeocin treatment (300 µg/ml; Invitrogen; #250-01) for 5 days. Conditioned media was collected after 5 and 10 days, centrifuged (300 x g, 15 min) and sterile filtrated (0.22 µm filter).	293T WNT3A cell line from ATTC CRL-2647TM

Table 2.5. Recombinant proteins added to primary cell culture.

Recombinant protein	Concentration [ng/ml]	Supplier and catalog number

BMP2	30	R&D systems, 355-BM-010
BMP4	30	R&D systems, 5020-BP-010
CHRDL1	300	R&D systems, 1808-NR-050
GREM1	500	R&D systems, 956-GR-050
GREM2	500	R&D systems, 2069-PR-050
IFNγ	100	R&D systems, 485-MI-100
Noggin	100	Peprotech, 250-38-1000

2.1.4 BUFFERS AND SOLUTIONS

Table 2.6. General buffers and solutions.

Name	Preparation	Supplier
BHI medium	Ultrapure water, 36g/l BHI	-
Blocking Buffer	3% BSA, 1% Saponin, 2% Triton X-100, 0.02% Na Azide	-
DNase/RNase Free Water	-	Gibco, Life Technologies
FACS buffer	PBS, 1% FCS, 1% HEPES, 0,5% DNase I, 3µl/ml Rock inhibitor	-
PBS: 1xDPBS without Ca, Mg	-	Gibco, Life Technologies
PFA (3,7-4%)	37-40g paraformaldehyde, 600ml ddH_2O at 60-70°C, clear solution with NaOH, 100ml 10x PBS and ddH_2O to 1l; pH 7.4	-

2.1.5 CHEMICALS AND REAGENTS

Table 2.7. General chemicals and reagents.

Name	Supplier
Bacto Brain Heart Infusion (BHI)	BD Bioscience
Bovine serum albumin (BSA), Fraction V	Life Technologies
Brucella Broth	Sigma Aldrich
Chloramphenicol	Sigma Aldrich
Columbia agar	Oxoid
Defibrinates horse blood	Oxoid
Dithiothreitol (DTT)	AppliChem
DNase I	Qiagen
EDTA	Roth
Eosin Y solution	Roth
Ethanol	Merck
LE agarose	Biozym
Mayer's hematoxylin solution	Roth
Paraformaldehyde (PFA)	Sigma Aldrich
Roti-Histokitt	Roth
Saponin	Riedel-de Haën
Tamoxifen	Sigma Aldrich
Triton X-100	Calbiochem
Vancomycin	MP Biomedicals
Vectashield	Vector
Xylene	Roth

2.1.6 COMMERCIAL KITS

Table 2.8. Commercial kits and their application.

Name	Application	Supplier	Catalog number
AB Power SYBR® Green RNA-to-CT™ 1-Step Kit	qRT-PCR	Thermo Scientific	4389986
Click-iT EdU Alexa Fluor 594 Imaging Kit	Proliferation assay for myofibroblasts culture	Thermo Scientific	C10339
GeneJET RNA Purification Kit	RNA extraction from cultured cells	Thermo Scientific	K0731
HiSeq PE Rapid Cluster Kit v2	RNAseq – cluster generation on flow-cell	Illumina	PE-402-4002
HiSeq Rapid SBS Kit v2	RNAseq – sequencing	Illumina	FC-402
Mouse GE 4x44K v2 Microarray Kit	Microarrays - cRNA fragmentation and hybrydization	Agilent Technologies	G4846A
Nextera XT DNA Library Preparation Kit	RNAseq – library preparation	Illumina	FC-131
Quick Amp Labeling Kit, two-color	Microarrays – RNA labeling	Agilent Technologies	5190-0444
RNAscope 2.5 HD Reagent Kit- RED	Single-molecule RNA *in situ* hybridization of tissue	Advanced Cell Diagnostics	322350
RNeasy Mini Kit	RNA extraction from the tissue	Qiagen	74104
RNeasy Plus Micro Kit	RNA extraction from sorted myofibroblasts	Qiagen	74034
SMART-Seq v4 Ultra Low Input RNA Kit	RNAseq – mRNA transcription and pre-amplification	Takara Clontech	6348
TaqMan Fast Virus 1-Step Master Mix	qRT-PCR	Thermo Scientific	4444432

2.1.7 ANTIBODIES

Table 2.9. Primary antibodies for immunofluorescence analysis.

Protein	Donor species	Dilution	Supplier	Catalog number
DAPI	-	1:300	Roche	10236276001
Ki67	rabbit	1:100	Cell Signaling Technology	9129S
Lectin GS-II Alexa Fluor 647 Conjugated	Griffonia simplicifolia	1:100	Thermo Scientific	L32451
MUC5AC	mouse	1:100	Thermo Scientific	MA5-12178
Phalloidin Alexa Fluor 594	-	1:100	Thermo Scientific	A12381
Vimentin	rabbit	1:100	Cell Signaling Technology	5741S
α-SMA	rabbit	1:100	Abcam	ab5694

Table 2.10. Secondary antibodies for immunofluorescence analysis.

Protein	Reactivity	Donor species	Dilution	Supplier	Catalog number

IgG (H+L) Alexa-Fluor 488	rabbit	chicken	1:100	Thermo Scientific	A21441
IgG (H+L) Alexa-Fluor 647	rabbit	chicken	1:100	Thermo Scientific	A21443

Table 2.11. Antibodies for flow cytometric analysis.

Protein	Donor species	Dilution	Supplier	Catalog number
CD326 EpCAM-APC	mouse	1:10	Milteny Biotec	130-080-234
Propidium iodide solution (PI)	-	1:400	Sigma Aldrich	P4864

2.1.8 ISH PROBES

Table 2.12. Single-molecule in situ hybridization probes.
All probes were ordered as murine probes from Advanced Cell Diagnostics company.

Gene name	Target region	Catalog number
Bmp2	854 – 2060	406661
Bmp4	586 – 1673	401301
Bmp6	1001 – 2389	488801
Bmp7	2637 – 3585	407901
Grem1	398 – 1359	314741
Grem2	231 – 826	491631
Chrdl1	406 – 1469	442811
Noggin	78 – 1774	467391

2.1.9 qRT-PCR PRIMERS

Table 2.13. Primers for reverse transcription and quantitative PCR.
Primers were designed as murine primers using BLAST online tool, obtained from Sigma Aldrich or Thermo Scientific and diluted to 10µM. The melting temperature was determined to 60°C. Abbreviations: For- forward, Rev- reverse.

Gene name	Accession number	Primer Sequence (5' – 3')	Supplier
Axin2	NM_015732.4	For: TGACTCTCCTTCCAGATCCCA Rev: TGCCCACACTAGGCTGACA	Sigma Aldrich
Bmp1	NM_009755.3	For: TGGCCATATCCAGTCTCCCA Rev: TGTCGTGACGCTCAATCTCA	Sigma Aldrich
Bmp2	NM_007553.3	For: GACTGCGGTCTCCTAAAGGTCG Rev: CTGGGGAAGCAGCAACACTA	Sigma Aldrich
Bmp4	NM_007554.3	For: CCGGAAGCTAGGTGAGTTCG Rev: GGAATGGCTCCATTGGTTCCT	Sigma Aldrich
Bmp5	NM_007555.4	For: CAGACCCTGGTACACCTGATG Rev: CACAGGCACTTCCAGCTAGT	Sigma Aldrich
Bmp6	NM_007556.3	For: TGGGATGGCAGGACTGGAT Rev: TGGCATTCATGTGTGCGTTG	Sigma Aldrich
Bmp7	NM_007557.3	For: GGCCTGCAAGAAACATGAGC Rev: AGTGAACCAGTGTCTGGACG	Sigma Aldrich
Chga	NM_007693.2	For: CAAGCACAGAGACGCAGCAG Rev: GGCTGGTTGGTGATTGGGTA	Sigma Aldrich
Chrdl1	NM_001114385.1	For: CACTGCCCCAATCGATACCC Rev: GGTTCTTCTGGGCACACCTTG	Sigma Aldrich
Gapdh	NM_001289726.1	For: TCACCATCTTCCAGGAGCG	Sigma Aldrich

		Rev: AAGCAGTTGGTGGTGCAGG	
Gapdh	NM_001289726.1	TaqMan Gapdh probe Mm99999915_g1	Thermo Scientific
Gast	NM_010257.4	For: AGGGGACACCAAGGTGATGA Rev: AGCAGATTCTGGTGTCGCAG	Sigma Aldrich
Gif	NM_008118.3	For: AAGCACAGCGCAAAAACTCC Rev: GCAACCCCTTCATCCAAAGG	Sigma Aldrich
Ifnγ	NM_008337.4	TaqMan Ifnγ probe Mm01168134_m1	Thermo Scientific
Id1	NM_010495.3	For: GCTCTACGACATGAACGGCT Rev: AACACATGCCGCCTCGG	Sigma Aldrich
Irf1	NM_008390.2	For: ATCTCGGGCATCTTTCGCTT Rev: TCTGCATCTCTAGCCAGGGT	Sigma Aldrich
Itln1	NM_010584.3	For: GTTGCTACCAGAGGTTGCAGT Rev: AGACCATCTTGTGCCTTTGTGT	Sigma Aldrich
Lgr5	NM_010195.2	For: CCTACTCGAAGACTTACCCAGT Rev: GCATTGGGGTGAATGATAGCA	Sigma Aldrich
Muc5ac	NM_010844.1	For: CCTGAGGGTATGGTGCTTGA Rev: TGTGTTGGTGCAGTCAGTAGAG	Sigma Aldrich
Muc6	NM_001330001.1	For: CAGCTCAACAAGGTGTGTGC Rev: GGTCTCCTCGTAGTTGCAGG	Sigma Aldrich
Rspo3	NM_028351.3	For: TTGACAGTTGCCCAGAAGGG Rev: CTGGCCTCACAGTGTACAATACT	Sigma Aldrich
Reg3b	NM_011036.1	For: TCCCAGGCTTATGGCTCCTA Rev: GCAGGCCAGTTCTGCATCA	Sigma Aldrich
Reg3g	NM_011260.2	For: TCTGCAAGACAGACAAGATGCT Rev: GCAACTTCACCTTGCACCTG	Sigma Aldrich

2.1.10 LABORATORY INSTRUMENTS

Table 2.14. Laboratory instruments.

Machine	**Application**	**Company**
Agilent 2100 Bioanalyzer	Quality control of RNA	Agilent
BD FACSAria II flow cytometer	Flow cytometry	BD Bioscience
DR/2000 Spectrophotometer	Measuring optical density for bacteria cultivation	HACH
Eppendorf centrifuge 5417C	Eppendorf tubes centrifugation	Eppendorf
Eppendorf centrifuge 5810R	Primary cell culture centrifugation	Eppendorf
FormaSeries II Water-Jacketed CO2 Incubators	Bacterial incubator	Thermo Scientific
G2565CA high-resolution laser microarray scanner	Microarray	Agilent Technologies
Hera cell 150 Incubator	Primary cell culture	Heraeus
HybEZ Oven	Single-molecule RNA *in situ* hybridization	Advanced Cell Diagnostics
Illumina HiSeq 1500	RNAseq	Illumina
IX50-S8F inverted microscope	Light microscopy	Olympus
Leica SP-8	Confocal microscopy	Leica
Logos One automat	Tissue paraffin embedding	Milestone

NanoDrop 1000 UV-Vis spectrophotometer	Measurments of RNA concentration	Kisker
Olympus CKX41 and U-HGLGPS Fluorescence Illumination Source	Fluorescence microscopy	Olympus
StepOnePlus Real-Time PCR System	qRT-PCR	Applied Biosystems
Vibrating blade microtome VT100 S	Tissue processing	Leica

2.1.11 SOFTWARE

Table 2.15. Software.

Name	Application	Supplier	Version
BD FACSDiva software	Flow cytometry	BD Bioscience	8.0.1
FlowJo	Flow cytometry	FlowJo, LLC	X.0.6
CellSensEntry	Image processing	Olympus	-
EndNote	Literature	Clarivate Analytics	X8.2
Excel	Calculations, data processing	Microsoft	2016
Illustrator CS4	Image processing	Adobe	14.0.0
Image Analysis and Feature Extraction G2567AA	Microarray analysis	Agilent Technologies	A.11.5.1.1
ImageJ	Image processing and quantification	Open source	1.47
Leica Application Suite X (LAS X)	Confocal imaging	Leica Microsystems GmbH	-
NCBI	Biological databases	https://www.ncbi.nlm.nih.gov/	-
Prism	Data analysis and statistic	GraphPad	8
Rosetta Resolver Biosoftware	Microarray analysis	Rosetta Biosoftware	Build 7.2.2 SP1.31
StepOne Software	qRT-PCR analysis	Life technologies	2.3
Volocity	Image processing and quantification	Improvision	6.3

2.2 MURINE CELL ACQUISITION

2.2.1 ISOLATION AND CULTURE OF GASTRIC ORGANOIDS

To obtain organoids from murine gastric tissue, mice were sacrificed by cervical dislocation and stomach was separated from the mice. Next, fore-stomach was eliminated and glandular part was opened by the cut along the lesser curvature and dissected into two parts. Corpus part was removed and antrum part with transitional zone was taken for further preparation. It was disinfected by incubation in 5ml of 0.04% sodium hypochlorite diluted in phosphate buffered saline (PBS) solution for 15 minutes

at room temperature and washed with PBS. Tissue was then incubated on a roller platform for 90 minutes at room temperature in falcon tubes wrapped with aluminum foil containing 12ml of 0.5mM dithiothreitol (DTT) and 3mM ethylenediaminetetraacetic acid (EDTA) diluted in PBS to weaken the intercellular junctions and allow the release of the glands. After incubation, tissue was washed with PBS, placed in new, cold PBS and shaken vigorously. Residual tissue was removed and supernatant with released glands was centrifuged at 300g for 5 minutes at 4°C and resuspended in 1ml of ADF++ (Advanced DMEM/F12, supplemented with Hepes and Glutamax) medium. Glands concentration was estimated by counting their number under the microscope in 10µl aliquot and approximately 100 glands per well were obtained by centrifugation at 300g for 5 minutes at 4°C. Glands pellet was resuspended in ice cold matrigel (50µl/well), seeded on 24 well plate and incubated for 10 minutes at 37°C to let the matrigel solidify. Afterwards, 500µl/well of prewarmed medium (Table 2.16.) was added to wells to support organoid growth. Murine gastric organoids were cultivated at 37 °C and 5 % CO_2 and every 2-3 days medium was replaced.

Table 2.16. Composition of gastric organoids medium.
The final concentrations of the reagents are indicated in Table 2.3.

Reagent	Volume (ul) for 1ml medium
B27	20
N2	10
NAC	2.5
Noggin	1
EGF*	1
FGF	1
Gastrin*	1
ROCK Inhibitor	3
WNT3a conditioned medium	500
R-spondin 1 conditioned medium	100
Pen/Strep	10
ADF++	350.5

*(prediluted 1:10)

For experiments with recombinant BMP2, BMP4, CHRDL1, GREM1, GREM2 and IFNγ proteins (Table 2.5.), organoids were cultivated for 2 days after seeding to grow and develop. First dose of recombinant protein was added on day 2, second on day 5 followed by microscopic imaging and RNA extraction on day 6. Factors were added

directly to the wells. For experiments with RSPO and WNT withdrawal, organoids were cultured without RSPO and with 50% WNT from the beginning of the culture. For experiments with simultaneous BMP2 and IFNγ treatment, IFNγ was added followed by BMP2 4 hours later.

For analyzing stemness capacity by organoid forming efficiency, after the treatment with recombinant proteins, organoids were passaged on day 6 and cultured further with normal medium without any addition of recombinant proteins. To passage the cells, protocol described by Schlaermann and others (Schlaermann et al. 2016) was adapted. Briefly, organoids were harvested by dissolving the matrigel with cold ADF++ (Advanced DMEM/F12, supplemented with HEPES and Glutamax). The cells were pelleted with centrifugation at 300g for 5 minutes at 4 °C. Next, the pellet was resuspended in 1ml TrypLE and incubated for 5 minutes at 37°C. A Pasteur pipet, where the opening was narrowed by melting the tip with the fire of a Bunsen burner, was used for pipetting up and down to completely dissociate organoids into single cells. Cells were then counted using a Neubauer Chamber and approximately 10 000 cells per well were obtained by centrifugation at 300g for 5 minutes at 4°C. Glands pellet was resuspended in ice cold matrigel (50µl/well), seeded on 24 well plate and incubated for 10 minutes at 37°C to let the matrigel solidify. Afterwards, 500µl/well of prewarmed medium (Table 2.16.) was added.

For experiments with Lgr5 lineage tracing in organoids, glands were isolated from *Lgr5CreErt2/Rosa26-tdTomato* (Table 2.1.) mice and treated with recombinant proteins as described above. However, simultaneously with second dose of recombinant proteins on day 5, 3µM 4OH-tamoxifen was added to the culture. Next, organoids were passaged on day 6 as described above.

To quantify experiments with organoids, their morphology, number and size were analyzed. Microscope imaging was performed with IX50-S8F inverted microscope or Olympus CKX41 and U-HGLGPS® Fluorescence Illumination Source Microscope. Numbers of organoids per well were quantified by manual counting. Diameter of organoids was measured using ImageJ1.47v software.

2.2.2 ISOLATION AND CULTURE OF MYOFIBROBLASTS

Mouse stomach separation and tissue preparation was performed as described above. Antrum with transitional zone was isolated, placed on ice in PBS and taken for further treatment based on protocol published by Stzepourginski and others (Stzepourginski et al. 2017). Tissue was incubated on the shaker for 20 minutes at 37°C with 2ml of 10mM EDTA diluted in PBS to weaken the intercellular interactions and allow the release of glands. After incubation, tissue was washed four times with PBS and each time vigorously shaken to removed epithelial cells and obtained clear supernatant. Remained tissue was cut into pieces of approximately 0.3 cm^2 size by using scalpel and incubated for 20 minutes at 37°C in a dissociation mix composed of 2ml Hank's balanced salt solution (HBSS), Liberase low-thermolysin (TL) (1U/ml) and DNase I (1U/ml). To improve dissociation, tissue pieces were gently mixed by pipetting up and down every 10 minutes with truncated pipet tip. After 20 minutes, supernatant was harvested and one volume of HBSS containing 10% fetal calf serum (FCS) was added to block enzymes digestion, while remaining tissue pieces were further processed with new dose of dissociation mix. This step was repeated three times for total time of 60 minutes. After completion of the three cycles, remaining tissue fragments were mechanically disaggregated on 70µm filter by using syringe plunger. Supernatant with cells was centrifugated at 300g for 5 minutes at 4°C, resuspended in medium (Table 2.17.) and seeded in 6 wells on 12 well plate.

Table 2.17. Composition of myofibroblasts medium.

Reagent	Volume (ul) for 1ml medium
ROCK Inhibitor	3
Pen/Strep	10
MSC	1000

Myofibroblasts were cultivated at 37 °C and 5 % CO_2 and every 2 to 3 days the medium was replaced. However, to obtain pure population of myofibroblasts, cells were cultured for 2 passages until experiments were performed. To passage the myofibroblasts, medium was removed and wells were washed with PBS. Next, cells were incubated with 1ml/well of TrypLE for 5 minutes at 37°C. After incubation, myofibroblasts were

collected, 1 volume of cold ADF++ was added to block TrypLE function and cells were centrifugated at 300g for 5 minutes at 4°C. Pellet was resuspended in medium and myofibroblasts were cultured further on 6-well plates.

For experiments with recombinant BMP2 and Noggin proteins (Table 2.5.), myofibroblasts were cultivated for 2 days after passaging to obtain stable and confluent culture. First dose of recombinant protein was added on day 2, next, cells were passaged again on day 5 and simultaneously a second dose of recombinant protein was added, finally third and last dose was added on day 7 followed by RNA extraction on the next day.

For experiments with myofibroblasts staining, 3µM 4OH-tamoxifen was added to myofibroblasts on passage 1 isolated from *Myh11CreErt2/Rosa26-mTmG* (Table 2.1.) mice. After 24 hours, cells were passaged again and seeded on collagen coated coverslip. To prepare collagen coated coverslip, 15mm round coverslips were sterilized, covered with 0,02M acetic acid and 15µg bovine collagen I, incubated for 45 minutes at 37°C and washed two times with warm PBS. Cells were seeded for 3 days until they reached 90-100% confluence, washed with PBS and fixed for 20 minutes with 4% paraformaldehyde (PFA) at room temperature. Next, myofibroblasts were washed with PBS and blocked for 20 minutes with Blocking Buffer (Table 2.6.) followed by incubation with Blocking Buffer and Vimentin (Table 2.9.) antibody overnight, in darkness at 4°C. Next day, samples were washed three times with Blocking Buffer and incubated for 1 hour with Alexa Fluor 647 secondary antibody and 4',6-diamidino-2-phenylindole (DAPI) (Table 2.9. and 2.10.) diluted in Blocking Buffer. Finally, myofibroblasts were washed and prepared for confocal microscopy with Vectashield mounting medium (Table 2.7.) and nail polish to seal the cover slip.

For proliferation assay, Click-iT EdU proliferation kit was used and assay was performed according to the manufacturer's protocol. Briefly, myofibroblasts were seeded on coverslip and incubated overnight with 10µM 5-ethynyl-2'-deoxyuridine (EdU). Next day, cells were fixed with 3,7% PFA for 15 minutes, permeabilizated with 0,5% Triton X-100 for 20 minutes and incubated with reaction cocktail provided by the company. Additional step for DNA staining with Hoechst 33342 was performed.

Myofibroblast's staining and proliferation assay was analyzed using confocal laser scanning with Leica Sp8 confocal microscope. Pictures were analyzed by using ImageJ1.47v and Volocity 6.3. Live cell imaging software. For proliferation assay, number of EdU positive cells was counted, compared to DAPI positive cells and presented as percentage.

2.2.3 FLOW CYTOMETRY OF MYH11+ CELLS

To obtain pure population of Myh11+ myofibroblasts for RNA sequencing (RNAseq) analysis, fluorescence-activated cell sorting was performed with collaboration with the FACS Core facility of the Max Planck Institute for Infection Biology (MPIIB). *Myh11CreErt2/Rosa26-mTmG* heterozygotes were intraperitoneally injected with one dose of Tamoxifen (4mg per 25g body weight, diluted in 200µl corn oil) for Cre-driven fluorophore expression in the Myh11+ cell lineage, sacrificed 2 days later and myofibroblasts population was isolated as described above. Next, cells were washed twice with PBS, centrifuged at 300g for 5 minutes at 4°C, suspended in 400µl FACS buffer (Table 2.6.) and pipetted through 40µm filter into the FACS tube. Shortly before sorting, propidium iodide (PI) antibody (Table 2.11.) was added to stained dead cells.

Flow cytometric analysis was performed using a BD FACSAria II flow cytometer and the BD FACSDiva and FlowJo vX.0.6 software. First sorting gate eliminated cell debris and dead cells that showed a lower level of forward scatter (FSC) in the FSC and SSC (side scatter) density plot. Similarly, a density plot of FSC-W (FSC-width) and FSC-H (FSC-height), as well as SSC-W and SSC-H were used to exclude cell doublets. The fourth gate was used to distinguish between dead (PI positive) and alive cells. Finally, fifth gate separated Myh11+ myofibroblasts (green fluorescence in FITC channel) from the rest of the cells. Myofibroblasts were collected into the Lysis Buffer and proceed further with RNA extraction.

For experiment with epithelial cell adhesion molecule (Epcam) sorting, *Myh11CreErt2/Rosa26-tdTomato* mice were sacrificed and myofibroblasts were isolated as described above. Next, cells were suspended in PBS with 0,5% bovine serum albumin (BSA) and 2mM EDTA at pH 7,2, CD326-epcam-APC mouse antibody was added

in dilution 1:10 and incubated 10 minutes at 4°C. After incubation, myofibroblasts were washed twice with FACS buffer (Table 2.6.), suspended in 400µl of this buffer and pipetted through 40µm filter into the FACS tube. Sorting gates were set as described previously, except fifth gate which separated Myh11+ myofibroblasts (red fluorescence caught by PE-Texas Red-A) from the Epcam+ epithelial cells (green fluorescence in APC-A channel).

2.3 *H. PYLORI* INFECTION

2.3.1 CULTIVATION OF BACTERIA

H. pylori strains were thawed from frozen stocks of the departmental collection (Table 2.2.), diluted in 3-10ml brain heart infusion (BHI) medium, spread over the blood agar plate with Vancomycin or Vancomycin/Chloramphenicol and cultivated overnight at 37 °C and 5% CO_2. After 48 hours, bacteria were collected from the plate and transferred to falcon tube by using cotton swab. Measurements of optical density (OD) 550nm was performed by using spectrophotometer. Indicated concentration of bacteria was incubated further overnight with BHI medium and 10% FCS at 37°C, 110 revolutions per minute (rpm) in humid culture flask with microaerophilic conditions.

2.3.2 *IN VIVO* INFECTION WITH *H. PYLORI*

Viability of cultivated bacteria was determined by its movement and shape followed by OD measurements of the liquid culture. Medium and bacteria were placed in falcon tubes, centrifuged and bacteria at OD_{550} was resuspended in DMEM with 5% FCS and 10% Brucella Broth. Mice were intragastrically infected with 5µl of bacteria suspension containing 10^8 *H. pylori.*

2.3.3 COLONY FORMING UNIT ANALYSIS

Serial of dilutions were performed immediately after infection to verify the bacteria input.100µl of bacterial suspension was diluted to 10^{-6}, 10^{-7} and 10^{-8} and plated on blood agar plates in 3 replicates. After 72 hours, bacterial colonies were counted and the real amount of given bacteria was estimated.

After 2 months of infection, mice were sacrificed and small piece of corpus tissue was collected in previously weighed tubes with BHI medium for colony forming unit (CFU) analysis to estimate infection efficiency. Weight of the tissue was determined and tissue was homogenized in 400µl BHI medium. Next, homogenate was diluted 1:5, 1:25 and 1:125 and plated in three replicates for each dilution on blood agar plates. Culture was cultivated at 37 °C and 5% CO_2 for 72h and the obtained bacterial colonies were counted. Dilution with the least varied numbers of colonies for each tissue was chosen and average from three replicates was calculated. The result was normalized and the number of bacteria was calculated as CFUs per gram of stomach tissue.

2.4 TISSUE PROCESSING AND MICROSCOPY

For tissue collection, the fore-stomach was removed and the glandular stomach was opened along the lesser curvature and flattened on paper. Stomach contents were removed and tissue was divided into three parts along greater curvature. To minimalize sampling error, in each experiment, right part of the stomach was used for confocal microscopy analysis, central for ISH and histopathology and the left for CFU analysis.

2.4.1 CONFOCAL MICROSCOPY

For confocal microscopy, stomach sections were placed in plastics cassettes, fixed with 4% PFA solutions for 1 hour and washed three times with PBS. Next, samples were embedded in 4% agarose as described previously by Sigal and others (Sigal et al. 2015). 300µm thick longitudinal sections were prepared with vibrating blade microtome and permeabilized in Blocking Buffer (Table 2.6.) prior to staining. The samples were then stained overnight with primary antibodies (Table 2.9.), followed by 2 hours incubation with secondary antibodies (Table 2.10.), counterstained with DAPI for nucleus visualization and with phalloidin for visualization of F actin. Confocal laser scanning was done on Leica Sp8 confocal microscope and pictures were analyzed by using ImageJ1.47v and Volocity 6.3. cell imaging software.

Quantification of fluorescent signal for TdTomato positive glands and green fluorescence protein (GFP) positive myofibroblasts in *Myh11CreErt2/Rosa26-mTmG*

mice treated with Tamoxifen was performed by automatic measuring of red and green signal in Volocity 6.3. cell imaging program and quantification of Ki67+ cells was performed by manual counting of Ki67 positive cells labelled with a Alexa488 conjugated secondary antibody per gland.

2.4.2 HISTOPATHOLOGY

Histopathology was performed with stomach sections placed in plastics cassettes, fixed with 4% PFA solutions for 24 hours at 4°C and washed 3 times with PBS. Samples were paraffin-embedded overnight in Logos One automat, cut into 5µm thick sections and stained with hematoxylin and eosin by Anja Kuehl from Charité Core Unit Immunopathology for Experimental Models. Hematoxylin and eosin staining was made by serial incubation steps. First, 2 minutes with xylene, followed by another 1 minute with xylene, 1 minute 100% ethanol, 1 minute 96% ethanol, 1 minute 96% ethanol, 1 minute 70% ethanol, 1 minute distilled water, 2 minutes with hematoxylin, 1 minute with tap water, 1 minute with 70% ethanol, 1 minute with 96% ethanol, 1 minute with eosin, 1 minute with 96% ethanol, 1 minute with 100% ethanol, 2 minutes with xylene, 1 minute with xylene and finally permanently covered with Histokitt. Pictures of the section were made with IX50-S8F inverted microscope or Olympus CKX41 and U-HGLGPS® Fluorescence Illumination Source Microscope and analyzed in ImageJ1.47v software. Gland height was measured manually in every third gland of a longitudinal section.

2.4.3 SINGLE-MOLECULE RNA *IN SITU* HYBRIDIZATION

For ISH, stomach sections were placed in plastic cassettes, fixed with 4% PFA solutions for 24 hours at 4°C and washed three times with PBS. Samples were paraffin-embedded overnight in Logos One automat and cut into 5µm thick sections by the Charité Core Unit Immunopathology for Experimental Models.

RNA *in situ* detection was performed with the RNAscope Red Detection Kit (Table 2.8.) according to the manufacturer's protocol. Slides were baked for 1 hour at 60°C and deparaffinizated with two times 5-minutes xylene incubation followed by two times 5-minutes 100% alcohol incubation. Hydrogen peroxide was applied for 10 minutes and

target retrieval was performed by incubating samples in boiled Target Retrieval Reagents for 15 minutes. Slides were washed with distilled water followed by 100% alcohol incubation. Hydrophobic barrier was created with Immedge pen around the stomach sections. Next day, Protease Plus was applied for 20 minutes at 40°C and washed with distilled water. Hybridization with respective probes (Table 2.12.) and amplification of the signal was performed in 6 steps with washing in Washing Buffer after each incubation. First, slides were incubated for 2 hours at 40°C with probes, then 30 minutes at 40°C with AMP1, 15 minutes at 40°C with AMP2, 30 minutes at 40°C with AMP3, 15 minutes at 40°C with AMP4, 45 minutes at room temperature with AMP5 and finally 15 minutes at room temperature with AMP6. Next, sections were incubated in Fast Red-A and Fast Red-B reaction mix for 10 minutes in room temperature to detect the signal, counterstained in 50% Hematoxylin solution for 2 minutes, washed with 0,02% Ammonia water, dried for 30 minutes at 60°C, briefly dehydrated with xylene and mounted in EcoMount medium. Slides were stored in -20°C.

Pictures of the section were made with IX50-S8F inverted microscope or Olympus CKX41 and U-HGLGPS® Fluorescence Illumination Source Microscope and analyzed in ImageJ1.47v software. Signal was measured automatically per picture or in the indicated glands area.

2.5 RNA TECHNIQUES

2.5.1 RNA ISOLATION

RNA from organoids and myofibroblasts was isolated with GeneJET RNA Purification Kit (Table 2.8.). Organoids from 3 wells were released from matrigel by washing with cold PBS and myofibroblasts from 2 wells were collected by trypsinization with TrypLE, blocked further with ADF++. Next, cells were centrifuged at 300g for 5 minutes at 4°C, washed with PBS and lysed in 600µl Lysis Buffer supplemented with DTT and ethanol. RNA isolation was performed as described in manufacturer's protocol. Total RNA was eluted in 40µl RNase-free water followed by concentration and purity measurements with the NanoDrop® ND-1000 Spectrophotometer for quantitative reverse transcription

polymerase chain reaction (qRT-PCR) analysis or with Agilent 2100 Bioanalyzer and NanoDrop 1000 UV-Vis spectrophotometer for microarrays. The samples were stored at -80°C until further usage.

RNA from the whole tissue was isolated with RNeasy Mini Kit (Table 2.8.). Antrum with transitional zone was separated from mice, placed in Eppendorf tube and snap frozen in liquid nitrogen. Tissue was mashed by using plastic sticks, lysed for 5 minutes in 600µl RLT buffer and homogenized with syringe by moving up and down several times until it was homogenous. RNA isolation was performed as described in manufacturer's protocol, including on-column DNase digestion and step to dry the membrane. Total RNA was eluted in 50µl RNase-free water followed by concentration and purity measurements with the NanoDrop® ND-1000 Spectrophotometer. The samples were stored at -80°C until qRT-PCR analysis.

RNA for RNAseq was isolated with RNeasy Plus Micro Kit (Table 2.8.). Myh11+ myofibroblasts were sorted directly to 400µl RLT buffer supplemented with DTT and kept on ice during sorting process. RNA isolation was performed as described in manufacturer's protocol. Total RNA was eluted in 17µl RNase-free water followed by concentration and purity measurements with Agilent 2100 Bioanalyzer. The samples were stored at -80°C until RNAseq library preparation.

2.5.2 QUANTITATIVE RT-PCR

qRT-PCR was performed with Power SYBR Green RNA-to-Ct 1-Step Kit containing master mix with nucleic acid dye SYBR Green, Taq DNA-Polymerase and dNTPs as well as reverse transcription (RT) enzyme mix with the reverse transcriptase and RNase inhibitors. Apart from kit components, primers and DNase/RNase Free Water was added. Primers used for qRT-PCR analysis (Table 2.13.) were validated by serial dilutions of RNA-template, which was plotted against the threshold cycle (C_t) to create a standard curve.

The qRT-PCR reaction mixture (Table 2.18.) was prepared without RNA and 15µl/well was pipetted into a 96-well plate.

Table 2.18. qRT-PCR reaction mixture.

Component	per 1 well
SYBR® green master mix	10 µL
Primer mix (for+rev primer)	0.5 µL
H_2O	4.3 µL
RT enzyme mix	0.2 µL

10µl/well of RNA diluted to 5ng/µl was added to the wells with reaction mixture, resulting in a total volume of 25µl per well. The plate was covered with a film and put into the StepOnePlus Real-Time PCR System in which the two steps of reverse transcription and quantitative PCR proceeded using the program suggested by manufacturer (Table 2.19.).

Table 2.19. Power SYBR Green RNA-to-Ct 1-Step qRT-PCR program.

Stage	Step	Time	Temp.
Holding	reverse transcription	30 min	48°C
Holding	inactivation of RT and activation of Taq polymerase	10 min	95°C
Cycling	melting of double strands	15 sec	95°C
(40 cycles)	primer annealing and elongation	1 min	60°C
Melting curve	denaturation	15 sec	95°C
	annealing	15 sec	60°C
	denaturation	15 sec	95°C

For each primer pair and RNA-sample the reaction was done in technical duplicate or triplicate. The amplification plots obtained from the qRT-PCR were analyzed with the Step One Software v2.1. The expression levels were relatively quantified calculating ΔC_t as well as $2^{-\Delta\Delta Ct}$ with glyceraldehyde-3-phosphate dehydrogenase (Gapdh) as an endogenous reference.

qRT-PCR for Ifnγ was performed by Stefanie Muellerke from the MPIIB Department of Molecular Biology with TaqMan Fast Virus 1-Step Master Mix. Briefly, reaction mixture was prepared with 5µl/well TaqMan master mix, 1µl/well TaqMan probe and 14µl/well of RNA diluted to 5ng/µl and run with the program suggested by manufacturer (Table 2.20.).

Table 2.20. TaqMan Fast Virus 1-Step Master Mix qRT-PCR program for Fast real-time PCR systems.

Step	Cycles	Time	Temp.
reverse transcription	1	5 min	50°C
RT inactivation/initial denaturation	1	20 sec	95°C
Amplification	40	3 sec	95°C
		30 sec	60°C

Relative quantification of gene expression was analyzed by me with the Step One Software v2.1 using TaqMan Gapdh probe as an endogenous reference.

2.5.3 MICROARRAY ANALYSIS

Microarray experiments were performed by Hans Mollenkopf from the MPIIB Microarray Core Facility as independent dual-color dye hybridizations using two biological replicates. RNA labeling was performed with the dual-color Quick-Amp Labeling Kit (Table 2.8.). In brief, mRNA was reverse transcribed and amplified using an oligo-dT-T7 promoter primer, and resulting cRNA was labeled with cyanine 3-CTP or cyanine 5-CTP. After precipitation, purification, and quantification, 1.25µg of each labeled cRNA was fragmented and hybridized to Agilent Technologies whole genome mouse 4 × 44k multipack microarrays (Table 2.8.) according to the supplier's protocol. Scanning of microarrays was performed with 5µm resolution using a G2565CA high-resolution Agilent Technologies laser microarray scanner with extended dynamic range (XDR). Microarray image data were analyzed with the Agilent Technologies Image Analysis/Feature Extraction software G2567AA v. A.11.5.1.1 using default settings and the GE2_1105_Oct12 extraction protocol. The extracted MAGE-ML files were analyzed further with the Rosetta Resolver Biosoftware Build 7.2.2 SP1.31. Ratio profiles comprising single hybridizations were combined in an error-weighted fashion to create ratio experiments. A 1.5-fold change expression cut-off for ratio experiments was applied together with anti-correlation of dye-swapped ratio profiles, rendering the microarray analysis highly significant ($P < 0.01$), robust, and reproducible (Churchill 2002). Microarray data was also analyzed using R (R Core R Core Team 2014) version v3.4 and package limma (Ritchie et al. Ritchie et al. 2015) for further analysis. Gene Set Enrichment Analysis (GSEA) was performed on genes pre-ranked by gene expression-

based t-score between PMSS1 infected and uninfected mice and between IFNγ-treated and untreated organoids using the fgsea R package (Sergushichev 2016) with 5,000 permutations. Gene sets from MSigDB v6.2 (Liberzon et al. 2011; Subramanian et al. 2005) were used. P-values were adjusted for multiple testing by a global false discovery rate (FDR) according to the method described by Benjamini and Hochberg (Benjamini and Hochberg 1995).

2.5.4 RNA SEQUENCING

For gene expression analysis of sorted cells, RNAseq libraries were generated together with Jeroen Maertzdorf from the MPIIB Department of Immunology. Messenger RNA (mRNA) was reverse transcribed and pre-amplified using the SMART-Seq v4 ultra low input RNA kit, followed by library generation using a Nextera XT DNA library prep kit (Table 2.8.). Sequencing of the libraries was done on an Illumina HiSeq 1500 machine by Jeroen Maertzdorf and Hans Mollenkopf and data was analyzed by Hilmar Berger from the MPIIB Department of Molecular Biology.

Briefly, first-strand cDNA synthesis from total RNA was primed by the 3’ SMART-Seq CDS Primer II A and template was switched at the 5’ end of the transcript with the SMART-Seq v4Oligonucleotide. cDNA from the SMART sequences introduced by 3’ SMART-Seq CDS Primer II A and the SMART-Seq v4 Oligonucleotide was amplified by PCR Primer II A in 12 cycles. PCR-amplified cDNA was purified by immobilization on AMPure XP beads. The beads were then washed with 80% ethanol and cDNA was eluted with 17µl Elution Buffer. Next, 800pg cDNA was used as input material for library generation and tagmented by the Nextera XT transposome, which fragmented the input DNA and simultaneously added sequences for sequencing primers to the ends of template DNA. Next, adapters were attached to the tagmented DNA fragments for library amplification via a limited-cycle PCR program. These sequencing adapters were required for cluster formation on the flow-cell and also contained the index 1 (i7) and index 2 (i5) sequences for assigning sequence reads to samples during data conversion. Finally, AMPure XP beads were used to purify the library DNA and equimolar amounts of sample libraries were pooled. The pooled libraries were size-selected (200-1500 bp) on a Pippin Prep

platform to remove unbound sequence adapters and create a pool of defined sequence lengths.

Sample loading and cluster generation on the flow-cell was done with the HiSeq PE Rapid Cluster Kit v2. Sequencing was run in paired-end (2x50bp) rapid mode with the HiSeq Rapid SBS Kit v2 on an Illumina HiSeq 1500 machine. Following bcl-to-fastq conversion of the imaging data, sequenced data were further analyzed in our bioinformatics pipeline. STAR v2.4 (Dobin et al. 2013) was used to align sequences against mouse genome version GRCm38 and htseq-count (Anders, Pyl, and Huber 2015) was used to obtain read counts per gene using gene models from Ensembl (www.ensmbl.org) GRCm38 v76. Gene expression was analyzed using package DESeq2 (Love, Huber, and Anders 2014) and heatmaps were generated in R.

3 Results

3.1 MYH11+ MYOFIBROBLASTS RESPOND TO *H. PYLORI* INFECTION

3.1.1 MOUSE MODEL

Epithelial stem cells drive constant regeneration of stomach epithelium and thereby play a crucial role in gland organization and turnover (Barker et al. 2007; Matsuo et al. 2017). Our previous studies have shown that myofibroblasts surrounding epithelial cells express and secrete RSPO3, which appeared to be relevant factor in context of epithelial stem cell proliferation (Sigal et al. 2017). Thus, further investigation of stem cell microenvironment is important to obtain a more complete view on the impact of niche cells for epithelial gland homeostasis. For this purpose, a mouse model enabling visualization of the niche myofibroblasts for their further characterization was developed. *Myh11CreErt2* mice (Herring et al. 2014) with CreErt2 recombinase expression under smooth muscle myosin promotor (Myh11) were bred to *Rosa26-mTmG* reporter mice (Muzumdar et al. 2007) with membrane activated expression of TdTomato (mT) and membrane inactivated, by loxP-flanked genes, expression of green fluorescence protein (mG). As a consequence, *Myh11CreErt2/Rosa26-mTmG* mice were generated and in myofibroblasts, which expressed CreErt2 enzyme under the Myh11 promotor, addition of Tamoxifen enabled excision of loxP-flanked sites, which induced conditional expression of GFP specifically in Myh11 lineage (Figure 3.1.a).

Myh11CreErt2/Rosa26-mTmG mice were treated with 4mg Tamoxifen per 25g mouse body weight to induce Cre-driven recombination, sacrificed 7 days later and tissue was isolated for further analysis. A protocol enabling confocal microscopy of tissues without loss of their fluorescence was developed and consisted of three steps: 1h fixation in 4% PFA, immobilization in 4% agarose and vibratome sectioning. Confocal microscopy identified GFP+ cells both beneath and between the glands, in direct proximity to epithelial cells, whereas the gland epithelium appeared free of GFP. Moreover, staining with α-smooth muscle actin (SMA) antibody showed co-localization with GFP fluorescence (Figure 3.1.b), indicating that GFP signal in our mice is specific to myofibroblasts. Thus, *Myh11CreErt2/Rosa26-mTmG* mouse model was suitable to investigate the regulation of epithelial stem cells by the microenvironment focusing on a defined myofibroblasts population.

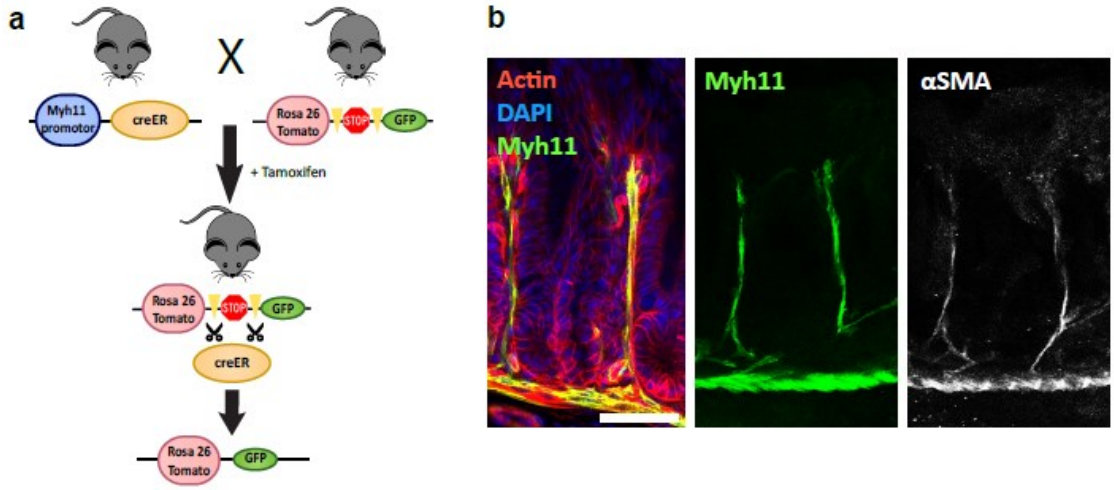

Figure 3.1. *Myh11CreErt2/Rosa26-mTmG* mice model visualizing myofibroblasts
Schematic representation of *Myh11CreErt2/Rosa26-mTmG* mouse (a) and confocal microscopy of stomach antrum from mice sacrificed 7 days after Tamoxifen treatment (b). Images show localization of GFP signal in Myh11+ myofibroblasts beneath and between the epithelial cells and co-localization of GFP signal with αSMA staining. Images are representative of 3 biological replicates. Scale bar 100µm.

Further validation of Myh11+ myofibroblasts was done to confirm that Myh11 gene is only expressed in these cells and not in epithelial cells. For this particular experiment, *Myh11CreErt2/Rosa26-tdTomato* mice with TdTomato expression inactivated by loxP-flanked genes were used. Tamoxifen treatment 7 days before sacrificing excised loxP-flanked sites and induced TdTomato fluorescence in cells with Myh11 promoter. The whole antrum tissue was isolated, dissociated to single cells by incubations with Liberase enzymes, stained with EPCAM antibody, which is a specific marker for epithelial cells, and taken for FACS sorting. Flow cytometric gating eliminated cell debris and dead cells (Figure 3.2.a) and distinguished between dead, PI positive and alive, PI negative cells (Figure 3.2.b). Finally, last gate separated Myh11+ myofibroblasts with red fluorescence in PE-Texas Red-A channel and EPCAM+ epithelial cells with green fluorescence in APC-A channel (Figure 3.2.c). FACS plots clearly showed a separation between TdTomato+ cells and EPCAM stained cells, and almost none of Myh11+ myofibroblasts were present in EPCAM+ gate. This confirmed that TdTomato indeed specifically labelled non-epithelial cells.

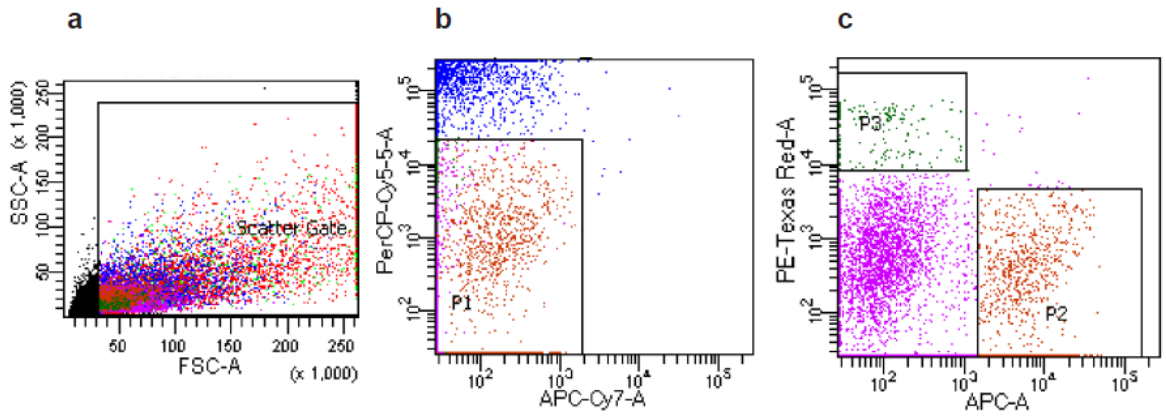

Figure 3.2. Flow cytometric analysis of Myh11+ and EPCAM+ cells
Flow cytometric analysis of *Myh11CreErt2/Rosa26-tdTomato* antrum tissue showing gates set up for cell morphology by SCC-A and FSC-A (a) and living cells stained with PI (b). Last sorting gate distinguished Myh11+ myofibroblasts in PE-Texas Red-A channel from EPCAM+ epithelial cells in APC-A channel (c). Results are representative of 3 biological replicates.

3.1.2 *H. PYLORI* INFECTION

As described before, epithelial stem cells constantly repopulate gastric glands and therefore maintain homeostatic turnover. However, environmental changes such as infections can promote structural alterations in the glands resulting in pathological lesions such as gland hyperplasia, atrophy or metaplasia (Sigal et al. 2015). To get a comprehensive view on how the microenvironment changes upon infection and whether this drives gland alterations, *Myh11CreErt2/Rosa26-mTmG* mice were used to study how infection with the gastric pathogen *H. pylori* affects the cells which surround the epithelium. Three *Myh11CreErt2/Rosa26-mTmG* mice were infected for two months with WT PMSS1 *H. pylori* and three mice from the same strain were used as an uninfected control. Mice were treated with Tamoxifen, sacrificed 7 days later and antral tissue together with transitional zone (zone between antrum and corpus) were processed. Focus was put on this part of the stomach because *H. pylori* gland colonization and infection-driven expansion of stem cells was previously described in this location (Sigal et al. 2015). Experiment confirmed that infection induces gland hyperplasia in antrum and transitional zone, which is consistent with phenotype observed by Sigal and others (Sigal et al. 2015). Next, Myh11+ cell lineage that expresses GFP in the model were visualized and showed that the increased gland height upon infection was accompanied by an expansion of Myh11+ myofibroblasts that surround

the gland (Figure 3.3.a). Quantification was done using Volocity software by measuring red signal area per picture to determinate gland expansion and green signal area per picture to determinate Myh11+ signal in uninfected and infected tissues (Figure 3.3.b). Obtained results showed significant increase in TdTomato+ cells due to hyperplasia as well as increase of GFP+ Myh11+ myofibroblasts area upon infection with *H. pylori*.

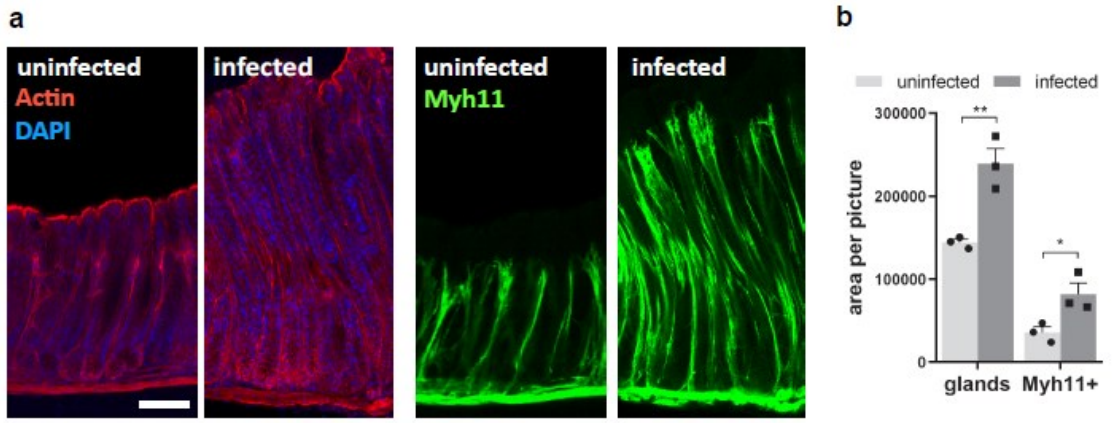

Figure 3.3. Confocal microscopy of *H. pylori* infected *Myh11CreErt2/Rosa26-mTmG* mice 2 months post infection (p.i.).
Representative images of confocal microscopy showing gland hyperplasia with red fluorescence for actin or green fluorescence for Myh11+ myofibroblasts expansion (a) and quantification of red or green signal area per picture (b) in uninfected and *H. pylori* infected *Myh11CreErt2/Rosa26-mTmG* mice 2 months p.i. Images are representative of 3 biological replicates. Scale bar 100µm. Data are presented as mean ± standard error of the mean (SEM) from 3 biological replicates, analyzed by Student's t-test.

The fact that myofibroblasts respond to *H. pylori* infection led to the hypothesis that not only the number of these cells changed, but also the gene expression pattern. Therefore, another three *Myh11CreErt2/Rosa26-mTmG* mice were infected for two months with WT PMSS1 *H. pylori* and again three mice from the same strain were used as an uninfected control. Mice were treated with Tamoxifen and sacrificed 7 days later. Infection efficiency was confirmed by cultivating the homogenized part of the infected stomach on blood agar plates, counting *H. pylori* colonies and performing CFU calculations, which showed 5-7 log10 colonization (Figure 3.4.a). Myofibroblasts were isolated from the antrum and transitional zone and taken for FACS sorting to exclude debris, dead cells and receive pure Myh11+ myofibroblasts population as described above, which was taken further for RNA extraction, library preparation and RNA sequencing. Analysis was done by Hilmar Berger from the MPIIB Department of Molecular Biology using STAR v2.4 to align sequences against mouse genome (Dobin et

al. 2013) and htseq-count to obtain read counts per gene using gene models from Ensembl GRCm38 v76 (Anders, Pyl, and Huber 2015). Gene expression was analyzed using package DESeq2 (Love, Huber, and Anders 2014) and heatmaps were generated in R version3.4 (R Core Team 2014R Core Team 2014). Data analysis from uninfected control mice revealed that myofibroblasts express a variety of genes that encode for factors involved in regulation of epithelial stem cells through signals such as Wnt, Rspo as well as Bmp, and that myofibroblasts express both activators and inhibitors of these pathways (Figure 3.4.b). Upon infection with *H. pylori*, 104 genes were significantly upregulated, while 93 genes showed down-regulation compared to uninfected myofibroblasts (Figure 3.4.b), indicating that these cells actively respond to *H. pylori* infection. Interestingly, multiple of these genes were from the Bmp signaling pathway. Further analysis revealed significant increase in expression of Bmp inhibitors, such as Crim1 and Chrdl1 and the same trend for Grem1 and Bambi in myofibroblasts upon infection. Moreover, changes in Bmp ligands were observed: significant down-regulation of Bmp2, Bmp6 and Bmp7, as well as a shift towards reduction for Bmp1, Bmp3, Bmp4, Bmp5 and Bmp pathway target genes Id1 and Id2 (Figure 3.4.c). Next, to validate these results obtained by RNAseq, qRT-PCR for significantly changed genes with the same RNA as used for sequencing was performed. Down-regulation in Bmp1, Bmp2, Bmp4, Bmp5, Bmp6 and Bmp7, as well as up-regulation in Chrdl1 expression was confirmed (Figure 3.4.d). However, results were significant only for Bmp2, Bmp6, Bmp7 and Chrdl1, but not for Bmp1, Bmp4 and Bmp5. Thus, *H. pylori* infection induced overall an increased expression of Bmp inhibitors and decreased expression of several Bmp ligands in myofibroblasts.

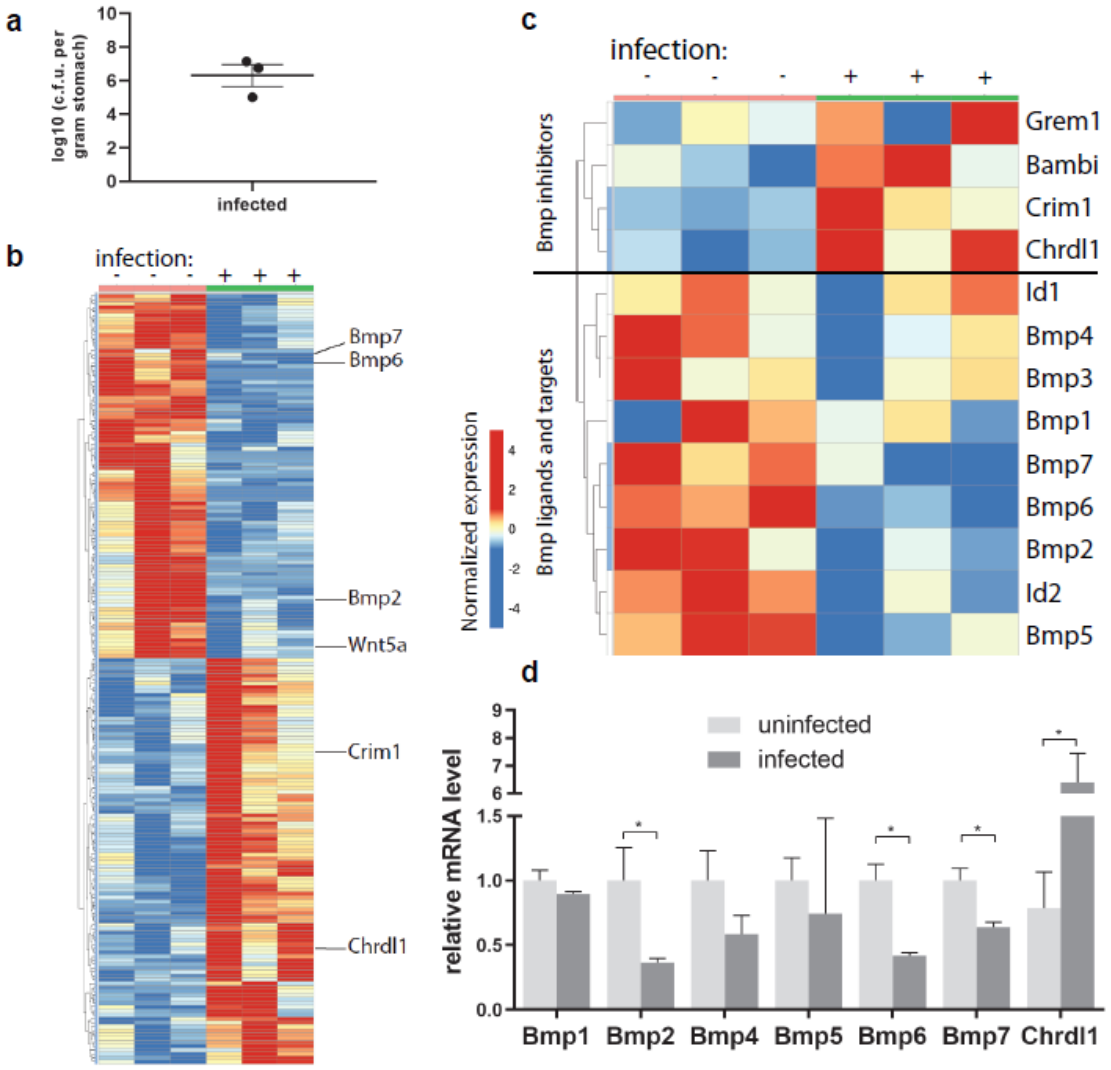

Figure 3.4. RNAseq and qRT-PCR validation of Myh11+ myofibroblasts from 2 months *H. pylori* infected mice.

Number of colony forming units for *H.pylori* infected Myh11CreErt2/Rosa26-mTmG cells 2 months p.i.(a). Heatmap of RNAseq data with genes differentially expressed in uninfected and *H.pylori* infected Myh11+ myofibroblasts 2 months p.i. (b) and highlight of differentially expressed genes involved in Bmp signaling (c). qRT-PCR validation of RNAseq data for Bmp-involved genes with the same RNA as used for sequencing (d). RNAseq data are from 3 biological replicates per group. qRT-PCR data are presented as mean ±SEM from three biological replicates per group, analyzed by Student's t-test.

3.2 BMP SIGNALING IS SPATIALLY ORGANIZED IN THE STOMACH

3.2.1 BMP LIGANDS DISTRIBUTION

Since Bmp signaling showed multiple alterations in infected myofibroblasts, in the next step this pathway in the stomach was further investigated. Because both activators and inhibitors were expressed in myofibroblasts, the question how they are spatially distributed *in situ* appeared. Bmp ligand distribution in uninfected antrum tissue was

examined by performing ISH for Bmp2, Bmp6 and Bmp7, which were significantly decreased, and for Bmp4, which showed reduction trend in infected myofibroblasts. Bmp2 showed the highest expression and was present in both epithelial and stromal cells. Moreover, expression was predominant in the surface of the gland and gradually decreased towards the base. The base itself was free of Bmp2 (Figure 3.5.a). Other Bmp ligands were expressed at lower levels, Bmp4 expression was restricted to the stroma and equally distributed along the gland axis (Figure 3.5.b), whereas expression of Bmp6 and Bmp7 was much lower (Figure 3.5.c) and therefore it was not further examined. To quantify the distribution along the gland axis, tissue was divided into the surface and bottom part and signal for Bmp2 and Bmp4 was quantified using ImageJ1.47v software. In the top of the gland, average Bmp2 expression was 15 times higher than in the bottom and there was no Bmp2 signal within the stem cell compartment (Figure 3.5.d). Quantification of Bmp4 ligand confirmed our observations showing no significant changes in the expression between the top and the bottom of the gland (Figure 3.5.e). In summary, Bmp2 expression was dominant in the surface of the gland, whereas Bmp4 is equally distributed along gland.

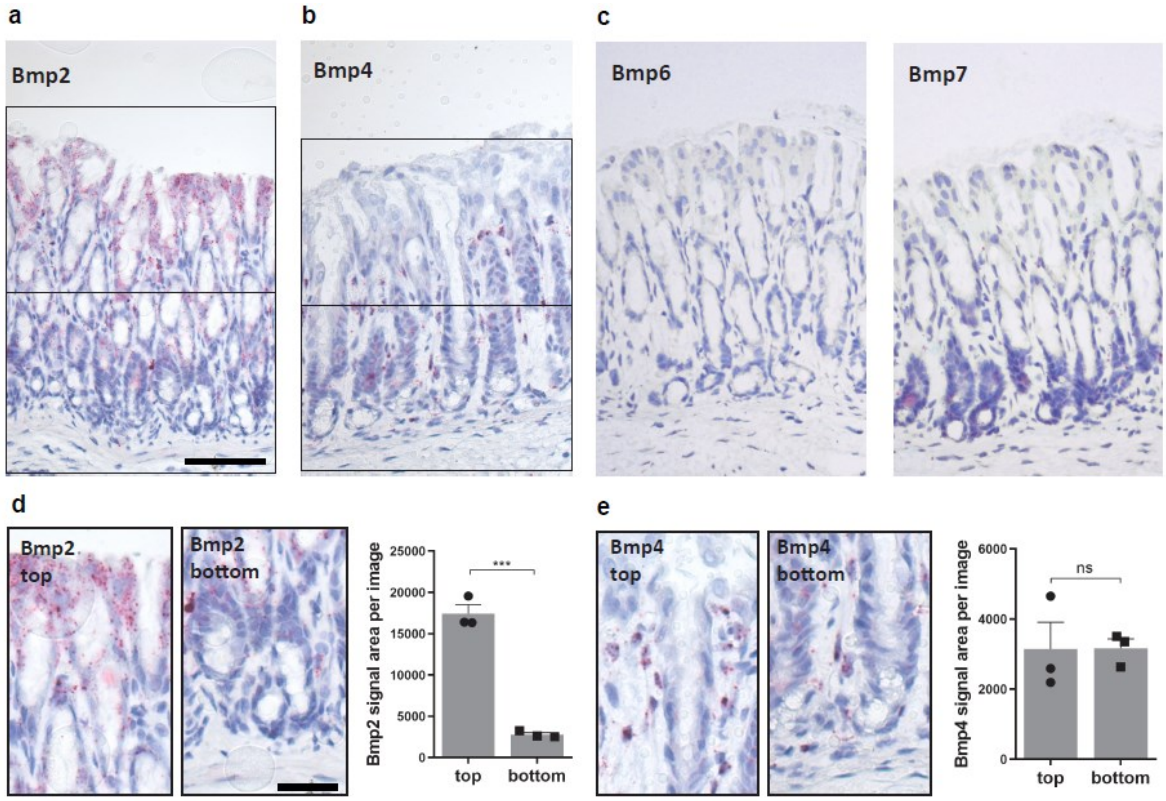

Figure 3.5. ISH for Bmp ligands in antrum tissue.

Light microscope pictures of ISH for Bmp2 (a), Bmp4 (b), Bmp6 and Bmp7 (c). High magnification and quantification divided for top and bottom of the gland for Bmp2 (d) showing Bmp2 dominant expression in the surface of the gland and for Bmp4 (e) showing equal distribution along gland height. Images are representative of at least 3 biological replicates. Scale bar 100µm. Data are presented as mean ±SEM from 3 biological replicates, analyzed by Student's t-test.

3.2.2 BMP INHIBITORS DISTRIBUTION

RNAseq of infected myofibroblasts showed not only alterations in Bmp ligand expression but also up-regulation of Bmp inhibitors. Therefore, Bmp inhibitors distribution in uninfected antrum tissue was also examined by performing ISH. Inhibitors changed in RNAseq like Chrdl1 and Grem1 were chosen for the assay as well as Noggin, which is described as a main Bmp inhibitor in the intestine (He et al. 2004) and Grem2 by its similarity to Grem1. ISH showed high expression of Grem1, Grem2 and Chrdl1 in the stroma located beneath the glands (Figure 3.6.a), so in the close proximity to the epithelial stem cell compartment. Surprisingly, Noggin, which is commonly present in the intestine was not detected in the mouse stomach (Figure 3.6.b). Next, these observations were quantified using ImageJ1.47v software. However, since Bmp inhibitors expression was strongly limited to the base, this time the tissue was divided into the base and rest of the gland to quantify the distribution along the gland axis, as indicated on Figure 3.6.a. Quantification analysis of ISH showed that Grem1 and Grem2 and especially Chrdl1 expression was limited to the base (Figure 3.6.c). Together, these data depict the highly organized distribution of Bmp signaling molecules in gastric glands, with strong expression of Bmp2 in the surface region and absence of Bmp2 as well as expression of Bmp inhibitors in the base.

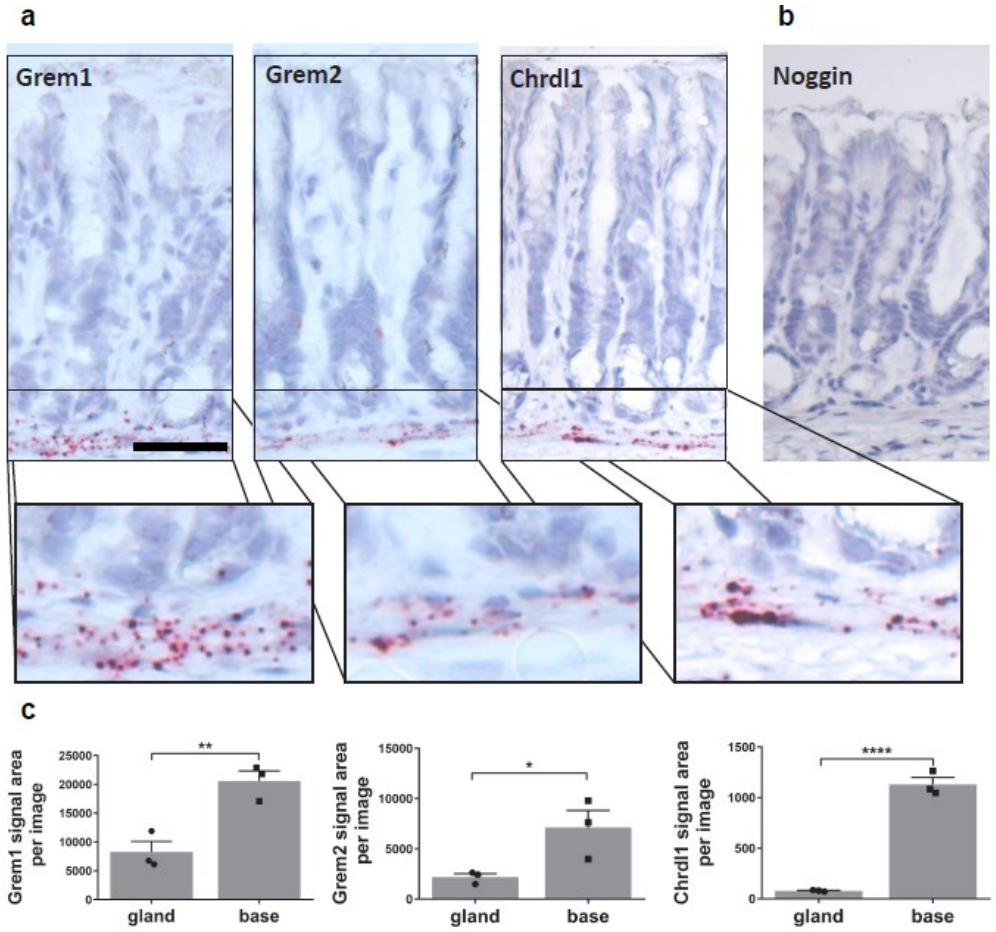

Figure 3.6. ISH for Bmp inhibitors in antrum tissue.
Light microscope pictures and high magnifications of ISH for Grem1, Grem2, Chrdl1 (a) and Noggin (b). ISH quantification divided for base and rest of the gland for Grem1, Grem2 and Chrdl1 (c) showing inhibitors distribution limited to the base. Images are representative of at least 3 biological replicates. Scale bar 100µm. Data are presented as mean ±SEM from 3 biological replicates, analyzed by Student's t-test.

3.3 *H. PYLORI* INFECTION ALTERS BMP SIGNALING

3.3.1 BMP LIGANDS UPON INFECTION

To further characterize Bmp signaling and its changes upon *H. pylori* infection, Bmp ligand distribution was investigated in infected samples by ISH. Three C57BL/6 mice were infected for 2 months with WT PMSS1 *H. pylori* and three uninfected C57BL/6 mice served as controls. Stomach was separated, processed further, ISH for Bmp2 and Bmp4 was performed and investigated in the antral part of the stomach. ISH revealed strong decrease in Bmp2 expression in the gland surface including both stroma and epithelial cells, which confirmed the results of the RNAseq. Despite the increase of gland height, Bmp4 expression remained at a similar level (Figure 3.7.a) in infected samples compared to uninfected. To confirm those observations, signal area was quantified per picture

using ImageJ1.47v software, which revealed almost seven times lower expression of Bmp2 in the infected samples compared to uninfected and no significant changes for Bmp4 expression were detected (Figure 3.7.b). Thus, *H. pylori* infection down-regulated Bmp2 in the top of the gland and did not affect Bmp4 distribution.

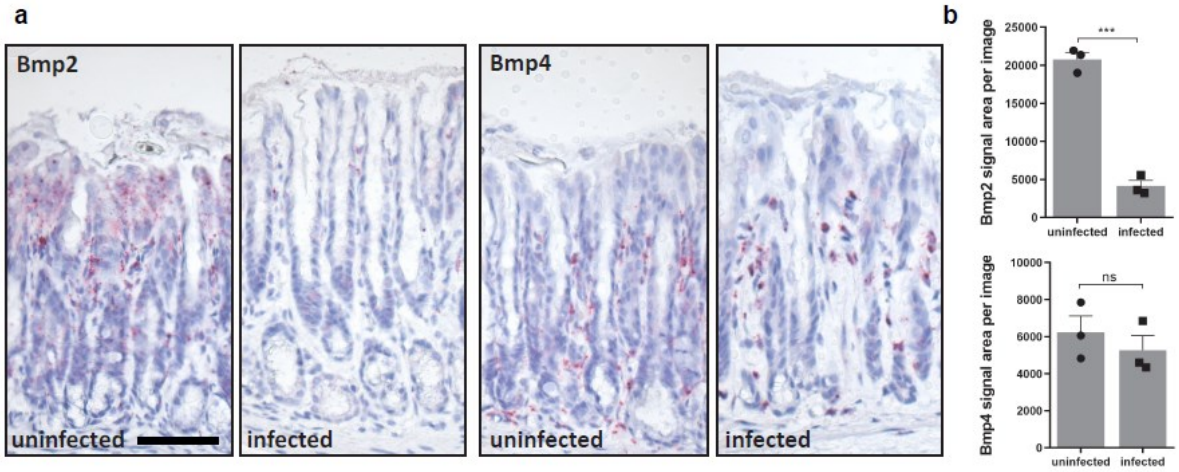

Figure 3.7. ISH for Bmp ligands in 2 months *H. pylori* infected antrum.
Light microscope pictures of ISH for Bmp2 and Bmp4 in antrum tissue from 2 months *H. pylori* infected C57BL/6 mice (a). ISH quantification of signal area per picture for Bmp2 showing Bmp2 decrease upon infection and for Bmp4 showing no significant changes (b). Images are representative of at least 3 biological replicates. Scale bar 100µm. Data are presented as mean ±SEM from 3 biological replicates, analyzed by Student's t-test.

3.3.2 BMP INHIBITORS UPON INFECTION

In the next step, changes in Bmp inhibitors distribution upon *H. pylori* infection were investigated by ISH with the same 2 months infected and uninfected tissues, which were used for Bmp ligands examination. Microscope pictures visualized an increased expression of Chrdl1 as well as Grem2 in infected samples, which was quantified and confirmed the observation. Surprisingly, Grem1 did not show a significant increase upon infection when quantified in the antrum (Figure 3.8.a-b). However, focus specifically on the transitional zone between antrum and corpus showed significant increase of Grem1 and Grem2 upon infection in this area (Figure 3.8.c-d). This area is highly colonized by gland-associated *H. pylori* (Van Zanten, Dixon, and Lee 1999) and gland hyperplasia as well as antral metaplasia is often observed in this part of the stomach. Taken together, *H. pylori* infection affects the spatial distribution of Bmp signaling molecules, it down-regulates Bmp2 in the top of the gland and up-regulates Bmp inhibitors located in the gland base.

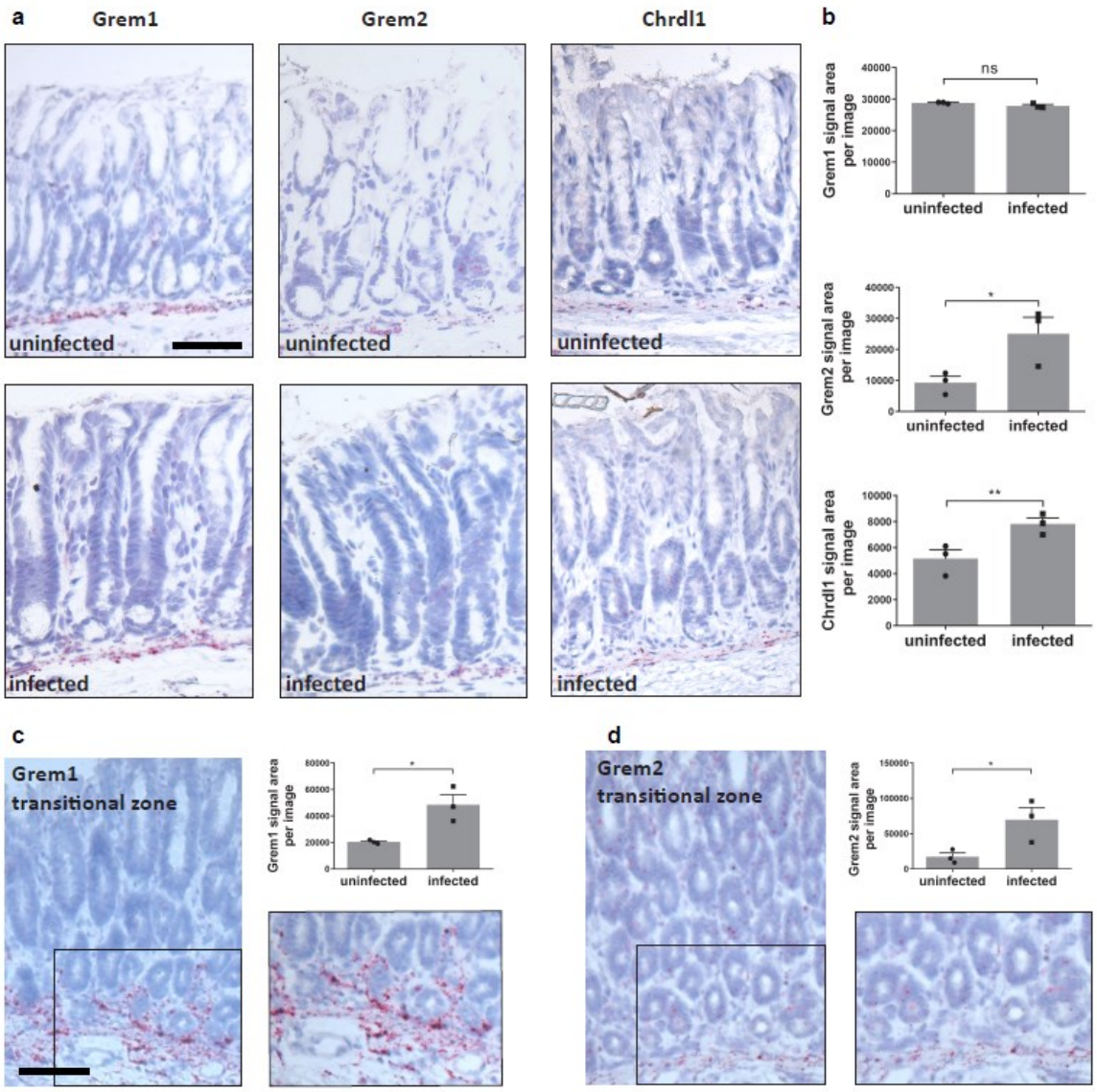

Figure 3.8. ISH for Bmp inhibitors in 2 months *H. pylori* infected antrum and transitional zone.
Light microscope images of ISH for Grem1, Grem2 and Chrdl1 in antrum tissue from 2-months *H. pylori* infected C57BL/6 mice and uninfected controls (a) and ISH quantification of signal area per picture for Bmp inhibitors showing significant increase for Grem2 and Chrdl1 upon infection (b). Light microscopy pictures and quantification of ISH for Grem1 (c) and Grem2 (d) 2 months *H. pylori* infected transitional zone showing significant increase. Images are representative of at least 3 biological replicates. Scale bar 100µm. For quantification 10 images per mouse were analyzed and the average value per image was calculated. Data are presented as mean ±SEM from 3 biological replicates, analyzed by Student's t-test.

3.4 BMP PROMOTES SURFACE AND INHIBITS BASAL PHENOTYPE

3.4.1 DIFFERENTIATION MARKERS

While the data presented in the previous sections described Bmp distribution and changes upon *H. pylori* infection, the function of BMP signaling in the stomach remained not clear. The cellular distribution with gastric antral glands appears highly

compartmentalized so the question whether this could be driven by the discovered spatial restriction of Bmp signaling appeared. Antrum gland contains various cells such as subpopulations of Lgr5+ cells in the base that are either proliferative stem cells or secretory cells expressing markers such as Muc6+ and Gif+ (Sigal et al. 2019), the highly proliferative Axin2+ stem cells in the lower isthmus and Muc5ac+ mucous pit cells in the surface region (Figure 3.9.a). Examining the influence of BMP signaling on cellular differentiation in the stomach required a cell culture model that represented all gastric cell types. Therefore, three-dimensional (3D) organoids model, which enables *in vitro* differentiation of epithelial cells by selection of medium factors was used. Once organoids were established in full medium, they were exposed to recombinant BMP2 or BMP4 and a rapid growth inhibition compared to controls kept without BMPs was observed (Figure 3.9.b). As described above, the stem cell compartment in the antrum is exposed to Bmp inhibitors that are robustly expressed in the stroma underlying the gland base. Therefore, the function of these factors was also investigated and indeed, addition of BMP inhibitors such as CHRDL1, GREM1 and GREM2 to the culture with BMP ligands was sufficient to block the effect of BMPs resulting in organoids that were phenotypically similar to the ones cultured in normal medium (Figure 3.9.b). Next, qRT-PCR for differentiated genes in organoids treated with BMP2 and BMP4 was performed to examine cell differentiation state. Strong increase in expression of BMP target gene Id1 upon treatment with BMP was observed, confirming that addition of recombinant BMP indeed efficiently induced the BMP pathway. Next, genes, which are known to be specific for cellular populations in the gland were selected. A strong down-regulation of the stem cell marker Lgr5 as well as secretory gland base cell marker Muc6 upon BMP treatment was observed, whereas the surface pit cell marker Muc5ac was strongly and significantly up-regulated. Expression of isthmus stem cell gene Axin2 and enteroendocrine cell markers such as Gast and Chga remained unchanged. BMP2 and BMP4 had a similar effect on the expression of the selected genes, although changes in expression were slightly stronger for BMP2 (Figure 3.9.c). To ask how BMP inhibitors affect differentiation, Qrt-PCR for the same markers with RNA from organoids treated with BMP4 together with Bmp inhibitors was run and confirmed that each of them was sufficient to block the BMP-driven differentiation (Figure 3.9.d). Thus, the conducted

experiments demonstrated that BMP promotes differentiation into gland surface cells and inhibits gland base cell identity, which can be maintained by BMP inhibitors.

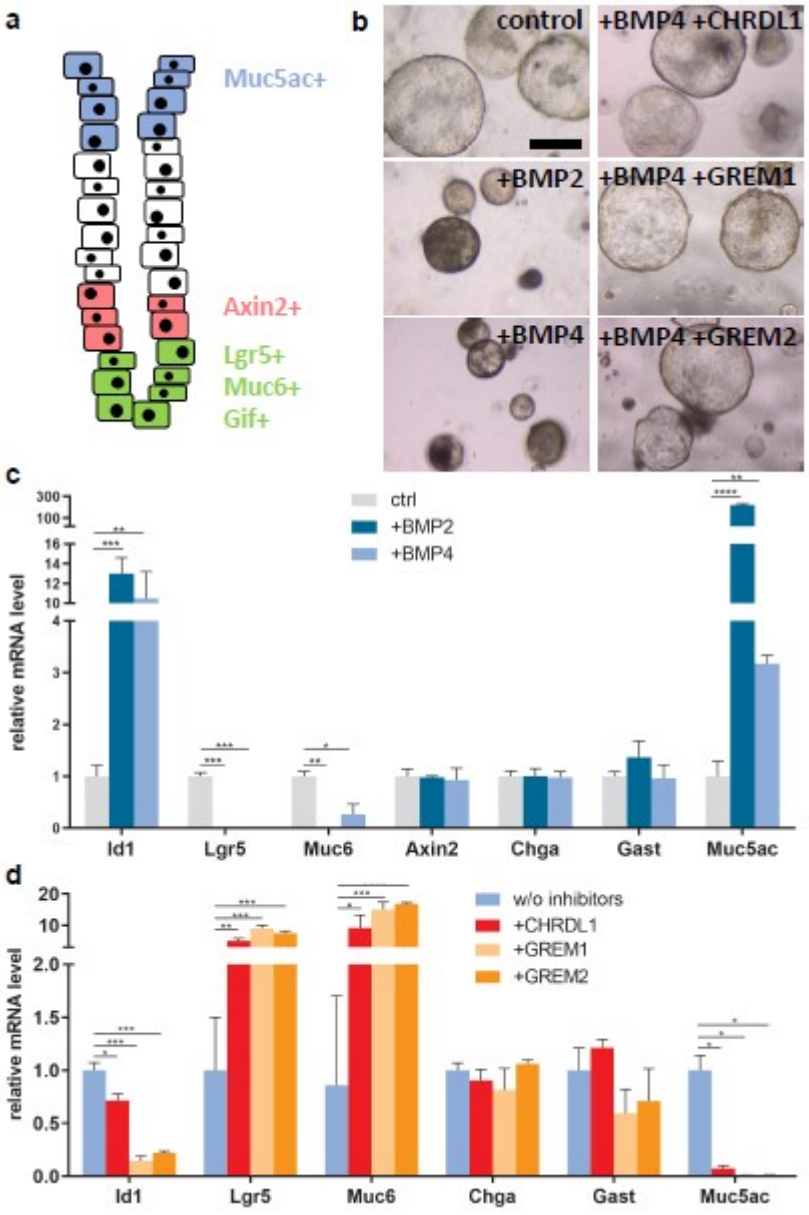

Figure 3.9. BMP ligands and inhibitors treatment in 3D organoids model.
Schematic representation of different gastric antrum cells and their markers (a). Images of organoids from antral epithelium grown in full organoid medium and either untreated and treated with BMP2 and BMP4 separately or BMP4 together with BMP inhibitors: CHRDL1, GREM1 and GREM2 (b) showing inhibited growth of organoids upon treatment with BMP ligands and restored phenotype by addition of BMP inhibitors. qRT-PCR for BMP target gene and markers characteristic for specific gland cells from organoids untreated and treated with BMP2 and BMP4 (c) and organoids treated with BMP4 separately or together with BMP inhibitors: CHRDL1, GREM1 and GREM2 (d) showing induction of differentiation into gland surface cells and inhibition of gland base markers, induced by BMP and restored by inhibitors. Images are representative of at least 3 biological replicates. Scale bar 250µm. Data are presented as mean ±SEM from 3 biological replicates, analyzed by Student's t-test.

Since BMP signaling was altered upon *H. pylori* infection and effects of BMP2 on cellular differentiation in organoids were identified, it was further investigated whether similar differentiation changes occur upon infection in vivo. Thus, tissue from uninfected and 2-months *H. pylori*-infected mice was stained with markers that showed the highest level of alteration upon BMP treatment of organoids. Indeed, MUC5AC signal in the surface decreased upon infection (Figure 3.10.a) and GSII+ gland base secretory cells (reminiscent of Muc6+ cells) increased upon infection (Figure 3.10.b). These observations are consistent with our previous findings showing an expansion of Lgr5+ stem cells as well as gland base secretory cells upon infection (Sigal et al. 2017; Sigal et al. 2019). In summary, changes upon infection resemble changes observed upon BMP inhibition, indicating that loss of BMP signaling could drive these processes *in vivo*.

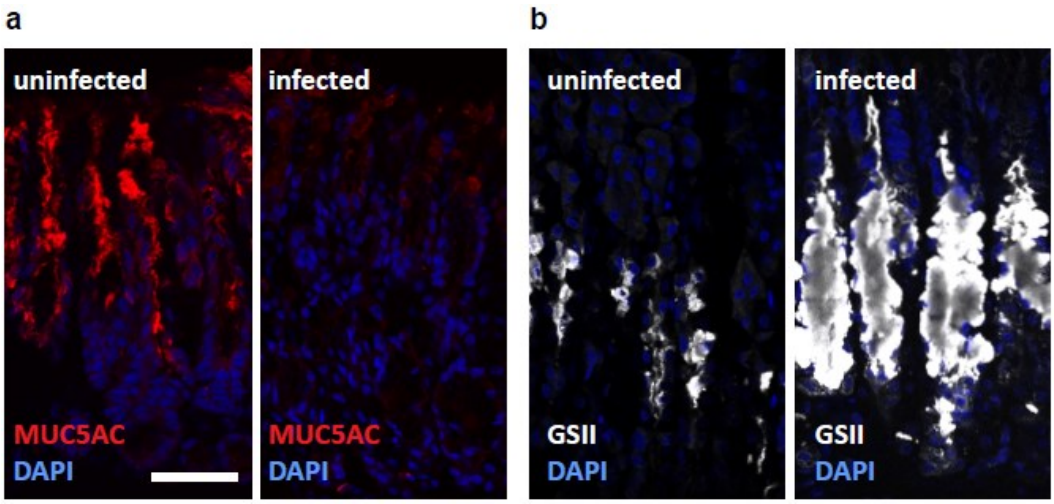

Figure 3.10. Confocal microscopy of stomachs stained for differentiation markers in 2 months *H. pylori*-infected mice.
Confocal microscopy images of uninfected and 2 months *H. pylori* infected mice labeled with MUC5AC (a) and GSII (b) showing reduction of gland surface markers and induction of gland base cells upon infection. Images are representative of at least 3 biological replicates. Scale bar 100µm. Data are presented as mean ±SEM from 3 biological replicates, analyzed by Student's t-test.

3.4.2 ANTIMICROBIAL GENES

Our previous studies have identified that a subpopulation of basal Lgr5+ cells are able to secrete antimicrobial factors such as Intelectin 1 (Itln1) and Regenerating family member 3 beta/gama (Reg3b/g) to counterbalance *H. pylori* infection (Sigal et al. 2019). Since BMP inhibition appeared to shape the gland base compartment, it was

hypothesized that BMP has an impact on the expression of these antimicrobial genes. Itln1, Reg3b and Reg3g expression was examined in organoids cultured with exogenous BMP2 and BMP4. qRT-PCR showed strong decrease for all antimicrobial genes in samples treated with both BMP2 and BMP4. However, down-regulation was stronger in organoids cultured with BMP2 (Figure 3.11.a). Next, influence of BMP inhibitors on antimicrobial genes was examined and expression of Itln1, Reg3b and Reg3g was found to be restored with all the inhibitors, compared to expression in samples treated with BMP4 only (Figure 3.11.b). Together, these data demonstrate that BMP signaling is a critical determinant not only in gastric epithelial differentiation but may play also crucial role in the antimicrobial response to *H. pylori* infection.

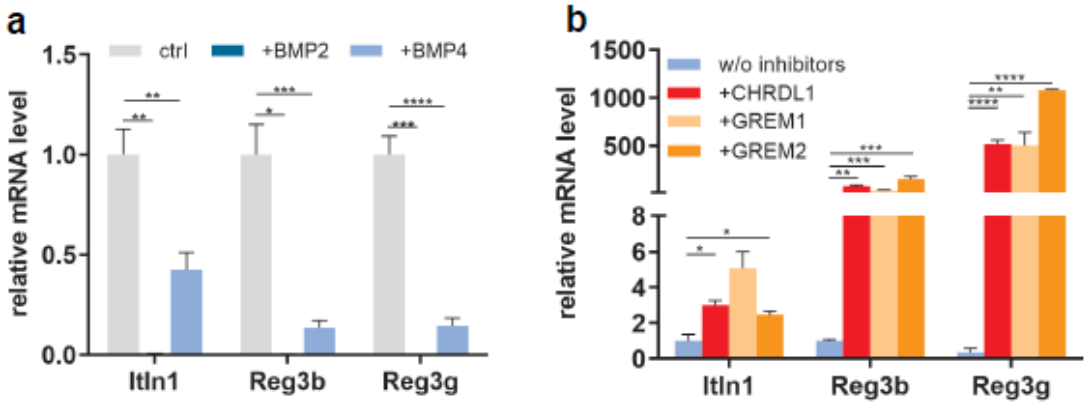

Figure 3.11. qRT-PCR results of antimicrobial respond to BMP treatment in 3D organoids model. qRT-PCR for antimicrobial genes from organoids untreated and treated with BMP2 and BMP4 (a) and organoids treated with BMP4 separately or together with BMP inhibitors: CHRDL1, GREM1 and GREM2 (b) showing reduction in antimicrobial genes expression upon BMP ligands treatment and restored expression with BMP inhibitors. Data are presented as mean ±SEM from 3 biological replicates, analyzed by Student's t-test.

3.5 BMP2 DRIVES FULL DIFFERENTIATION OF SURFACE MUCOUS CELLS

3.5.1 COMPARISON OF THE ROLES OF WNT AND BMP IN ORGANOIDS MODEL

Gastric gland homeostasis, including epithelial differentiation and proliferation, is shaped by different pathways and factors (de Lau et al. 2011; Demitrack et al. 2015). Our previous work has shown that myofibroblasts below the epithelial stem cells expressed high levels of WNT/β-catenin signaling modulator Rspo3 (Sigal et al. 2017). It has been described that the location and amount of this factor correlates with the concentration of WNT target genes in the gland base and lower isthmus epithelium.

Experiments with organoid culture has confirmed that RSPO is important for epithelial stem cells. Removal of WNT or RSPO from the culture medium increased differentiation and led to enrichment of surface markers, indicating that once cells exit the gland base compartment they start to differentiate into surface cells. Therefore, roles of Bmp and Wnt/RSPO were compared. Effects of RSPO-depletion and BMP activation were juxtaposed by culturing organoids epithelium in medium without RSPO only, without RSPO and with 50% reduced WNT3A and with addition of recombinant BMP2. As expected, both reduction of WNT signaling and activation of BMP pathways decreased in organoids growth. Quantification of organoids diameters showed that all the conditions induced similar reduction in organoids size (Figure 3.12.a), indicating that inhibition of WNT and activation of BMP have comparable influence on epithelial proliferation. However, investigating gene expression levels revealed significant differences in the effects of the studied pathways. Depletion of RSPO from culture medium was not sufficient to induce increase of Id1, together with reduced WNT it slightly up-regulated this BMP target gene, whereas BMP2 treatment led to 10-fold change in expression (Figure 3.12.b). Expression of gland base cell markers showed that both, reduction of WNT signaling and addition of BMP2 induced significant down-regulation of Lgr5, Muc6 and Gif genes, but the effect of BMP2 was much stronger leading to an almost complete loss of all these markers. The same pattern was observed when examining expression of Muc5ac surface marker. As expected, removal of WNT/RSPO induced Muc5ac expression, but BMP2 treatment induced it three times stronger (Figure 3.12.c).

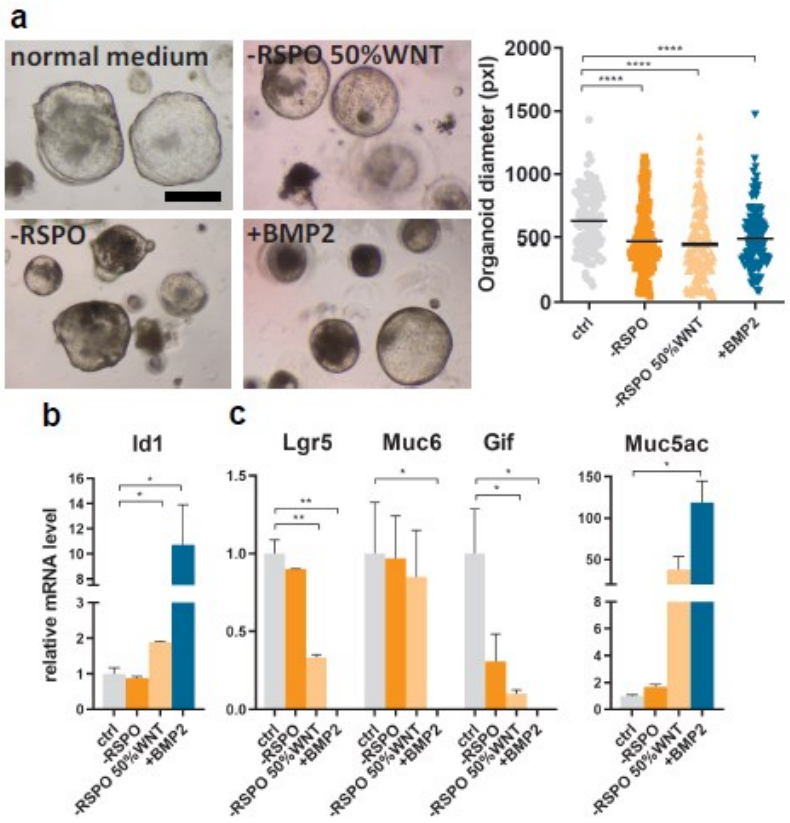

Figure 3.12. Organoids size and qRT-PCR analysis of cells cultured with reduced WNT/RSPO or addition of BMP2.

Organoids pictures and size quantification of cells cultured with reduced WNT/RSPO and addition of BMP2 (a) showing similar reduction of organoids growth in indicated conditions. qRT-PCR analysis of BMP target gene (b), basal and surface markers (c) showing reduction in basal genes and induction in Muc5ac expression with reduced WNT/RSPO and addition of BMP2, but much stronger effect for BMP2 treatment. Images are representative of 3 biological replicates. Scale bar 250µm. Data are presented as mean ±SEM from 3 biological replicates, analyzed by Student's t-test.

Since BMP had much stronger influence on epithelial cell plasticity than the reduction of WNT signaling, question of its influence on stemness appeared. To compare the effect of both conditions on stemness, organoids were cultured with or without exogenous BMP2 in normal medium, medium without RSPO only or without RSPO together with 50% reduced WNT. Next, organoid forming efficiency from passaged organoid cells seeded in the same cell number for all the conditions and cultured further in normal gastric organoid medium was measured. After the passage, cells kept in different medium conditions without BMP2, even upon removal of WNT/RSPO were able to create organoids when put back in normal medium. However, cells treated with BMP2, irrespectively of WNT/RSPO signaling, did not create any organoids (Figure 3.13.a-b),

indicating that exposure to BMP2 protein completely blocked stemness. Taken together, these data show that BMP signaling inhibits basal markers, induces differentiation into surface cells, leads to loss of stemness and promotes differentiation to surface mucous cells much stronger than reduction of WNT signaling.

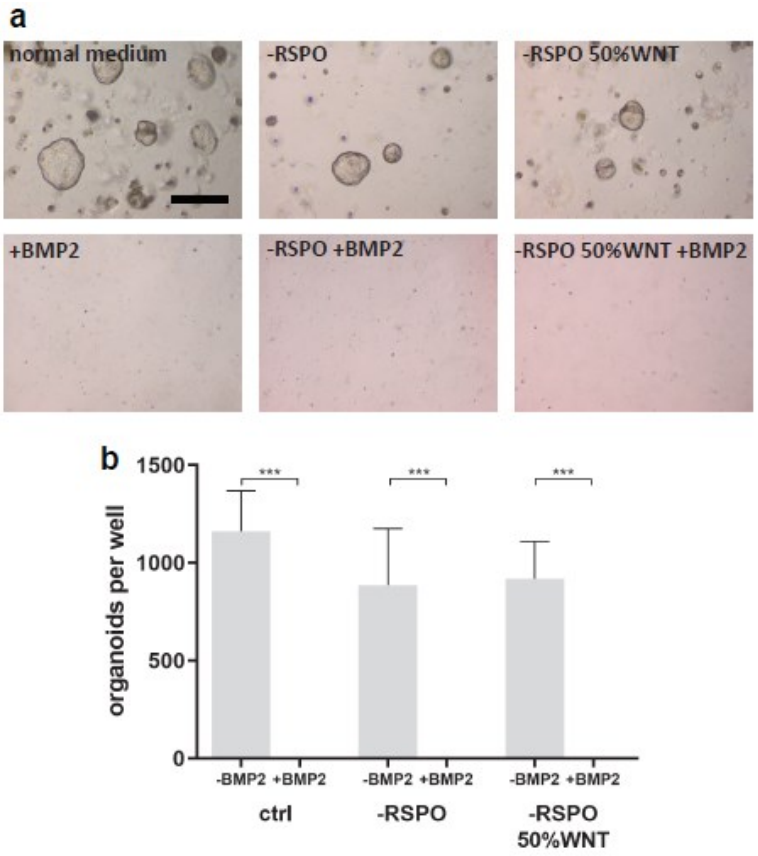

Figure 3.13. Pictures and numbers of passaged organoids cultured with reduced WNT/RSPO or addition of BMP2.

Pictures (a) and quantification (b) of organoids cultured with reduced WNT/RSPO or addition of BMP2, passaged and cultured further in normal organoids medium showing loss of stemness properties after treatment with BMP2, but not after the culture with reduced WNT/RSPO. Images are representative of 3 biological replicates. Scale bar 250µm. Data are presented as mean ±SEM from 3 biological replicates, analyzed by Student's t-test.

3.5.2 BMP2 AUTOCRINE LOOP

As showed above BMP ligands appear to be critical drivers of epithelial differentiation and question how Bmp2 expression, that is found in the surface and not base of the gland, is regulated appeared. To identify the condition that influences Bmp2 expression, qRT-PCR for Bmp2 expression was performed with organoids cultured with different conditions elaborated above such as reduced WNT/RSPO or addition of BMP2 and BMP4 in the medium. While WNT/RSPO depletion did not influence on Bmp2 expression,

strong and significant increase was observed upon BMP2 and BMP4 treatment (Figure 3.14.a). This led us hypothesize that Bmp2 induces itself in auto-paracrine loop, where once the cell encounters Bmp2, it starts to express it and turns on an autocrine loop, which further stabilizes and enhances the effect of Bmp2. To address this, organoids experiment with different BMP2 concentrations was performed with the help of Manqiang Lin from the MPIIB Department of Molecular Biology. Organoids were cultured with BMP2 concentrations from 0 to 50 ng/ml and their size, number and genes expression were examined. Indeed, significant alterations in differentiation genes expression identified previously by us as effect of BMP2 treatment were observed with the BMP2 concentration sufficient to induce Bmp2 expression. Once the expression of Bmp2 was induced, expression of differentiation markers changed significantly – expression of Muc5ac was strongly induced, whereas expression of Muc6 and Lgr5 almost completely lost (Figure 3.14.b). Additionally, organoids after the treatment with different BMP2 concentrations were passaged and cultured further with normal medium to investigate the organoid forming capacity. Interestingly, the number of formed organoids after passage corresponded with previous observations – BMP2 concentration that was sufficient to induce endogenous Bmp2 expression was the breaking point in which organoids number dropped significantly to almost zero (Figure 3.14.b). In contrast, organoids cultured with doses of BMP2 that was below the threshold to induce Bmp2 expression were still able to re-grow and developed into organoids after passage. (Figure 3.14.c). Taken together, these experiments indicated that Bmp2 expression in epithelial cells is regulated by BMP2 auto/paracrine loop, which, when switched on, leads to differentiated phenotype and loss of stemness properties.

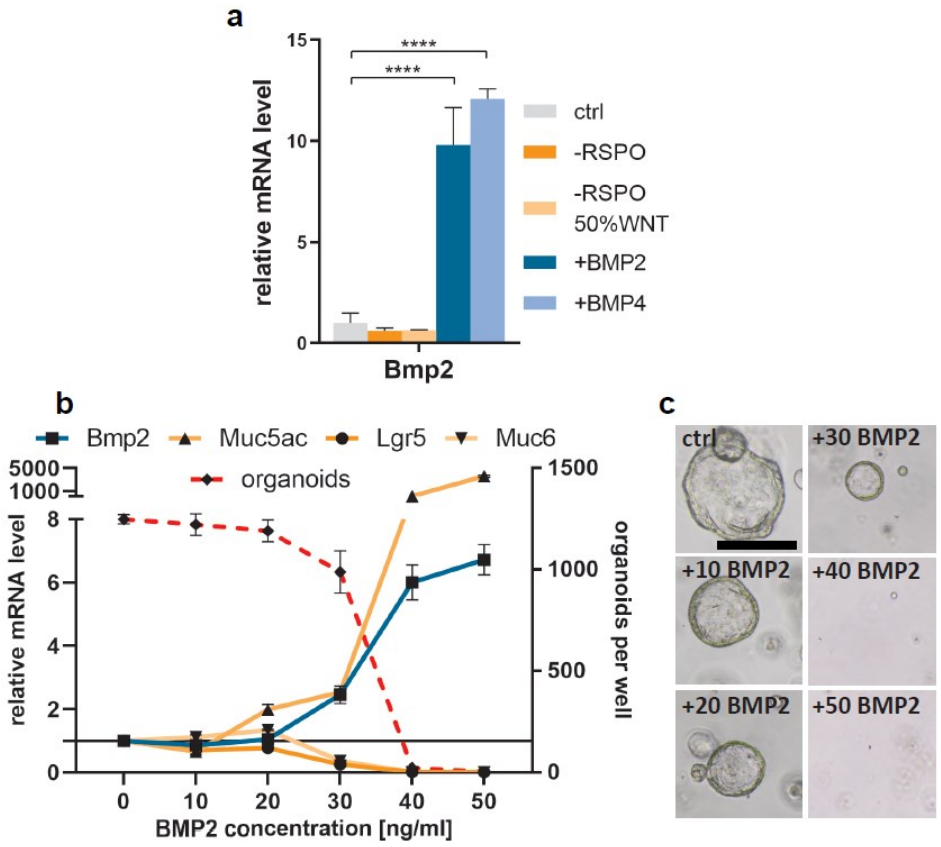

Figure 3.14. qRT-PCR, number and morphology analysis of organoids cultured with different BMP2 concentrations.

qRT-PCR for Bmp2 in organoids cultured with reduced WNT/RSPO or addition of BMP2 and BMP4 (a) showing induced Bmp2 expression upon BMP2 and BMP4 treatment. Expression of differentiated genes, organoids number (b) and organoids phenotype (c) in culture treated with different BMP2 concentration indicating that effect of BMP2 on differentiated genes and impaired colony forming efficiency corresponds with induction of Bmp2 expression in epithelial cells. Images are representative of 3 biological replicates. Scale bar 250µm. Data are presented as mean ±SEM from 3 biological replicates, analyzed by Student's t-test.

3.5.3 BMP AND RSPO REGULATION IN MYOFIBROBLASTS

As mentioned above, our previous studies showed that Rspo3, which is an important modulator of WNT signaling in epithelial stem cells, is expressed exclusively in myofibroblasts beneath the gastric gland (Sigal et al. 2017). In contrast, stroma surrounding surface of the gland showed no signal for this factor, whereas the current study revealed that it is enriched in Bmp2 expression (Figure 3.5.a, d). Mutually exclusive sites of expression led us hypothesize that these signaling pathways negatively affect each other. To investigate this relationship, primary myofibroblasts from *Myh11CreErt2/Rosa26-tdTomato* mice were isolated and a culture of these cells was established. Confocal imaging of cultured cells, which were extracted from the tissue

showed that after two passages they mainly consist of Myh11+ myofibroblasts. Moreover, staining with vimentin as marker of mesenchymal cells was performed and demonstrated strong enrichment of the signal, which was mostly co-located with Myh11 fluorescence confirming mesenchymal character of the cells (Figure 3.15.).

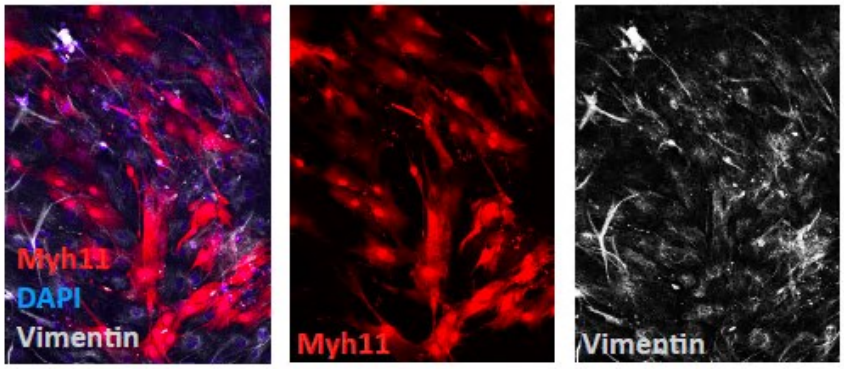

Figure 3.15. Confocal microscopy of myofibroblasts culture from *Myh11CreErt2/Rosa26-tdTomato* mice. Representative images of confocal microscopy with Myh11+ myofibroblasts stained with Vimentin antibody, confirming mesenchymal character of the cells. Images are representative of 3 biological replicates.

Next, myofibroblasts were treated with exogenous recombinant RSPO3 or BMP2. While addition of RSPO3 did not induce any changes in Bmp2 expression (data not shown), myofibroblasts responded to BMP treatment and showed a significant decrease in Rspo3 expression. Additionally, BMP inhibition using rNoggin was further examined. Expression of BMP target gene Id1 was induced by addition of BMP2 and reduced with Noggin, indicating that myofibroblasts actively respond to the treatment. Moreover, expression of Rspo3 in myofibroblasts was inversely correlated with BMP activation. With addition of rNoggin, when Id1 was down-regulated, expression of Rspo3 increased almost 2-fold, whereas during BMP2 treatment and up-regulation of Id1, expression of Rspo3 decreased almost by half (Figure 3.16.a). Investigation of different BMP2 concentrations showed that the induction of Bmp2 target gene Id1 was increasing with higher concentration and that loss of Rspo3 expression showed the same concentration dependency (Figure 3.16.b). To ask whether BMP2 reduced Rspo3 expression or whether it selectively affected the expansion of subpopulations of Rspo3 positive versus Rspo3 negative cells, EdU proliferation assay was performed and no significant difference in proliferation upon BMP2 treatment was observed (Figure 3.16.c). Thus, the data indicated that Rspo3 expression in myofibroblasts is inhibited by BMP signaling,

which may explain the spatial separation of Bmp2+ cells versus Rspo3-positive cells. Moreover, it may be an explanation for increased Rspo3 expression upon infection with *H. pylori*.

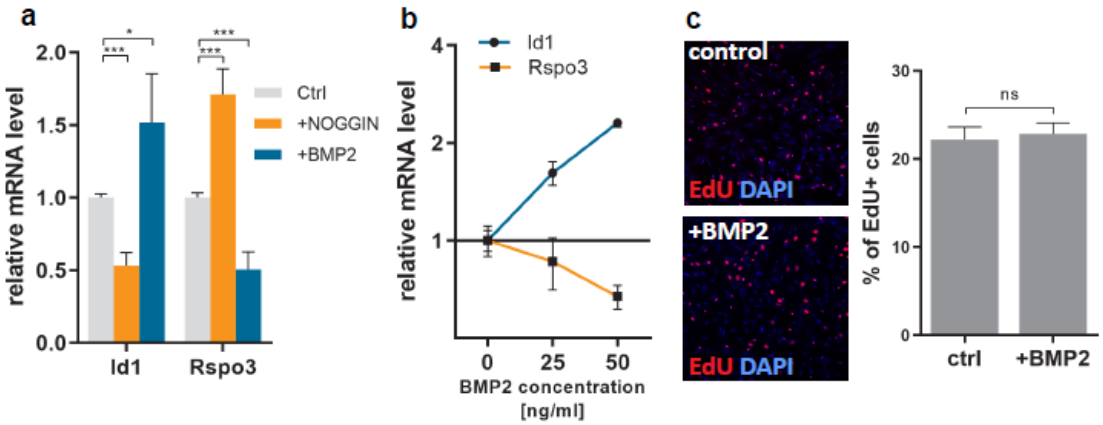

Figure 3.16. qRT-PCR and EdU assay of myofibroblasts culture treated with BMP2 and Noggin.
qRT-PCRs of myofibroblasts cultured with BMP2, Noggin (a) and with different BMP2 concentrations (b) showing inverse correlation between induction of BMP pathway and Rspo3 expression. Edu proliferation assay with myofibroblasts treated with BMP2 (c) showing no differences in proliferation upon the treatment. Images are representative of 3 biological replicates. Data are presented as mean ±SEM from 3 biological replicates, analyzed by Student's t-test.

3.6 *H. PYLORI* REGULATES BMP SIGNALING THROUGH IFNγ

3.6.1 ROLE OF *H. PYLORI* T4SS IN BMP2 REGULATION

Finally, a connection between infection with *H. pylori* and reduction of BMP signaling was further explored. To address this, tissue responses to *H. pylori* infection were revisited. *H. pylori* T4SS represents a well-studied virulence machinery of *H. pylori*, required for injection of *CagA* and other virulence factors such as ADP heptose into host cells and is required for the full expansion of Lgr5+ cell upon infection (Sigal et al. 2015). To examine whether functional T4SS is required for Bmp2 inhibition upon infection, isogenic mutant lacking the *CagE* gene, making the T4SS dysfunctional was used (Arnold, Lee, et al. 2011). Stomachs from mice infected with ΔCagE PMSS1, compared to stomachs infected with the wild-type PMSS1 strain for two months, showed less hyperplasia (Figure 3.17.a) and less Ki67+ proliferating cells (Figure 3.17.b). Next, Bmp2 changes in mice infected with both strains were examined by ISH. WT PMSS1 infected mice had an almost complete loss of Bmp2 expression. However, mice infected with ΔCagE PMSS1 still expressed Bmp2 on high level, indicating that Bmp2 loss depends on

a functional T4SS (Figure 3.17.c). To identify the specific factor or signal responsible for Bmp2 down-regulation, microarray with uninfected and 2 months *H. pylori* infected WT PMSS1 mice was performed and GSEA showed the highest level of enrichment for IFNγ response genes (Figure 3.17.d). Expression of Ifnγ was then examined in mice infected with WT and ΔCagE PMSS1. qRT-PCR data revealed significantly higher expression of Ifnγ in WT infected animals indicating that the strong induction of Ifnγ expression upon infection requires the T4SS (Figure 3.17.e).

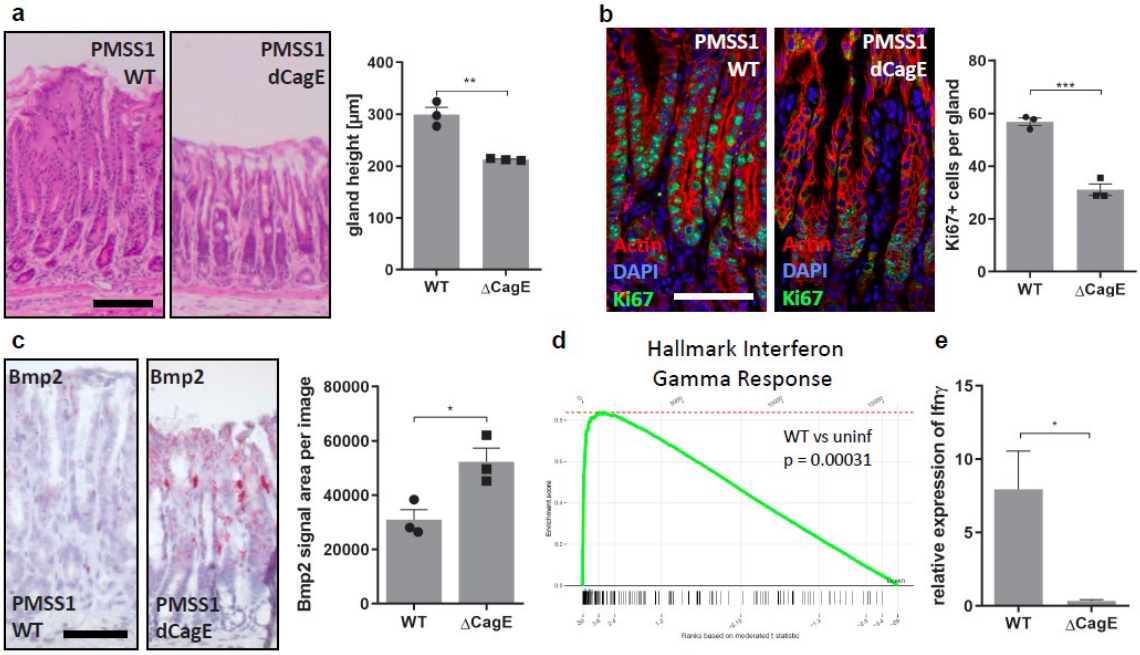

Figure 3.17. Tissue analysis, microarray and qRT-PCR of mice infected with WT and ΔCagE mutant. H&E staining (a), confocal images of Ki67 staining (b) and ISH for Bmp2 (c) of stomachs infected with WT and ΔCagE mutant showing less hyperplasia, less proliferation and high levels of Bmp2 in ΔCagE mutant compared to WT. Microarray GSEA in WT infected stomachs compared to uninfected (d) showing high enrichment in IFNγ response genes. qRT-PCR for Ifnγ showing significantly higher expression in WT infected animals. Images are representative of at least 3 biological replicates. Scale bar 100µm. Data are presented as mean ±SEM from 3 biological replicates, analyzed by Student's t-test.

3.6.2 IFNγ INFLUENCE ON ORGANOIDS PLASTICITY

As showed above, both induction of Ifnγ signaling and reduction of Bmp2 expression were induced in T4SS dependent manner. Similar phenotype and connection to infection made us wonder whether IFNγ will affect organoids growth, stemness and Bmp2 expression. To address this, gastric organoids were treated with recombinant IFNγ and changes in gene expression level were investigated. To confirm that cells respond

to IFNγ, Ifnγ target gene Irf1 was selected and confirmed a strong increase in expression upon treatment. Next, examination whether IFNγ is affecting BMP signaling was performed by investigating changes in Id1 expression. Interestingly, Id1 expression was significantly down-regulated, whereas the expression of Lgr5 was significantly increased. Strikingly, expression of Bmp2 was also down-regulated in IFNγ treated organoids, indicating that IFNγ could block the induction of endogenous Bmp2 signaling cascade (Figure 3.18.a). To determine whether these effects depend on the IFN-γ receptor, experiments were repeated with organoids isolated from IFNγ receptor KO mice (Huang et al. 1993). This time, there was no increase in Irf1 expression as well as no changes in Bmp2, Id1 and Lgr5 expression, indicating that IFNγ-driven effects are via its interaction with the IFNγ receptor (Figure 3.18.b). Moreover, culture with different concentrations of IFNγ showed that already low concentration of 3ng/ml of IFNγ is sufficient to induce changes of indicated genes. Expression stays on the similar level even with 500ng/ml, indicating that IFNγ driven changes in Irf1, Bmp2, Id1 and Lgr5 expression are induced at low concentration and don't increase further (Figure 3.18.c).

To examine in detail the response of organoids to IFNγ, microarray from organoids culture with addition of IFNγ was performed. Interestingly, GSEA showed a significant enrichment of genes identified as down-regulated BMP2 targets by Lee et al in the mouse uterus upon KO of Bmp2 (Lee et al. 2007) (Figure 3.18.d), whereas genes described as up-regulated BMP2 targets in the same system were significantly reduced upon IFNγ treatment (Figure 3.18.e), which demonstrates that IFNγ suppressed the BMP2 signaling. Of note, there was no significant enrichment for gene sets associated with Wnt signaling such as "Beta catenin targets". Therefore, the induction of Lgr5 expression upon IFNγ was more likely to be induced by loss of BMP2 signaling than by induction of WNT pathway (Figure 3.18.f).

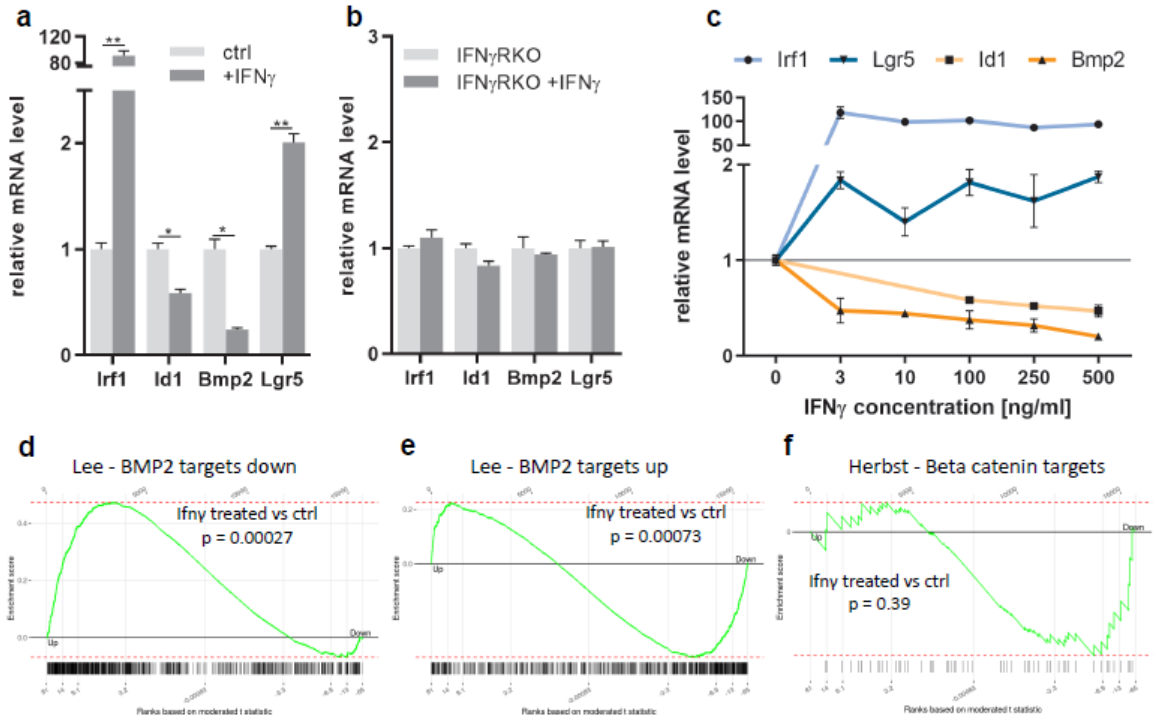

Figure 3.18. qRT-PCR and microarray analysis of organoids treated with IFNγ.
qRT-PCR for WT (a) and IFNγRKO (b) organoids cultured with IFNγ showing Bmp2 inhibition upon IFNγ treatment. qRT-PCR with different IFNγ concentrations (c) showing that gene expressions levels do not changed with higher IFNγ concentration. Microarray analysis of organoids treated with IFNγ showing enrichment for down-regulated BMP2 targets (d), reduction for up-regulated BMP2 targets (e) and no significant changes for Beta catenin targets (f). For qRT-PCR results data are presented as mean ±SEM from 3 biological replicates, analyzed by Student's t-test. For microarrays analysis 2 biological replicates were used.

Since IFNγ inhibits anti-proliferative Bmp2 and increases Lgr5 expression, addition of IFNγ to the culture should induce organoids growth and development. However, treatment with this recombinant protein led to a rather decreased organoid growth and less outgrowth of organoids after passage (Figure 3.19.a). To understand this further, Lgr5+ cell lineage tracing was performed in organoids: organoids from *Lgr5CreEr/Rosa26tdTomato* mice were cultured with IFNγ as previously, then treated with 4OH-tamoxifen for 24h to induce lineage tracing, passaged, seeded as single cells and proportion of organoids created from tdTomato positive to tdTomato negative organoids was calculated. Interestingly, the proportion of Lgr5+ to Lgr5- organoids was higher in cells treated with IFNγ before the passage compared to cells untreated with IFNγ (Figure 3.19.b). Thus, this experiment showed that IFNγ-reduced stemness in Lgr5+ cells, whereas Lgr5-negative cells had a higher likelihood to grow into organoids, overall being an indicator for an altered stem cell hierarchy.

Since IFNγ inhibited Bmp2 expression, question whether the terminal differentiation induced by Bmp2 signaling will be lost by co-treatment of cells with IFNγ appeared. Organoids were treated with BMP2 or IFNγ, but also with BMP2 and IFNγ together and qRT-PCR was performed. Addition of IFNγ together with BMP2 blocked the overexpression of Muc5ac and Bmp2 induced by BMP2 only, but there were no changes in the decreased expression of Lgr5 (Figure 3.19.c). Next, colony forming efficiency was examined by passaging treated organoids and culturing them further in normal medium. As previously, cells treated with BMP2 created only 5 organoids per well and mostly stayed on single cell level. However, cells cultured with BMP2 and IFNγ could be passed and developed organoids, indicating that IFNγ blocked BMP2-induced terminal differentiation and enhanced stem cell plasticity in differentiating cells (Figure 3.19.d).

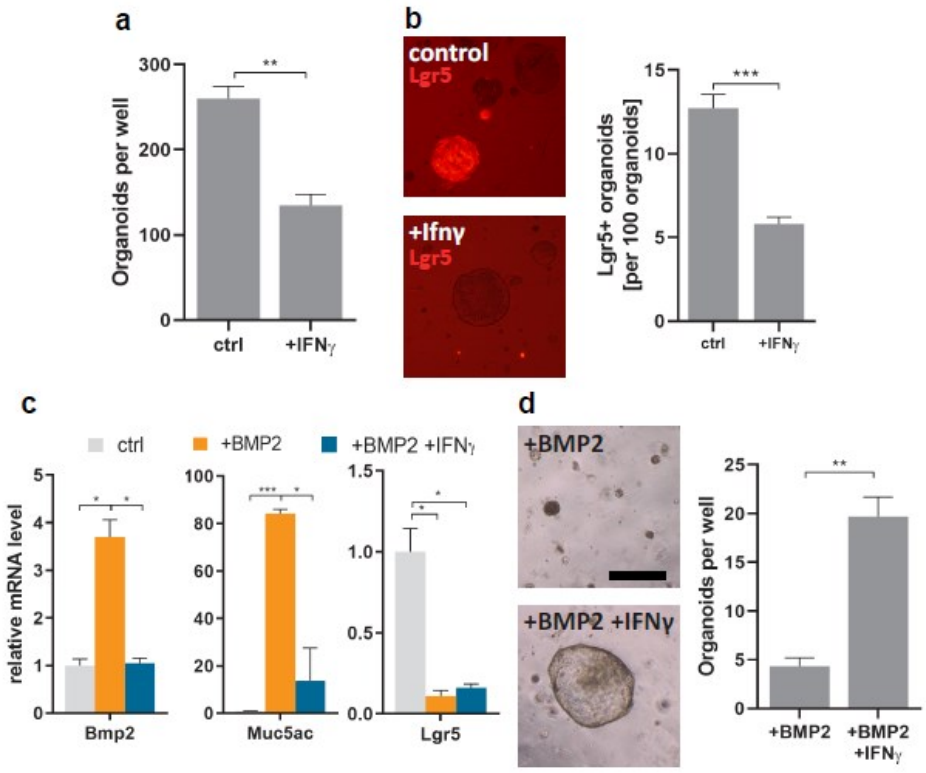

Figure 3.19. Organoids culture and qRT-PCR of cells treated with BMP2 and IFNγ.
Organoids number quantification (a) and Lgr5 lineage tracing induced by Tamoxifen 24h before the passage (b) of organoids treated with IFNγ showing reduced stemness capacity and reduced Lgr5+ driven organoids formation. qRT-PCR for Bmp2, Muc5ac and Lgr5 treated with BMP2, IFNγ or with both factors together (c) showing that IFNγ blocks BMP2-driven overexpression of Muc5ac and Bmp2, but no changes for Lgr5. Colony forming efficiency for cells treated with BMP2 and BMP2 together with IFNγ (d) showing increased stemness capacity after IFNγ addition. Images are representative of 3 biological replicates. Scale bar 250µm. Data are presented as mean ±SEM from 3 biological replicates, analyzed by Student's t-test.

4 Discussion

H. pylori is one of the most widespread bacteria and colonizes more than 50% of the world population (Pounder and Ng 1995). Thanks to Barry Marshall and Robin Warren it has been identified as the causing agent of chronic gastritis as well as other gastric pathologies (Marshall et al. 1985). Further examination of *H. pylori* influence revealed its contribution to gastric precancerous processes. Accordingly, it has been classified as a class I carcinogen in 1994 by the WHO (IARC 1994). The important role of *H. pylori* in cancer development evoked interest in understanding the mechanisms of disease development. Many studies focusing on bacterial factors required for colonization and adaptation to gastric environment were performed. Moreover, epidemiological and mechanistic studies enabled defining bacterial virulence factors, especially VacA, bacterial adhesins and cagPAI (Palframan, Kwok, and Gabriel 2012; Sheu et al. 2012; Khatoon et al. 2017). On the other hand, gastric alterations induced by *H. pylori* that define pathological states ranging from gastritis, through atrophy, intestinal metaplasia, dysplasia to gastric cancer were characterized in patients (Correa et al. 1975; Correa and Piazuelo 2012).

However, little is known about the mechanistic principles of epithelial cell responses to infection and the development of tissue pathology. In this study, I explored the mechanistic basis of gastric epithelial regeneration, plasticity and differentiation in both uninfected healthy state as well as upon infection with *H. pylori*. In this context, my study aimed at characterizing the molecular linkages between the infection, inflammation and epithelial pathology.

I identified myofibroblasts surrounding the epithelial gland cells as cells that generate a BMP signaling gradient along the gland axis from BMP inhibition in the base to high BMP signaling in the surface. This gradient guides epithelial cell differentiation from the basal stem cells towards secretory mucous cells at the gland surface. Once BMP signaling is activated in epithelial cells, it induces an auto-/paracrine feed-forward BMP2 loop in epithelial cells that stabilizes the BMP signaling pathway and therefore limits plasticity leading to terminal differentiation. Moreover, my results showed strong induction of IFNγ signaling in the stomach upon infection and I identified its inhibitory effect on BMP

signaling. This leads to a termination of paracrine BMP activation and limits BMP signaling overall in the stomach thus, triggering an increased number of proliferative cells and inhibition of terminal differentiation.

Therefore, these studies provide a molecular explanation for both, terminal differentiation of cells in the healthy condition and enhanced plasticity observed in gastrointestinal pathologies (Yu et al. 2018; Schwitalla et al. 2013; Stange et al. 2013; Tetteh et al. 2016).

4.1 GASTRIC STEM CELLS MICROENVIROMENT UPON *H. PYLORI* INFECTION

Gastric glands are characterized by a constant, rapid and highly organized turnover. Role of specific epithelial cell types and their responses to *H. pylori* infection have been widely studied. Gao and colleagues have identified hyperproliferation of epithelium (Gao et al. 2000), Murakami et al. have investigated parietal cell atrophy (Murakami et al. 2013), Matsuzwa and colleagues have described increase of gland mucous cells (Matsuzwa et al. 2003) and Sigal et al. have shown expansion of stem cells compartment (Sigal et al. 2015) and its antimicrobial properties (Sigal et al. 2019) upon *H. pylori* infection. However, molecular processes behind these changes still remain not understood.

In the intestine, mesenchymal cells have been described as crucial cells, which create epithelial stem cell niche, providing specific microenvironment signals for different types of epithelial cells. As a consequence, they play an essential role in homeostasis maintenance as well as in disease development (Roulis and Flavell 2016; Tan and Barker 2014). Mesenchymal cells have been reported to express WNT signaling factors such as Wnt2b, Wnt4, Wnt5a, Wnt5b and Rspo1, Rspo2 and Rspo3 (Gregorieff et al. 2005; Lei et al. 2014). Since Paneth cells are a critical source of canonical WNT signaling in the intestine, mesenchymal cells have been suggested to complement this mechanism and support non-canonical WNT pathway (Powell et al. 2011). Moreover, they have been described as a source of BMP ligands and antagonists. Noggin, GREM1, GREM2 and CHRDL1 expression was identified in the crypt base, while BMP4 signal was present in the stroma through the whole villi axis and BMP2 expression was limited to the top, but also observed in the epithelium (He et al. 2004; Kosinski et al. 2007; Haramis et al. 2004;

van Dop et al. 2009). Co-culture experiments showed significant support of epithelial organoids growth and development in the presence of mesenchymal cells indicating that these cells create microenvironment for epithelial stem cells (Lahar et al. 2011; Lei et al. 2014). Moreover, *in vivo* studies confirmed significant influence of myofibroblasts on goblet and Paneth cells differentiation and thus revealed their role in generation of the niche also for differentiated cells (Stzepourginski et al. 2017). Additionally, myofibroblasts have been reported as an important factor in intestinal responses to tissue injury and bacteria. They are not only responsible for mechanical wound healing but also promote compensatory epithelial proliferation by induction of proinflammatory tumor progression locus-2 (Tpl2), which promotes arachidonic acid metabolism and cyclooxygenase-2 (Cox-2)/prostaglandin E2 activation (Tomasek et al. 2002; Roulis et al. 2014).

Although investigation of myofibroblasts in the small intestine clearly showed their essential role in epithelial homeostasis and disease, they have not been well studied in stomach. Two independent studies have identified gastric myofibroblasts as the main source of RSPO3, which induced expansion of stem cell compartment (Chen et al. 2019; Sigal et al. 2017). Moreover, it has been reported that stromal RSPO3 increased upon *H. pylori* infection and induced antimicrobial secretion by Lgr5+ stem cells (Sigal et al. 2019). Additionally, air liquid interface culture model showed that gastric stromal cells of the lamina propria, which are located between, but not beneath, the glands, have not supported the epithelial growth and even reduced their stemness (Boccellato et al. 2018).

This study applies an unbiased approach to explore the gastric stem cells microenvironment in homeostasis and in the context of *H. pylori* infection. For the first time, a mouse model was used to visualize gastric myofibroblasts and identify their alterations upon infection. *Myh11CreErt2/Rosa26-mTmG* mice enabled localization of these cells between and beneath the gastric epithelium (Figure 3.1.b) as well as negative labeling for EPCAM antibody (Figure 3.2.c). RNAseq from sorted Myh11 cells revealed potential role of myofibroblasts in epithelial cells regulation by expressing factors like Wnt, Rspo and Bmp (Figure 3.4.b), which is similar to findings in the small intestine (Gregorieff et al. 2005; Kosinski et al. 2007). Additionally, infection of mice showed that

H. pylori is not only inducing hyperplasia of epithelial cells, but also that Myh11+ myofibroblasts population expands upon infection (Figure 3.3.). Further analysis of infected myofibroblasts implicates their active role in *H. pylori* infection by identifying significant changes in 197 genes, including strong reduction of BMP ligands and induction of BMP inhibitors (Figure 3.4.).

Exploration of BMP distribution within the tissue demonstrated a spatial gradient similar to the one observed in the small intestine with the BMP antagonists in the base of the gland and Bmp2 dominant in its top part in both myofibroblasts and epithelial cells (Figure 3.5. and 3.6.) (Kosinski et al. 2007; van Dop et al. 2009). Interestingly, Noggin, described as the main BMP antagonist present in the base of small intestine crypt, was not detected in the mouse stomach glands (Figure 3.6.b) (He et al. 2004). In contrast, other Bmp inhibitors such as GREM1/2 and CHRDL1 were present exclusively in the base. Gremlins specifically binds BMP ligands and therefore has a similar function to Noggin.

Boccellato et al. describe that different subtypes of stromal cells have differential effects on epithelial proliferation and differentiation. He has observed that stroma from lamina propria between the gastric glands reduces epithelial stemness capacity and induces differentiation (Boccellato et al. 2018), whereas cells isolated from the base have been described as a source of factors inducing stemness (Sigal et al. 2017). My findings on spatial distribution of Bmp activators versus inhibitors in myofibroblasts may explain the differential influence of subpopulations of stromal cells on epithelial stem cells described by Boccellato et al. Gastric stromal cells of the lamina propria used by them correspond to cells that I find to be enriched in BMP2 and lack BMP antagonists, which enhance stemness.

Expression of different BMP factors in other parts of gastric gland observed by me and expression of Rspo3 limited to basal myofibroblasts described by Sigal et al. (Sigal et al. 2017) indicate different stroma populations in the top and in the base of gastric gland. These findings are consistent with observation reported in the small intestine, which distinguished basal cell population enriched in Wnt2b, Grem1 and Rspo1 and stroma population in the villus region expressing Bmp2, Bmp7, Ptch1 and Acta2 (Stzepourginski et al. 2017). Finally, I was able to confirm RNAseq results by ISH and show up-regulation of Grem1, Grem2 and Chrdl1 in the myofibroblasts compartment and strong down-

regulation of Bmp2 in the upper parts of gland within the tissue upon infection (Figure 3.7. and 3.8.), which provides another evidence of their active response to *H. pylori* infection. Thus, this study is the first to describe the spatial distribution of BMP-associated molecules in myofibroblasts and their changes upon *H. pylori* infection.

4.2 ROLE OF BMP SIGNALING IN EPITHELIAL DIFFERENTIATION

BMP pathway has been reported to play an essential role in growth and differentiation of the developing gastrointestinal tract as an coordinator of endodermal and ectodermal patterning (Batts et al. 2006). In the stomach development it is responsible for regionalization of specific stomach regions and KO of BMP receptor leads to increase of the forestomach at the expense of the corpus part (Maloum et al. 2011). Moreover, BMP is required for establishment of the pyloric sphincter and its deletion in both mesenchymal and endoderm layers leads to impaired pyloric sphincter formation (Smith et al. 2000; Smith and Tabin 1999; Zhang and Que 2019).

In the adult, developed stomach BMP signaling has been identified as a crucial pathway. Inhibition of BMP signaling in different cell types in the murine stomach results in increase of gland height, hyperproliferation, loss of parietal cells, increased number of cells expressing GSII, formation of cystic structures and even induction of CD44 and C-Myc expression, which are involved in gastric carcinogenesis (Shinohara et al. 2010; Ye et al. 2018; Takabayashi et al. 2014). However, most of the studies induced alteration in BMP signaling in selected cells and focus on specific responses in this compartment. Therefore, in this study, to create a systematic picture of the function of BMP signaling, I performed 3D organoid cultures with BMP ligands and inhibitors and investigated alterations in gene expression of markers characteristic for all antral gland cell types. These experiments clearly showed BMP as a factor which promotes differentiation into surface mucous cells and reduces expression of basal markers as well as inhibition of proliferation (Figure 3.9.). This is consistent with previous *in vivo* observations, which identified hyperplasia, hyperproliferation, loss of surface mucous cells and induction of mucous neck cells in stomach with overexpression of BMP inhibitor Noggin or inhibition of BMPR1a in both mesenchymal and epithelial cells (Maloum et al. 2011; Roy et al. 2016; Todisco et al. 2015). However, I did not observe any changes in expression of

enteroendocrine markers like Chga or Gast upon BMP treatment or inhibition, which has been identified in the corpus with Bmpr1a KO (Maloum et al. 2011). The difference may be due to investigation of different regions of stomach or involvement of some other signaling, which can be limited during *in vitro* cultures. Moreover, organoids experiments revealed Lgr5+ stem cell inhibition by BMP ligands that has been widely examined in the small intestine and not fully explored in the stomach (Qi et al. 2017; Ye et al. 2018). Studies from small intestine have shown direct suppression of Lgr5+ stem cell signature genes, but not WNT target genes such as Axin2, by BMP activation, which can be reversed by BMP inhibitors (Qi et al. 2017). This observation is consistent with Lgr5 down-regulation in organoids upon BMP2 and BMP4 treatment, which was re-induced by BMP inhibitors as well as no changes in Axin2 expression upon indicated treatments (Figure 3.9.c-d). Furthermore, as a confirmation of these findings, experiments performed in the stomach presented Lgr5 induction in mice with Bmpr1a KO or Noggin overexpression under the Lgr5 promotor (Ye et al. 2018).

Additionally, I discovered that factors, which regulate Bmp2 expression in the epithelium are BMP ligands themselves (Figure 3.14.a). Experiments involving organoids showed reduction of growth, stemness, basal identity and induction of differentiation into surface mucous cells with concentration of BMP2 sufficient to induce Bmp2 expression (Figure 3.14.b-c). This indicates the presence of BMP2 auto-paracrine loop, which, referring to Bmp distribution and function, maintains and enhances BMP signaling-driven differentiation of the epithelial cells on their way to the surface. BMP2 auto-paracrine loop may explain epithelial hyperplasia observed in mice with BMP signaling inhibition not only in epithelial cells but also in stromal cells. Inhibition of Bmp2 in either cell type could lead to loss of positive feedback loop, lower level of Bmp signaling and therefore increased proliferation and reduced differentiation (Roy et al. 2016; Shinohara et al. 2010). I could demonstrate how BMP signaling is self-enhanced and stabilized in the surface through Bmp2 autocrine loop. Investigations of maintenance of BMP gradient have not been done in the healthy gastrointestinal tract. However, data from colon have shown similar regulatory pathway: Bmp4 expression was reduced by the inhibition of BMP signaling in colorectal cancer, indicating that BMP forward loops may be a general mechanism (Yokoyama et al. 2017).

Since WNT signaling is inducing proliferation, reducing differentiation and also creates the gradient within the gastric gland (which is opposite to BMP with high WNT in the base and low WNT in the surface), it has been suggested as a driver of gastric gland turnover (Fischer and Sigal 2019). Therefore, I compared the influence of WNT and BMP pathways on epithelial differentiation, proliferation and stemness by culturing gastric epithelial organoids with BMP signaling induction or WNT signaling reduction. Experiments showed that both conditions are inhibiting proliferation and growth of the organoids and both conditions are sufficient to block expression of gland base cell markers and induce differentiation into surface mucous cells (Figure 3.12.). However, changes caused by BMP activation were much stronger and irreversible. BMP treatment induced terminal differentiation and led to complete loss of stemness properties in cultured organoids (Figure 3.13.), which indicates that BMP is a main driver of gastric gland turnover. These results are consistent with observation made in the small intestine by Qi and colleagues (Qi et al. 2017). They have reported that BMP signaling suppresses expression of stem cells signature independently of WNT signaling by SMAD4 protein, which directly regulates promotor of these cells. On the other side, air liquid interface culture of gastric epithelium showed that WNT signaling can drive differentiation from MUC6+ to MUC5AC+ cells (Boccellato et al. 2018). It was confirmed *in vivo* by identifying WNT co-mediator RSPO3 as a crucial factor regulating stem cells compartment, promoting expression of basal markers and inhibiting differentiation into surface mucous cells (Sigal et al. 2017; Sigal et al. 2019). Although Rspo3 *in vivo* KO and *in vitro* withdrawal led to reduction of stem cell compartment, RSPO3 injection into the tissue was sufficient to induce only Axin2+ stem cells, but not Lgr5+ cells, indicating that there has to be another pathway regulating this compartment. This now can be explained by the identified BMP gradient, which inhibits particularly Lgr5+ cells, but not Axin2+ cells. Therefore, even when WNT signaling is induced in the Lgr5+ cells, they are still limited to the niche enriched by BMP inhibitors and cannot expand to the BMP2+ compartment.

While recent data suggest that BMP and WNT signaling act independently on expression of stem cell associated genes such as Lgr5 on cellular signaling level, I found that BMP pathway regulates expression of stromal Rspo3. RSPO3, an essential regulator of WNT

signaling in the stomach described by Sigal et al., has its source in myofibroblasts located beneath the glands (Sigal et al. 2017). Culture of the myofibroblasts isolated from the entire antrum (including subpopulations from beneath the gland as well as intraglandular cells) revealed that their expression of Rspo3 is reduced upon BMP activation and is induced with BMP inhibition (Figure 3.16.). These results suggest that Rspo3 is limited to the basal myofibroblasts, because it is suppressed elsewhere by BMP signaling and can be only expressed in the niche lacking BMP signaling. Moreover, its induction and expansion from the base to the stroma along the gland axis, which is observed upon *H. pylori* infection, may be explained by decreasing BMP gradient (Figure 3.7. and 3.8.) (Sigal et al. 2017). Taken together I could identify multiple intercellular communication routes that guide epithelial proliferation and differentiation, including an induction of a paracrine and autocrine Bmp feed forward loop that not only stabilizes epithelial differentiation but also blocks opposing stromal signals such as Rspo3 expression.

4.3 IFNγ INTERACTIONS WITH BMP SIGNALING

Infection with *H. pylori* induces changes in gland organization which further leads to gastric pathologies and even cancer (Correa and Piazuelo 2012). Since BMP2 signaling was identified as a main driver of gastric gland differentiation and its expression changed upon infection, its regulation in the context of infection was analyzed. The results revealed that inhibition of Bmp2 expression and subsequent hyperproliferation and hyperplasia upon infection depend on functional *H. pylori* T4SS (Figure 3.17.a-c), which is consistent with previous data that reported less severe gastric pathology evoked by strains lacking the cagPAI pathogenicity island compared to wildtype *H. pylori* (Sigal et al. 2015). Furthermore, functional T4SS has been demonstrated to be required to induce a recruitment of proinflammatory subsets of immune cells to the site of the infection (Arnold, Lee, et al. 2011). These cells, particularly Th1 cells, are mostly producing IFNγ as a response to the infection (Smythies et al. 2000). Consistently, my results showed that IFNγ and IFNγ target genes are highly upregulated upon *H. pylori* infection and that IFNγ induction is much lower in mice infected with mutants in the functional T4SS (Figure 3.17.d-e).

IFNγ function analysis with organoid model revealed its inhibitory effect on BMP signaling, which was obtained even with small concentrations of the protein. It did not only reduce the expression of overall BMP target gene Id1 by half, but also strongly decreased expression of Bmp2 itself (Figure 3.18.a-c). Microarray analysis confirmed these results and showed significant inhibition of BMP2 targets and induction of genes identified as down-regulated BMP2 targets in organoids treated with IFNγ (Figure 3.18.d-e). These data may explain the previously described gastric phenotypes induced by IFNγ, described by scientists: Sayi and colleagues have identified IFNγ as a factor responsible for induction of chronic inflammation, hyperplasia and atrophy upon *H. pylori* infection. Using IFNγ-deficient mice, they have not observed any of these pathological changes (Sayi et al. 2009). Additionally, Zuo et al. performed the opposite experiment, in which they injected recombinant IFNγ into the mice for 21 days and have reported epithelial hyperproliferation and atrophy (Zuo et al. 2019). These findings may be explained by changes in BMP signaling induced by IFNγ: IFNγ KO mice should not have any changes in Bmp2 expression, whereas injection of IFNγ should induce loss of BMP signaling and loss of Bmp2 expression. Indeed, effects of Bmp KO on gastric epithelial pathology appear to be resembled by IFNγ injection into mice.

Not only hyperplasia has been identified as an IFNγ-induced alteration of epithelial organization in the stomach. It has been reported that IFNγ is inducing gastric mucous neck cells hypertrophy and suppression of Muc5ac expression (Kang et al. 2005; Oyanagi et al. 2017). Additionally, in the small intestine IFNγ treatment results in release of antimicrobial products by Paneth cells (Farin et al. 2014). These observations inversely correlate with BMP function described here, which showed differentiation into Muc5ac+ cells, inhibition of basal markers and antimicrobial genes expressed by them upon BMP treatment (Figure 3.9. and 3.11.). Therefore, it is likely that the previously described IFNγ dependent phenotypes are mediated via reduction in BMP signaling. Further experiments would be required to determinate interactions between IFNγ and BMP signaling and specific role of IFNγ in different gastric cell types. For example, investigation of Bmp2 expression upon depletion of IFNγ specifically in the epithelium. Moreover, the effect of the IFNγ on stromal BMP signaling requires further attention.

Since BMP signaling inhibits proliferation and IFNγ is reducing BMP, I expected that addition of IFNγ to the organoid culture will improve their growth and development. However, number of organoids cultured with recombinant IFNγ was smaller compared to untreated control (Figure 3.19.a). This was consistent with observations reported by others, which described organoid cell apoptosis upon IFNγ treatment and overall anti-proliferative character of IFNγ (Osaki et al. 2019; Schroder et al. 2004). Lineage tracing for Lgr5+ stem cells performed in this study revealed that more organoids created upon IFNγ treatment are deriving from Lgr5-negative cells compared to untreated controls, suggesting the involvement of some other cell type (Figure 3.19.b). Therefore, to identify these cells, I decided to investigate IFNγ influence on cells differentiated by BMP2 and found that although IFNγ is inhibiting proliferation in stem cells, it appears to block terminal differentiation induced by BMPs, allowing recruitment of differentiating cells to the stem cell pool once exposed to stem cell signals (Figure 3.19.c-d). These results appear to be consistent to observations described in the murine stomach, which have shown induction of quiescence of multi-lineage progenitors upon IFNγ administration (Qiao et al. 2007). Moreover, it also provides an explanation for reported hyperplasia upon IFNγ treatment and its absence in IFNγ-deficient mice despite IFNγ anti-proliferative role (Sayi et al. 2009; Zuo et al. 2019). While IFNγ does not promote proliferation itself, it enhances the plasticity and extends pool of cells able to respond to pro-proliferative signals. Thus, these observations indicate a mechanism of epithelial re-arrangements upon *H. pylori*, which is driven by IFN-γ that blocks BMP2-driven terminal differentiation, thereby preserves plasticity in differentiating cells, finally resulting in hyperplasia, hyperproliferation, induction of basal and inhibition of surface cells (Figure 3.3. and 3.10.). However, some further *in vivo* experiments, for example with transgenic IFNγKO mice, are required to confirm these findings.

4.4 TISSUE ADAPTATION TO INFECTION AND CANCER PHENOTYPE

Gastric cancer development has been described as a process reflected by histological changes, termed Correa's cascade. This describes changes from normal gastric mucosa to chronic gastritis, atrophy, intestinal metaplasia, dysplasia and finally gastric cancer (Correa 1992; Correa and Piazuelo 2012). *H. pylori* has been identified as a factor

inducing inflammation, which leads to hyperplastic gastritis, atrophy and metaplasia (Sigal et al. 2015; Weck and Brenner 2008; Byrd and Bresalier 2000). Here, I identified IFNγ as a main regulator of epithelial organization and found that one of its effects is the inhibition of BMP signaling (Figure 3.18.). This Thesis has shown that BMP signaling directs differentiation of gastric epithelial cells into highly differentiated pit surface mucous cells (Figure 3.9.).

These observations provide new mechanistic links between infection, inflammation and epithelial homeostasis. Hyperproliferation and hyperplasia observed upon *H. pylori* infection (Abraham et al. 2001; Sigal et al. 2015) may be the result of BMP signaling inhibition via IFNγ (Figure 3.17 and 3.18.). Atrophy, which describes the loss of differentiated cells, as a second step of Correa's cascade (Kuipers et al. 1997) can be explained by impaired differentiation as a result of IFNγ-driven inhibition of terminal differentiation (Figure 3.19.). Moreover, infection with *H. pylori* has been correlated with disturbed mucus production: reduction of pit surface mucous producing cells and hypertrophy of mucous neck cells (Byrd and Bresalier 2000). Loss of pit surface mucous producing cells is the characteristic feature of intestinal metaplasia (Park et al. 2015), whereas expression of mucous neck cells in dysplastic lesions has been identified as a predictor for malignant progression (Marin et al. 2012). These findings may be also explained by the impaired BMP signaling upon infection, which regulates proper differentiation into pit surface mucous cells and inhibits expression of mucous neck cells during homeostasis (Figure 3.9.).

Taken together, my results suggest that BMP signaling reduction by IFNγ upon *H. pylori* infection contributes to development of premalignant lesions, such as hyperplasia, atrophy and metaplasia. Loss of differentiated cells and expansion of stem and progenitor cells upon infection may lead to a disrupter barrier and enhanced exposure of stem cells towards the potentially toxic luminal content in the stomach, which may not only lead to direct genomic damage in stem cells but also further perpetuate the inflammatory cascade overall enhancing the risk for development of gastric cancer.

4.5 OUTLOOK

These studies highlight a mechanism related to the molecular communication between inflammation and epithelial organization. The observations may not be limited to stomach and *H. pylori* infection but rather have broader implications. Accordingly, impaired differentiation appears to be a hallmark of inflammation in the whole gastrointestinal tract. Studies have reported loss of goblet cells in both colon during ulcerative colitis and small intestine during inflammatory bowel disease as well as loss of secretory cells in the stomach with infection or inflammatory conditions (Parker et al. 2019; Gersemann et al. 2009; Peek et al. 1997). Moreover, alternations in differentiation during inflammation refer not only to cell loss but also to enhanced plasticity. Injury in the colon leads to repopulation of the crypts by highly differentiated Atoh1+ and Krt20+ cells (Castillo-Azofeifa et al. 2019; Harnack et al. 2019). Irradiation of the small intestine is inducing proliferation and multipotency in mature Paneth cells as well as injury in the Alpi+ enterocytes (Yu et al. 2018; Tetteh et al. 2016). Even in the stomach, quiescent Troy+ chief cells have been reported to replenish entire gastric units upon tissue damage (Stange et al. 2013). These observations have shown that also in other organs upon inflammation stem cells properties are induced in highly differentiated cells. Together with the fact that BMP signaling is present in all organs and results showing BMP-driven differentiation mechanism presented in these studies, it suggests the potential role of BMP pathway as universal regulatory principle of tissue plasticity apart from classical inflammatory triggers in the entire gastrointestinal tract. Therefore, exploration of BMP signaling in context of the inflammation in different organs of the gastrointestinal tract will be important for generalizing based on my observations.

Furthermore, the involvement of *H. pylori* in gastric cancer development paired with the prominent regulatory function of BMP signaling in epithelial re-organization upon infection may implicate BMP involvement in cancer development. Respective observations from colon studies indeed revealed a strong reduction of BMP2 in cancer samples (Vishnubalaji et al. 2016). Moreover, the facts that *in vitro* re-expression of Bmp2 in cancer cell lines led to inhibition of cell growth and increased chemosensitivity and that overexpression of Bmp2 *in vivo* inhibited tumor formation suggests BMP2 is a critical suppressor of tumorigenesis, probably due to its effects on differentiation. It

implies that targeting Bmp2 could be used as a therapeutic strategy (Vishnubalaji et al. 2016). On the other hand, BMP7, which was not detected here in the normal homeostatic stomach, has been reported as a potential predictor of risk of tumor recurrence in gastric cancer (Aoki et al. 2011). Additionally, KO of Bmpr1a in gastric mesenchyme resulted in the induction of reactive mesenchyme, which expressed Cancer-Associated-Fibroblasts markers (Roy et al. 2016). Finally, studies from stomach addressing the role of BMP2 in gastric cancer cell lines indicated dual functions of BMP2 as both promotor and suppressor of the cancer (Kang et al. 2011; Zhang et al. 2012). Thus, the important role of BMP signaling in gland turnover, its alterations in chronic inflammation and its effects on gastric cancer cell lines are calling for further investigations on the role of BMP pathway in development of gastric cancer.

References

Abraham, S. C., V. K. Singh, J. H. Yardley, and T. T. Wu. 2001. 'Hyperplastic polyps of the stomach: associations with histologic patterns of gastritis and gastric atrophy', *Am J Surg Pathol*, 25: 500-7.

Alarmo, E. L., T. Korhonen, T. Kuukasjarvi, H. Huhtala, K. Holli, and A. Kallioniemi. 2008. 'Bone morphogenetic protein 7 expression associates with bone metastasis in breast carcinomas', *Ann Oncol*, 19: 308-14.

Allison, C. C., J. Ferrand, L. McLeod, M. Hassan, M. Kaparakis-Liaskos, A. Grubman, P. S. Bhathal, A. Dev, W. Sievert, B. J. Jenkins, and R. L. Ferrero. 2013. 'Nucleotide oligomerization domain 1 enhances IFN-gamma signaling in gastric epithelial cells during Helicobacter pylori infection and exacerbates disease severity', *J Immunol*, 190: 3706-15.

Alm, R. A., J. Bina, B. M. Andrews, P. Doig, R. E. Hancock, and T. J. Trust. 2000. 'Comparative genomics of Helicobacter pylori: analysis of the outer membrane protein families', *Infect Immun*, 68: 4155-68.

Alsayed, Y., S. Uddin, S. Ahmad, B. Majchrzak, B. J. Druker, E. N. Fish, and L. C. Platanias. 2000. 'IFN-gamma activates the C3G/Rap1 signaling pathway', *J Immunol*, 164: 1800-6.

Anders, S., P. T. Pyl, and W. Huber. 2015. 'HTSeq--a Python framework to work with high-throughput sequencing data', *Bioinformatics*, 31: 166-9.

Aoki, M., S. Ishigami, Y. Uenosono, T. Arigami, Y. Uchikado, Y. Kita, H. Kurahara, M. Matsumoto, S. Ueno, and S. Natsugoe. 2011. 'Expression of BMP-7 in human gastric cancer and its clinical significance', *Br J Cancer*, 104: 714-8.

Aoki, R., M. Shoshkes-Carmel, N. Gao, S. Shin, C. L. May, M. L. Golson, A. M. Zahm, M. Ray, C. L. Wiser, C. V. Wright, and K. H. Kaestner. 2016. 'Foxl1-expressing mesenchymal cells constitute the intestinal stem cell niche', *Cell Mol Gastroenterol Hepatol*, 2: 175-88.

Arnold, I. C., J. Y. Lee, M. R. Amieva, A. Roers, R. A. Flavell, T. Sparwasser, and A. Muller. 2011. 'Tolerance rather than immunity protects from Helicobacter pylori-induced gastric preneoplasia', *Gastroenterology*, 140: 199-209.

Arnold, K., A. Sarkar, M. A. Yram, J. M. Polo, R. Bronson, S. Sengupta, M. Seandel, N. Geijsen, and K. Hochedlinger. 2011. 'Sox2(+) adult stem and progenitor cells are important for tissue regeneration and survival of mice', *Cell Stem Cell*, 9: 317-29.

Arrabal, P. M., R. Visser, L. Santos-Ruiz, J. Becerra, and M. Cifuentes. 2013. 'Osteogenic molecules for clinical applications: improving the BMP-collagen system', *Biol Res*, 46: 421-9.

Asao, H., and X. Y. Fu. 2000. 'Interferon-gamma has dual potentials in inhibiting or promoting cell proliferation', *J Biol Chem*, 275: 867-74.

Auclair, B. A., Y. D. Benoit, N. Rivard, Y. Mishina, and N. Perreault. 2007. 'Bone morphogenetic protein signaling is essential for terminal differentiation of the intestinal secretory cell lineage', *Gastroenterology*, 133: 887-96.

Axelrod, J. D. 2009. 'Progress and challenges in understanding planar cell polarity signaling', *Semin Cell Dev Biol*, 20: 964-71.

Bach, D. H., H. J. Park, and S. K. Lee. 2018. 'The Dual Role of Bone Morphogenetic Proteins in Cancer', *Mol Ther Oncolytics*, 8: 1-13.

Baldridge, M. T., K. Y. King, N. C. Boles, D. C. Weksberg, and M. A. Goodell. 2010. 'Quiescent haematopoietic stem cells are activated by IFN-gamma in response to chronic infection', *Nature*, 465: 793-7.

Baldwin, D. N., B. Shepherd, P. Kraemer, M. K. Hall, L. K. Sycuro, D. M. Pinto-Santini, and N. R. Salama. 2007. 'Identification of Helicobacter pylori genes that contribute to stomach colonization', *Infect Immun*, 75: 1005-16.

Balfour, A. 1906. 'A haemogregarine of mammals and some notes on trypanosomiasis in the Anglo-Egyptian Sudan', *J Trop Med*, 9: 81-92.

Ban, S., and M. Shimizu. 2009. 'Muscularis mucosae in desmoplastic stroma formation of early invasive rectal adenocarcinoma', *World J Gastroenterol*, 15: 4976-9.

Bandyopadhyay, A., K. Tsuji, K. Cox, B. D. Harfe, V. Rosen, and C. J. Tabin. 2006. 'Genetic analysis of the roles of BMP2, BMP4, and BMP7 in limb patterning and skeletogenesis', *PLoS Genet*, 2: e216.

Barker, N., and H. Clevers. 2010. 'Leucine-rich repeat-containing G-protein-coupled receptors as markers of adult stem cells', *Gastroenterology*, 138: 1681-96.

Barker, N., M. Huch, P. Kujala, M. van de Wetering, H. J. Snippert, J. H. van Es, T. Sato, D. E. Stange, H. Begthel, M. van den Born, E. Danenberg, S. van den Brink, J. Korving, A. Abo, P. J. Peters, N. Wright, R. Poulsom, and H. Clevers. 2010. 'Lgr5(+ve) stem cells drive self-renewal in the stomach and build long-lived gastric units in vitro', *Cell Stem Cell*, 6: 25-36.

Barker, N., J. H. van Es, J. Kuipers, P. Kujala, M. van den Born, M. Cozijnsen, A. Haegebarth, J. Korving, H. Begthel, P. J. Peters, and H. Clevers. 2007. 'Identification of stem cells in small intestine and colon by marker gene Lgr5', *Nature*, 449: 1003-7.

Bartfeld, S., T. Bayram, M. van de Wetering, M. Huch, H. Begthel, P. Kujala, R. Vries, P. J. Peters, and H. Clevers. 2015. 'In vitro expansion of human gastric epithelial stem cells and their responses to bacterial infection', *Gastroenterology*, 148: 126-36 e6.

Batts, L. E., D. B. Polk, R. N. Dubois, and H. Kulessa. 2006. 'Bmp signaling is required for intestinal growth and morphogenesis', *Dev Dyn*, 235: 1563-70.

Bauer, B., E. Pang, C. Holland, M. Kessler, S. Bartfeld, and T. F. Meyer. 2012. 'The Helicobacter pylori virulence effector CagA abrogates human beta-defensin 3 expression via inactivation of EGFR signaling', *Cell Host Microbe*, 11: 576-86.

Beatty, G., and Y. Paterson. 2001. 'IFN-gamma-dependent inhibition of tumor angiogenesis by tumor-infiltrating CD4+ T cells requires tumor responsiveness to IFN-gamma', *J Immunol*, 166: 2276-82.

Benjamini, Y., and Y. Hochberg. 1995. 'Controlling the false discovery rate: a practical and powerful approach to multiple testing', *J. R. Statist. Soc.*, 57: 289-300.

Billiau, A., and P. Matthys. 2009. 'Interferon-gamma: a historical perspective', *Cytokine Growth Factor Rev*, 20: 97-113.

Blouin, C. M., Y. Hamon, P. Gonnord, C. Boularan, J. Kagan, C. Viaris de Lesegno, R. Ruez, S. Mailfert, N. Bertaux, D. Loew, C. Wunder, L. Johannes, G. Vogt, F. X. Contreras, D. Marguet, J. L. Casanova, C. Gales, H. T. He, and C. Lamaze. 2016. 'Glycosylation-Dependent IFN-gammaR Partitioning in Lipid and Actin Nanodomains Is Critical for JAK Activation', *Cell*, 166: 920-34.

Boccellato, F., S. Woelffling, A. Imai-Matsushima, G. Sanchez, C. Goosmann, M. Schmid, H. Berger, P. Morey, C. Denecke, J. Ordemann, and T. F. Meyer. 2018. 'Polarised epithelial monolayers of the gastric mucosa reveal insights into mucosal homeostasis and defence against infection', *Gut*.

Boonyanugomol, W., C. Chomvarin, C. Hahnvajanawong, B. Sripa, M. Kaparakis-Liaskos, and R. L. Ferrero. 2013. 'Helicobacter pylori cag pathogenicity island (cagPAI) involved in bacterial internalization and IL-8 induced responses via NOD1- and MyD88-dependent mechanisms in human biliary epithelial cells', *PLoS One*, 8: e77358.

Broda, T. R., K. W. McCracken, and J. M. Wells. 2019. 'Generation of human antral and fundic gastric organoids from pluripotent stem cells', *Nat Protoc*, 14: 28-50.

Budna, J., M. Rybska, S. Ciesiolka, A. Bryja, S. Borys, W. Kranc, K. Wojtanowicz-Markiewicz, M. Jeseta, E. Sumelka, D. Bukowska, P. Antosik, K. P. Brussow, M. Bruska, M. Nowicki, M. Zabel, and B. Kempisty. 2017. 'Expression of genes associated with BMP signaling pathway in porcine oocytes before and after IVM - a microarray approach', *Reprod Biol Endocrinol*, 15: 43.

Burkitt, M. D., C. A. Duckworth, J. M. Williams, and D. M. Pritchard. 2017. 'Helicobacter pylori-induced gastric pathology: insights from in vivo and ex vivo models', *Dis Model Mech*, 10: 89-104.

Byrd, J. C., and R. S. Bresalier. 2000. 'Alterations in gastric mucin synthesis by Helicobacter pylori', *World J Gastroenterol*, 6: 475-82.

Castillo-Azofeifa, D., E. N. Fazio, R. Nattiv, H. J. Good, T. Wald, M. A. Pest, F. J. de Sauvage, O. D. Klein, and S. Asfaha. 2019. 'Atoh1(+) secretory progenitors possess renewal capacity independent of Lgr5(+) cells during colonic regeneration', *EMBO J*, 38.

Castro, F., A. P. Cardoso, R. M. Goncalves, K. Serre, and M. J. Oliveira. 2018. 'Interferon-Gamma at the Crossroads of Tumor Immune Surveillance or Evasion', *Front Immunol*, 9: 847.

Chaudhry, S. R., M. N. P. Liman, and D. C. Peterson. 2019. 'Anatomy, Abdomen and Pelvis, Stomach.' in, *StatPearls* (Treasure Island (FL)).

Chen, J., B. T. Lau, N. Andor, S. M. Grimes, C. Handy, C. Wood-Bouwens, and H. P. Ji. 2019. 'Single-cell transcriptome analysis identifies distinct cell types and niche signaling in a primary gastric organoid model', *Sci Rep*, 9: 4536.

Chen, X., J. Liao, Y. Lu, X. Duan, and W. Sun. 2011. 'Activation of the PI3K/Akt pathway mediates bone morphogenetic protein 2-induced invasion of pancreatic cancer cells Panc-1', *Pathol Oncol Res*, 17: 257-61.

Cherwinski, H. M., J. H. Schumacher, K. D. Brown, and T. R. Mosmann. 1987. 'Two types of mouse helper T cell clone. III. Further differences in lymphokine synthesis between Th1 and Th2 clones

revealed by RNA hybridization, functionally monospecific bioassays, and monoclonal antibodies', *J Exp Med*, 166: 1229-44.

Choi, E., T. L. Lantz, G. Vlacich, T. M. Keeley, L. C. Samuelson, R. J. Coffey, J. R. Goldenring, and A. E. Powell. 2018. 'Lrig1+ gastric isthmal progenitor cells restore normal gastric lineage cells during damage recovery in adult mouse stomach', *Gut*, 67: 1595-605.

Choi, E., J. T. Roland, B. J. Barlow, R. O'Neal, A. E. Rich, K. T. Nam, C. Shi, and J. R. Goldenring. 2014. 'Cell lineage distribution atlas of the human stomach reveals heterogeneous gland populations in the gastric antrum', *Gut*, 63: 1711-20.

Christiansen, J. H., E. G. Coles, and D. G. Wilkinson. 2000. 'Molecular control of neural crest formation, migration and differentiation', *Curr Opin Cell Biol*, 12: 719-24.

Churchill, G. A. 2002. 'Fundamentals of experimental design for cDNA microarrays', *Nat Genet*, 32 Suppl: 490-5.

Co, J. Y., M. Margalef-Catala, X. Li, A. T. Mah, C. J. Kuo, D. M. Monack, and M. R. Amieva. 2019. 'Controlling Epithelial Polarity: A Human Enteroid Model for Host-Pathogen Interactions', *Cell Rep*, 26: 2509-20 e4.

Cooke, A. R. 1975. 'Control of gastric emptying and motility', *Gastroenterology*, 68: 804-16.

Correa, P. 1992. 'Human gastric carcinogenesis: a multistep and multifactorial process--First American Cancer Society Award Lecture on Cancer Epidemiology and Prevention', *Cancer Res*, 52: 6735-40.

Correa, P., W. Haenszel, C. Cuello, S. Tannenbaum, and M. Archer. 1975. 'A model for gastric cancer epidemiology', *Lancet*, 2: 58-60.

Correa, P., and M. B. Piazuelo. 2012. 'The gastric precancerous cascade', *J Dig Dis*, 13: 2-9.

Crabtree, J. E., J. D. Taylor, J. I. Wyatt, R. V. Heatley, T. M. Shallcross, D. S. Tompkins, and B. J. Rathbone. 1991. 'Mucosal IgA recognition of Helicobacter pylori 120 kDa protein, peptic ulceration, and gastric pathology', *Lancet*, 338: 332-5.

D'Amico M, A., B. Ghinassi, P. Izzicupo, L. Manzoli, and A. Di Baldassarre. 2014. 'Biological function and clinical relevance of chromogranin A and derived peptides', *Endocr Connect*, 3: R45-54.

De, A. 2011. 'Wnt/Ca2+ signaling pathway: a brief overview', *Acta Biochim Biophys Sin (Shanghai)*, 43: 745-56.

de Caestecker, M. 2004. 'The transforming growth factor-beta superfamily of receptors', *Cytokine Growth Factor Rev*, 15: 1-11.

de Lau, W. B., B. Snel, and H. C. Clevers. 2012. 'The R-spondin protein family', *Genome Biol*, 13: 242.

de Lau, W., N. Barker, T. Y. Low, B. K. Koo, V. S. Li, H. Teunissen, P. Kujala, A. Haegebarth, P. J. Peters, M. van de Wetering, D. E. Stange, J. E. van Es, D. Guardavaccaro, R. B. Schasfoort, Y. Mohri, K. Nishimori, S. Mohammed, A. J. Heck, and H. Clevers. 2011. 'Lgr5 homologues associate with Wnt receptors and mediate R-spondin signalling', *Nature*, 476: 293-7.

Decker, T., P. Kovarik, and A. Meinke. 1997. 'GAS elements: a few nucleotides with a major impact on cytokine-induced gene expression', *J Interferon Cytokine Res*, 17: 121-34.

DeGrado, W. F., Z. R. Wasserman, and V. Chowdhry. 1982. 'Sequence and structural homologies among type I and type II interferons', *Nature*, 300: 379-81.

Demitrack, E. S., G. B. Gifford, T. M. Keeley, A. J. Carulli, K. L. VanDussen, D. Thomas, T. J. Giordano, Z. Liu, R. Kopan, and L. C. Samuelson. 2015. 'Notch signaling regulates gastric antral LGR5 stem cell function', *EMBO J*, 34: 2522-36.

Dighe, A. S., E. Richards, L. J. Old, and R. D. Schreiber. 1994. 'Enhanced in vivo growth and resistance to rejection of tumor cells expressing dominant negative IFN gamma receptors', *Immunity*, 1: 447-56.

Dobin, A., C. A. Davis, F. Schlesinger, J. Drenkow, C. Zaleski, S. Jha, P. Batut, M. Chaisson, and T. R. Gingeras. 2013. 'STAR: ultrafast universal RNA-seq aligner', *Bioinformatics*, 29: 15-21.

Doenges, J. L. 1939. 'Spirochaetes in the gastric glands of Macacus rhesus and humans without definite history of related disease', *Arch Pathol*, 27: 469-77.

Dominici, P., S. Bellentani, A. R. Di Biase, G. Saccoccio, A. Le Rose, F. Masutti, L. Viola, F. Balli, C. Tiribelli, R. Grilli, M. Fusillo, and E. Grossi. 1999. 'Familial clustering of Helicobacter pylori infection: population based study', *BMJ*, 319: 537-40.

Duan, Y., W. Zhu, M. Liu, M. Ashraf, and M. Xu. 2017. 'The expression of Smad signaling pathway in myocardium and potential therapeutic effects', *Histol Histopathol*, 32: 651-59.

Dunn, B. E., H. Cohen, and M. J. Blaser. 1997. 'Helicobacter pylori', *Clin Microbiol Rev*, 10: 720-41.

Dutta, T., A. Spence, and L. A. Lampson. 2003. 'Robust ability of IFN-gamma to upregulate class II MHC antigen expression in tumor bearing rat brains', *J Neurooncol*, 64: 31-44.

Eidt, S., and M. Stolte. 1994. 'Prevalence of intestinal metaplasia in Helicobacter pylori gastritis', *Scand J Gastroenterol*, 29: 607-10.

Einhorn, T. A. 2003. 'Clinical applications of recombinant human BMPs: early experience and future development', *J Bone Joint Surg Am*, 85-A Suppl 3: 82-8.

Escobar, M. L., and E. Kawakami. 2004. 'Evidence of mother-child transmission of Helicobacter pylori infection', *Arq Gastroenterol*, 41: 239-44.

Evans, M. K., C. R. Yu, A. Lohani, R. M. Mahdi, X. Liu, A. R. Trzeciak, and C. E. Egwuagu. 2007. 'Expression of SOCS1 and SOCS3 genes is differentially regulated in breast cancer cells in response to proinflammatory cytokine and growth factor signals', *Oncogene*, 26: 1941-8.

Falk, P., K. A. Roth, and J. I. Gordon. 1994. 'Lectins are sensitive tools for defining the differentiation programs of mouse gut epithelial cell lineages', *Am J Physiol*, 266: G987-1003.

Farin, H. F., W. R. Karthaus, P. Kujala, M. Rakhshandehroo, G. Schwank, R. G. Vries, E. Kalkhoven, E. E. Nieuwenhuis, and H. Clevers. 2014. 'Paneth cell extrusion and release of antimicrobial products is directly controlled by immune cell-derived IFN-gamma', *J Exp Med*, 211: 1393-405.

Fischer, A. S., and M. Sigal. 2019. 'The Role of Wnt and R-spondin in the Stomach During Health and Disease', *Biomedicines*, 7.

Frucht, D. M., T. Fukao, C. Bogdan, H. Schindler, J. J. O'Shea, and S. Koyasu. 2001. 'IFN-gamma production by antigen-presenting cells: mechanisms emerge', *Trends Immunol*, 22: 556-60.

Fukuda, H., D. Saito, S. Hayashi, H. Hisai, H. Ono, S. Yoshida, Y. Oguro, T. Noda, T. Sato, M. Katoh, and et al. 1995. 'Helicobacter pylori infection, serum pepsinogen level and gastric cancer: a case-control study in Japan', *Jpn J Cancer Res*, 86: 64-71.

Gall, A., R. G. Gaudet, S. D. Gray-Owen, and N. R. Salama. 2017. 'TIFA Signaling in Gastric Epithelial Cells Initiates the cag Type 4 Secretion System-Dependent Innate Immune Response to Helicobacter pylori Infection', *MBio*, 8.

Gao, H., J. Y. Wang, X. Z. Shen, and J. J. Liu. 2000. 'Effect of Helicobacter pylori infection on gastric epithelial cell proliferation', *World J Gastroenterol*, 6: 442-44.

Gartner, K., and J. Pfaff. 1979. 'The forestomach in rats and mice, a food store without bacterial protein digestion', *Zentralbl Veterinarmed A*, 26: 530-41.

Gersemann, M., S. Becker, I. Kubler, M. Koslowski, G. Wang, K. R. Herrlinger, J. Griger, P. Fritz, K. Fellermann, M. Schwab, J. Wehkamp, and E. F. Stange. 2009. 'Differences in goblet cell differentiation between Crohn's disease and ulcerative colitis', *Differentiation*, 77: 84-94.

Gil, M. P., E. Bohn, A. K. O'Guin, C. V. Ramana, B. Levine, G. R. Stark, H. W. Virgin, and R. D. Schreiber. 2001. 'Biologic consequences of Stat1-independent IFN signaling', *Proc Natl Acad Sci U S A*, 98: 6680-5.

Goldenring, J. R., K. T. Nam, and J. C. Mills. 2011. 'The origin of pre-neoplastic metaplasia in the stomach: chief cells emerge from the Mist', *Exp Cell Res*, 317: 2759-64.

Gray, P. W., and D. V. Goeddel. 1982. 'Structure of the human immune interferon gene', *Nature*, 298: 859-63.

Gregorieff, A., D. Pinto, H. Begthel, O. Destree, M. Kielman, and H. Clevers. 2005. 'Expression pattern of Wnt signaling components in the adult intestine', *Gastroenterology*, 129: 626-38.

Groppe, J., J. Greenwald, E. Wiater, J. Rodriguez-Leon, A. N. Economides, W. Kwiatkowski, M. Affolter, W. W. Vale, J. C. Izpisua Belmonte, and S. Choe. 2002. 'Structural basis of BMP signalling inhibition by the cystine knot protein Noggin', *Nature*, 420: 636-42.

Han, S., J. Fink, D. J. Jorg, E. Lee, M. K. Yum, L. Chatzeli, S. R. Merker, M. Josserand, T. Trendafilova, A. Andersson-Rolf, C. Dabrowska, H. Kim, R. Naumann, J. H. Lee, N. Sasaki, R. L. Mort, O. Basak, H. Clevers, D. E. Stange, A. Philpott, J. K. Kim, B. D. Simons, and B. K. Koo. 2019. 'Defining the Identity and Dynamics of Adult Gastric Isthmus Stem Cells', *Cell Stem Cell*, 25: 342-56 e7.

Hanby, A. M., R. Poulsom, R. J. Playford, and N. A. Wright. 1999. 'The mucous neck cell in the human gastric corpus: a distinctive, functional cell lineage', *J Pathol*, 187: 331-7.

Haramis, A. P., H. Begthel, M. van den Born, J. van Es, S. Jonkheer, G. J. Offerhaus, and H. Clevers. 2004. 'De novo crypt formation and juvenile polyposis on BMP inhibition in mouse intestine', *Science*, 303: 1684-6.

Harnack, C., H. Berger, A. Antanaviciute, R. Vidal, S. Sauer, A. Simmons, T. F. Meyer, and M. Sigal. 2019. 'R-spondin 3 promotes stem cell recovery and epithelial regeneration in the colon', *Nat Commun*, 10: 4368.

Harris, D. P., L. Haynes, P. C. Sayles, D. K. Duso, S. M. Eaton, N. M. Lepak, L. L. Johnson, S. L. Swain, and F. E. Lund. 2000. 'Reciprocal regulation of polarized cytokine production by effector B and T cells', *Nat Immunol*, 1: 475-82.

Harrison, C. A., S. L. Al-Musawi, and K. L. Walton. 2011. 'Prodomains regulate the synthesis, extracellular localisation and activity of TGF-beta superfamily ligands', *Growth Factors*, 29: 174-86.

Hata, M., Y. Hayakawa, and K. Koike. 2018. 'Gastric Stem Cell and Cellular Origin of Cancer', *Biomedicines*, 6.

Hatakeyama, M. 2004. 'Oncogenic mechanisms of the Helicobacter pylori CagA protein', *Nat Rev Cancer*, 4: 688-94.

———. 2014. 'Helicobacter pylori CagA and gastric cancer: a paradigm for hit-and-run carcinogenesis', *Cell Host Microbe*, 15: 306-16.

Hayakawa, Y., H. Ariyama, J. Stancikova, K. Sakitani, S. Asfaha, B. W. Renz, Z. A. Dubeykovskaya, W. Shibata, H. Wang, C. B. Westphalen, X. Chen, Y. Takemoto, W. Kim, S. S. Khurana, Y. Tailor, K. Nagar, H. Tomita, A. Hara, A. R. Sepulveda, W. Setlik, M. D. Gershon, S. Saha, L. Ding, Z. Shen, J. G. Fox, R. A. Friedman, S. F. Konieczny, D. L. Worthley, V. Korinek, and T. C. Wang. 2015. 'Mist1 Expressing Gastric Stem Cells Maintain the Normal and Neoplastic Gastric Epithelium and Are Supported by a Perivascular Stem Cell Niche', *Cancer Cell*, 28: 800-14.

He, X. C., J. Zhang, W. G. Tong, O. Tawfik, J. Ross, D. H. Scoville, Q. Tian, X. Zeng, X. He, L. M. Wiedemann, Y. Mishina, and L. Li. 2004. 'BMP signaling inhibits intestinal stem cell self-renewal through suppression of Wnt-beta-catenin signaling', *Nat Genet*, 36: 1117-21.

Heldin, C. H., K. Miyazono, and P. ten Dijke. 1997. 'TGF-beta signalling from cell membrane to nucleus through SMAD proteins', *Nature*, 390: 465-71.

Herring, B. P., A. M. Hoggatt, C. Burlak, and S. Offermanns. 2014. 'Previously differentiated medial vascular smooth muscle cells contribute to neointima formation following vascular injury', *Vasc Cell*, 6: 21.

Hoeksema, M. A., B. P. Scicluna, M. C. Boshuizen, S. van der Velden, A. E. Neele, J. Van den Bossche, H. L. Matlung, T. K. van den Berg, P. Goossens, and M. P. de Winther. 2015. 'IFN-gamma priming of macrophages represses a part of the inflammatory program and attenuates neutrophil recruitment', *J Immunol*, 194: 3909-16.

Hooi, J. K. Y., W. Y. Lai, W. K. Ng, M. M. Y. Suen, F. E. Underwood, D. Tanyingoh, P. Malfertheiner, D. Y. Graham, V. W. S. Wong, J. C. Y. Wu, F. K. L. Chan, J. J. Y. Sung, G. G. Kaplan, and S. C. Ng. 2017. 'Global Prevalence of Helicobacter pylori Infection: Systematic Review and Meta-Analysis', *Gastroenterology*, 153: 420-29.

Horbelt, D., A. Denkis, and P. Knaus. 2012. 'A portrait of Transforming Growth Factor beta superfamily signalling: Background matters', *Int J Biochem Cell Biol*, 44: 469-74.

Horvath, L. G., S. M. Henshall, J. G. Kench, J. J. Turner, D. Golovsky, P. C. Brenner, G. F. O'Neill, R. Kooner, P. D. Stricker, J. J. Grygiel, and R. L. Sutherland. 2004. 'Loss of BMP2, Smad8, and Smad4 expression in prostate cancer progression', *Prostate*, 59: 234-42.

Hsu, M., and F. Lui. 2019. 'Physiology, Stomach.' in, *StatPearls* (Treasure Island (FL)).

Hua, J. S., P. Y. Zheng, and H. Bow. 1999. 'Species differentiation and identification in the genus of Helicobacter', *World J Gastroenterol*, 5: 7-9.

Huang, S., W. Hendriks, A. Althage, S. Hemmi, H. Bluethmann, R. Kamijo, J. Vilcek, R. M. Zinkernagel, and M. Aguet. 1993. 'Immune response in mice that lack the interferon-gamma receptor', *Science*, 259: 1742-5.

Hughes, C. S., L. M. Postovit, and G. A. Lajoie. 2010. 'Matrigel: a complex protein mixture required for optimal growth of cell culture', *Proteomics*, 10: 1886-90.

IARC. 1994. 'Schistosomes, liver flukes and Helicobacter pylori. IARC Working Group on the Evaluation of Carcinogenic Risks to Humans. Lyon, 7-14 June 1994', *IARC Monogr Eval Carcinog Risks Hum*, 61: 1-241.

Iemura, S., T. S. Yamamoto, C. Takagi, H. Uchiyama, T. Natsume, S. Shimasaki, H. Sugino, and N. Ueno. 1998. 'Direct binding of follistatin to a complex of bone-morphogenetic protein and its receptor inhibits ventral and epidermal cell fates in early Xenopus embryo', *Proc Natl Acad Sci U S A*, 95: 9337-42.

Ishijima, N., M. Suzuki, H. Ashida, Y. Ichikawa, Y. Kanegae, I. Saito, T. Boren, R. Haas, C. Sasakawa, and H. Mimuro. 2011. 'BabA-mediated adherence is a potentiator of the Helicobacter pylori type IV secretion system activity', *J Biol Chem*, 286: 25256-64.

Janda, C. Y., D. Waghray, A. M. Levin, C. Thomas, and K. C. Garcia. 2012. 'Structural basis of Wnt recognition by Frizzled', *Science*, 337: 59-64.

Jeanpierre, S., F. E. Nicolini, B. Kaniewski, C. Dumontet, R. Rimokh, A. Puisieux, and V. Maguer-Satta. 2008. 'BMP4 regulation of human megakaryocytic differentiation is involved in thrombopoietin signaling', *Blood*, 112: 3154-63.

Kang, M. H., S. C. Oh, H. J. Lee, H. N. Kang, J. L. Kim, J. S. Kim, and Y. A. Yoo. 2011. 'Metastatic function of BMP-2 in gastric cancer cells: the role of PI3K/AKT, MAPK, the NF-kappaB pathway, and MMP-9 expression', *Exp Cell Res*, 317: 1746-62.

Kang, W., S. Rathinavelu, L. C. Samuelson, and J. L. Merchant. 2005. 'Interferon gamma induction of gastric mucous neck cell hypertrophy', *Lab Invest*, 85: 702-15.

Kantani-Matsumoto, A., and K. Kataoka. 1987. 'Mucus release of surface mucous cells of the mouse stomach with special reference to cell maturation stages and dietary conditions', *Arch Histol Jpn*, 50: 273-82.

Kaplan, D. H., V. Shankaran, A. S. Dighe, E. Stockert, M. Aguet, L. J. Old, and R. D. Schreiber. 1998. 'Demonstration of an interferon gamma-dependent tumor surveillance system in immunocompetent mice', *Proc Natl Acad Sci U S A*, 95: 7556-61.

Keller, B., T. Yang, Y. Chen, E. Munivez, T. Bertin, B. Zabel, and B. Lee. 2011. 'Interaction of TGFbeta and BMP signaling pathways during chondrogenesis', *PLoS One*, 6: e16421.

Kessler, M., K. Hoffmann, V. Brinkmann, O. Thieck, S. Jackisch, B. Toelle, H. Berger, H. J. Mollenkopf, M. Mangler, J. Sehouli, C. Fotopoulou, and T. F. Meyer. 2015. 'The Notch and Wnt pathways regulate stemness and differentiation in human fallopian tube organoids', *Nat Commun*, 6: 8989.

Khatoon, J., K. N. Prasad, R. Prakash Rai, U. C. Ghoshal, and N. Krishnani. 2017. 'Association of heterogenicity of Helicobacter pylori cag pathogenicity island with peptic ulcer diseases and gastric cancer', *Br J Biomed Sci*, 74: 121-26.

Kim, J. S., J. H. Chang, S. I. Chung, and J. S. Yum. 1999. 'Molecular cloning and characterization of the Helicobacter pylori fliD gene, an essential factor in flagellar structure and motility', *J Bacteriol*, 181: 6969-76.

Kim, K. A., M. Kakitani, J. Zhao, T. Oshima, T. Tang, M. Binnerts, Y. Liu, B. Boyle, E. Park, P. Emtage, W. D. Funk, and K. Tomizuka. 2005. 'Mitogenic influence of human R-spondin1 on the intestinal epithelium', *Science*, 309: 1256-9.

Kim, T. H., and R. A. Shivdasani. 2016. 'Stomach development, stem cells and disease', *Development*, 143: 554-65.

Kimura, K., K. Satoh, K. Ido, Y. Taniguchi, T. Takimoto, and T. Takemoto. 1996. 'Gastritis in the Japanese stomach', *Scand J Gastroenterol Suppl*, 214: 17-20; discussion 21-3.

Kisonaite, M., X. Wang, and M. Hyvonen. 2016. 'Structure of Gremlin-1 and analysis of its interaction with BMP-2', *Biochem J*, 473: 1593-604.

Kleinman, H. K., M. L. McGarvey, L. A. Liotta, P. G. Robey, K. Tryggvason, and G. R. Martin. 1982. 'Isolation and characterization of type IV procollagen, laminin, and heparan sulfate proteoglycan from the EHS sarcoma', *Biochemistry*, 21: 6188-93.

Kopic, S., M. Murek, and J. P. Geibel. 2010. 'Revisiting the parietal cell', *Am J Physiol Cell Physiol*, 298: C1-C10.

Kortylewski, M., W. Komyod, M. E. Kauffmann, A. Bosserhoff, P. C. Heinrich, and I. Behrmann. 2004. 'Interferon-gamma-mediated growth regulation of melanoma cells: involvement of STAT1-dependent and STAT1-independent signals', *J Invest Dermatol*, 122: 414-22.

Kosinski, C., V. S. Li, A. S. Chan, J. Zhang, C. Ho, W. Y. Tsui, T. L. Chan, R. C. Mifflin, D. W. Powell, S. T. Yuen, S. Y. Leung, and X. Chen. 2007. 'Gene expression patterns of human colon tops and basal crypts and BMP antagonists as intestinal stem cell niche factors', *Proc Natl Acad Sci U S A*, 104: 15418-23.

Krause, C. D., E. Mei, J. Xie, Y. Jia, M. A. Bopp, R. M. Hochstrasser, and S. Pestka. 2002. 'Seeing the light: preassembly and ligand-induced changes of the interferon gamma receptor complex in cells', *Mol Cell Proteomics*, 1: 805-15.

Kuhnert, F., C. R. Davis, H. T. Wang, P. Chu, M. Lee, J. Yuan, R. Nusse, and C. J. Kuo. 2004. 'Essential requirement for Wnt signaling in proliferation of adult small intestine and colon revealed by adenoviral expression of Dickkopf-1', *Proc Natl Acad Sci U S A*, 101: 266-71.

Kuipers, E. J., E. C. Klinkenberg-Knol, C. M. Vandenbroucke-Grauls, B. J. Appelmelk, B. E. Schenk, and S. G. Meuwissen. 1997. 'Role of Helicobacter pylori in the pathogenesis of atrophic gastritis', *Scand J Gastroenterol Suppl*, 223: 28-34.

Kusters, J. G., A. H. van Vliet, and E. J. Kuipers. 2006. 'Pathogenesis of Helicobacter pylori infection', *Clin Microbiol Rev*, 19: 449-90.

Kuzaka, B., M. Janiak, K. H. Wlodarski, P. Radziszewski, and P. K. Wlodarski. 2015. 'Expression of bone morphogenetic protein-2 and -7 in urinary bladder cancer predicts time to tumor recurrence', *Arch Med Sci*, 11: 378-84.

Lahar, N., N. Y. Lei, J. Wang, Z. Jabaji, S. C. Tung, V. Joshi, M. Lewis, M. Stelzner, M. G. Martin, and J. C. Dunn. 2011. 'Intestinal subepithelial myofibroblasts support in vitro and in vivo growth of human small intestinal epithelium', *PLoS One*, 6: e26898.

Lazear, H. M., J. W. Schoggins, and M. S. Diamond. 2019. 'Shared and Distinct Functions of Type I and Type III Interferons', *Immunity*, 50: 907-23.

Lee, K. Y., J. W. Jeong, J. Wang, L. Ma, J. F. Martin, S. Y. Tsai, J. P. Lydon, and F. J. DeMayo. 2007. 'Bmp2 is critical for the murine uterine decidual response', *Mol Cell Biol*, 27: 5468-78.

Lei, H., J. Wang, P. Lu, X. Si, K. Han, T. Ruan, and J. Lu. 2016. 'BMP10 inhibited the growth and migration of gastric cancer cells', *Tumour Biol*, 37: 3025-31.

Lei, N. Y., Z. Jabaji, J. Wang, V. S. Joshi, G. J. Brinkley, H. Khalil, F. Wang, A. Jaroszewicz, M. Pellegrini, L. Li, M. Lewis, M. Stelzner, J. C. Dunn, and M. G. Martin. 2014. 'Intestinal subepithelial myofibroblasts support the growth of intestinal epithelial stem cells', *PLoS One*, 9: e84651.

Lenglinger, J., S. F. See, L. Beller, E. Cosentini, R. Asari, F. Wrba, M. Riegler, and S. F. Schoppmann. 2012. 'The cardia: esophageal or gastric? Critical reviewing the anatomy and histopathology of the esophagogastric junction', *Acta Chir Iugosl*, 59: 15-26.

Leushacke, M., A. Ng, J. Galle, M. Loeffler, and N. Barker. 2013. 'Lgr5(+) gastric stem cells divide symmetrically to effect epithelial homeostasis in the pylorus', *Cell Rep*, 5: 349-56.

Leushacke, M., S. H. Tan, A. Wong, Y. Swathi, A. Hajamohideen, L. T. Tan, J. Goh, E. Wong, Slij Denil, K. Murakami, and N. Barker. 2017. 'Lgr5-expressing chief cells drive epithelial regeneration and cancer in the oxyntic stomach', *Nat Cell Biol*, 19: 774-86.

Levine, J. S., P. K. Nakane, and R. H. Allen. 1980. 'Immunocytochemical localization of human intrinsic factor: the nonstimulated stomach', *Gastroenterology*, 79: 493-502.

Li, V. S., S. S. Ng, P. J. Boersema, T. Y. Low, W. R. Karthaus, J. P. Gerlach, S. Mohammed, A. J. Heck, M. M. Maurice, T. Mahmoudi, and H. Clevers. 2012. 'Wnt signaling through inhibition of beta-catenin degradation in an intact Axin1 complex', *Cell*, 149: 1245-56.

Liberzon, A., A. Subramanian, R. Pinchback, H. Thorvaldsdóttir, P. Tamayo, and JP. Mesirov. 2011. 'Molecular signatures database (MSigDB) 3.0', *Bioinformatics*, 27: 1739-40.

Love, M. I., W. Huber, and S. Anders. 2014. 'Moderated estimation of fold change and dispersion for RNA-seq data with DESeq2', *Genome Biol*, 15: 550.

MacDonald, B. T., and X. He. 2012. 'Frizzled and LRP5/6 receptors for Wnt/beta-catenin signaling', *Cold Spring Harb Perspect Biol*, 4.

MacDonald, B. T., K. Tamai, and X. He. 2009. 'Wnt/beta-catenin signaling: components, mechanisms, and diseases', *Dev Cell*, 17: 9-26.

MacNamara, K. C., M. Jones, O. Martin, and G. M. Winslow. 2011. 'Transient activation of hematopoietic stem and progenitor cells by IFNgamma during acute bacterial infection', *PLoS One*, 6: e28669.

Makhlouf, G. M., and M. L. Schubert. 1990. 'Gastric somatostatin: a paracrine regulator of acid secretion', *Metabolism*, 39: 138-42.

Malaty, H. M., V. Paykov, O. Bykova, A. Ross, D. P. Graham, J. F. Anneger, and D. Y. Graham. 1996. 'Helicobacter pylori and socioeconomic factors in Russia', *Helicobacter*, 1: 82-7.

Maloum, F., J. M. Allaire, J. Gagne-Sansfacon, E. Roy, K. Belleville, P. Sarret, J. Morisset, J. C. Carrier, Y. Mishina, K. H. Kaestner, and N. Perreault. 2011. 'Epithelial BMP signaling is required for proper specification of epithelial cell lineages and gastric endocrine cells', *Am J Physiol Gastrointest Liver Physiol*, 300: G1065-79.

Marin, F., C. Bonet, X. Munoz, N. Garcia, M. L. Pardo, J. M. Ruiz-Liso, P. Alonso, G. Capella, J. M. Sanz-Anquela, C. A. Gonzalez, and N. Sala. 2012. 'Genetic variation in MUC1, MUC2 and MUC6 genes and evolution of gastric cancer precursor lesions in a long-term follow-up in a high-risk area in Spain', *Carcinogenesis*, 33: 1072-80.

Marshall, B. J., J. A. Armstrong, D. B. McGechie, and R. J. Glancy. 1985. 'Attempt to fulfil Koch's postulates for pyloric Campylobacter', *Med J Aust*, 142: 436-9.

Marshall, B. J., and J. R. Warren. 1984. 'Unidentified curved bacilli in the stomach of patients with gastritis and peptic ulceration', *Lancet*, 1: 1311-5.

Matsuo, J., S. Kimura, A. Yamamura, C. P. Koh, M. Z. Hossain, D. L. Heng, K. Kohu, D. C. Voon, H. Hiai, M. Unno, J. B. So, F. Zhu, S. Srivastava, M. Teh, K. G. Yeoh, M. Osato, and Y. Ito. 2017. 'Identification of Stem Cells in the Epithelium of the Stomach Corpus and Antrum of Mice', *Gastroenterology*, 152: 218-31 e14.

Matsuzwa, M., H. Ota, M. Hayama, M. X. Zhang, K. Sano, T. Honda, I. Ueno, T. Akamatsu, and J. Nakayama. 2003. 'Helicobacter pylori infection up-regulates gland mucous cell-type mucins in gastric pyloric mucosa', *Helicobacter*, 8: 594-600.

McGee, D. J., and H. L. Mobley. 2000. 'Pathogenesis of Helicobacter pylori infection', *Curr Opin Gastroenterol*, 16: 24-31.

Meng, X., P. Zhu, N. Li, J. Hu, S. Wang, S. Pang, and J. Wang. 2017. 'Expression of BMP-4 in papillary thyroid carcinoma and its correlation with tumor invasion and progression', *Pathol Res Pract*, 213: 359-63.

Merchant, J. L. 2018. 'Parietal Cell Death by Cytokines', *Cell Mol Gastroenterol Hepatol*, 5: 636-37.

Meyer-Rosberg, K., D. R. Scott, D. Rex, K. Melchers, and G. Sachs. 1996. 'The effect of environmental pH on the proton motive force of Helicobacter pylori', *Gastroenterology*, 111: 886-900.

Mills, J. C., N. Andersson, C. V. Hong, T. S. Stappenbeck, and J. I. Gordon. 2002. 'Molecular characterization of mouse gastric epithelial progenitor cells', *Proc Natl Acad Sci U S A*, 99: 14819-24.

Mills, J. C., and O. J. Sansom. 2015. 'Reserve stem cells: Differentiated cells reprogram to fuel repair, metaplasia, and neoplasia in the adult gastrointestinal tract', *Sci Signal*, 8: re8.

Mills, J. C., and R. A. Shivdasani. 2011. 'Gastric epithelial stem cells', *Gastroenterology*, 140: 412-24.

Morey, P., L. Pfannkuch, E. Pang, F. Boccellato, M. Sigal, A. Imai-Matsushima, V. Dyer, M. Koch, H. J. Mollenkopf, P. Schlaermann, and T. F. Meyer. 2018. 'Helicobacter pylori Depletes Cholesterol in Gastric Glands to Prevent Interferon Gamma Signaling and Escape the Inflammatory Response', *Gastroenterology*, 154: 1391-404 e9.

Moustakas, A., S. Souchelnytskyi, and C. H. Heldin. 2001. 'Smad regulation in TGF-beta signal transduction', *J Cell Sci*, 114: 4359-69.

Mueller, T. D., and J. Nickel. 2012. 'Promiscuity and specificity in BMP receptor activation', *FEBS Lett*, 586: 1846-59.

Munera, J. O., N. Sundaram, S. A. Rankin, D. Hill, C. Watson, M. Mahe, J. E. Vallance, N. F. Shroyer, K. L. Sinagoga, A. Zarzoso-Lacoste, J. R. Hudson, J. C. Howell, P. Chatuvedi, J. R. Spence, J. M. Shannon, A. M. Zorn, M. A. Helmrath, and J. M. Wells. 2017. 'Differentiation of Human Pluripotent Stem Cells into Colonic Organoids via Transient Activation of BMP Signaling', *Cell Stem Cell*, 21: 51-64 e6.

Munoz-Sanjuan, I., and A. H. Brivanlou. 2002. 'Neural induction, the default model and embryonic stem cells', *Nat Rev Neurosci*, 3: 271-80.

Murakami, M., M. Fukuzawa, M. Yamamoto, K. Hamaya, Y. Tamura, A. Sugiyama, R. Takahashi, T. Murakami, K. Amagase, and K. Takeuchi. 2013. 'Effects of Helicobacter pylori infection on gastric parietal cells and E-cadherin in Mongolian gerbils', *J Pharmacol Sci*, 121: 305-11.

Muzumdar, M. D., B. Tasic, K. Miyamichi, L. Li, and L. Luo. 2007. 'A global double-fluorescent Cre reporter mouse', *Genesis*, 45: 593-605.

Nam, K. T., H. J. Lee, J. F. Sousa, V. G. Weis, R. L. O'Neal, P. E. Finke, J. Romero-Gallo, G. Shi, J. C. Mills, R. M. Peek, Jr., S. F. Konieczny, and J. R. Goldenring. 2010. 'Mature chief cells are cryptic progenitors for metaplasia in the stomach', *Gastroenterology*, 139: 2028-37 e9.

Neu, B., P. Randlkofer, M. Neuhofer, P. Voland, A. Mayerhofer, M. Gerhard, W. Schepp, and C. Prinz. 2002. 'Helicobacter pylori induces apoptosis of rat gastric parietal cells', *Am J Physiol Gastrointest Liver Physiol*, 283: G309-18.

Niswander, L., and G. R. Martin. 1993. 'FGF-4 regulates expression of Evx-1 in the developing mouse limb', *Development*, 119: 287-94.

Nohe, A., S. Hassel, M. Ehrlich, F. Neubauer, W. Sebald, Y. I. Henis, and P. Knaus. 2002. 'The mode of bone morphogenetic protein (BMP) receptor oligomerization determines different BMP-2 signaling pathways', *J Biol Chem*, 277: 5330-8.

Nusse, R. 2012. 'Wnt signaling', *Cold Spring Harb Perspect Biol*, 4.

O'Connor, A., and C. O'Morain. 2014. 'Digestive function of the stomach', *Dig Dis*, 32: 186-91.

Obonyo, M., D. G. Guiney, J. Harwood, J. Fierer, and S. P. Cole. 2002. 'Role of gamma interferon in Helicobacter pylori induction of inflammatory mediators during murine infection', *Infect Immun*, 70: 3295-9.

Odenbreit, S., K. Swoboda, I. Barwig, S. Ruhl, T. Boren, S. Koletzko, and R. Haas. 2009. 'Outer membrane protein expression profile in Helicobacter pylori clinical isolates', *Infect Immun*, 77: 3782-90.

Odenbreit, S., M. Till, D. Hofreuter, G. Faller, and R. Haas. 1999. 'Genetic and functional characterization of the alpAB gene locus essential for the adhesion of Helicobacter pylori to human gastric tissue', *Mol Microbiol*, 31: 1537-48.

Ohnishi, N., H. Yuasa, S. Tanaka, H. Sawa, M. Miura, A. Matsui, H. Higashi, M. Musashi, K. Iwabuchi, M. Suzuki, G. Yamada, T. Azuma, and M. Hatakeyama. 2008. 'Transgenic expression of Helicobacter pylori CagA induces gastrointestinal and hematopoietic neoplasms in mouse', *Proc Natl Acad Sci U S A*, 105: 1003-8.

Onichtchouk, D., Y. G. Chen, R. Dosch, V. Gawantka, H. Delius, J. Massague, and C. Niehrs. 1999. 'Silencing of TGF-beta signalling by the pseudoreceptor BAMBI', *Nature*, 401: 480-5.

Ootani, A., S. Toda, K. Fujimoto, and H. Sugihara. 2003. 'Foveolar differentiation of mouse gastric mucosa in vitro', *Am J Pathol*, 162: 1905-12.

Osaki, L. H., K. A. Bockerstett, C. F. Wong, E. L. Ford, B. B. Madison, R. J. DiPaolo, and J. C. Mills. 2019. 'Interferon-gamma directly induces gastric epithelial cell death and is required for progression to metaplasia', *J Pathol*, 247: 513-23.

Owen, R. J. 1998. 'Helicobacter--species classification and identification', *Br Med Bull*, 54: 17-30.

Oyanagi, T., T. Takizawa, A. Aizawa, O. Solongo, H. Yagi, Y. Nishida, H. Koyama, A. Saitoh, and H. Arakawa. 2017. 'Suppression of MUC5AC expression in human bronchial epithelial cells by interferon-gamma', *Allergol Int*, 66: 75-82.

Palframan, S. L., T. Kwok, and K. Gabriel. 2012. 'Vacuolating cytotoxin A (VacA), a key toxin for Helicobacter pylori pathogenesis', *Front Cell Infect Microbiol*, 2: 92.

Pangtey, B., J. M. Kaul, and S. Mishra. 2017. 'Histogenesis of Muscularis Mucosa and Muscularis Externa of Stomach: A Human Foetal Study', *J Clin Diagn Res*, 11: AC01-AC03.

Park, J. S., J. S. Yeom, J. H. Seo, J. Y. Lim, C. H. Park, H. O. Woo, H. S. Youn, J. S. Jun, J. H. Park, G. H. Ko, S. C. Baik, W. K. Lee, M. J. Cho, and K. H. Rhee. 2015. 'Immunohistochemical Expressions of MUC2, MUC5AC, and MUC6 in Normal, Helicobacter pylori Infected and Metaplastic Gastric Mucosa of Children and Adolescents', *Helicobacter*, 20: 260-8.

Park, Y., J. W. Kim, D. S. Kim, E. B. Kim, S. J. Park, J. Y. Park, W. S. Choi, J. G. Song, H. Y. Seo, S. C. Oh, B. S. Kim, J. J. Park, Y. H. Kim, and J. S. Kim. 2008. 'The Bone Morphogenesis Protein-2 (BMP-2) is associated with progression to metastatic disease in gastric cancer', *Cancer Res Treat*, 40: 127-32.

Parker, A., L. Vaux, A. M. Patterson, A. Modasia, D. Muraro, A. G. Fletcher, H. M. Byrne, P. K. Maini, A. J. M. Watson, and C. Pin. 2019. 'Elevated apoptosis impairs epithelial cell turnover and shortens villi in TNF-driven intestinal inflammation', *Cell Death Dis*, 10: 108.

Parsonnet, J., G. D. Friedman, N. Orentreich, and H. Vogelman. 1997. 'Risk for gastric cancer in people with CagA positive or CagA negative Helicobacter pylori infection', *Gut*, 40: 297-301.

Peek, R. M., Jr., S. F. Moss, K. T. Tham, G. I. Perez-Perez, S. Wang, G. G. Miller, J. C. Atherton, P. R. Holt, and M. J. Blaser. 1997. 'Helicobacter pylori cagA+ strains and dissociation of gastric epithelial cell proliferation from apoptosis', *J Natl Cancer Inst*, 89: 863-8.

Pernis, A., S. Gupta, K. J. Gollob, E. Garfein, R. L. Coffman, C. Schindler, and P. Rothman. 1995. 'Lack of interferon gamma receptor beta chain and the prevention of interferon gamma signaling in TH1 cells', *Science*, 269: 245-7.

Pfannkuch, L., R. Hurwitz, J. Traulsen, J. Sigulla, M. Poeschke, L. Matzner, P. Kosma, M. Schmid, and T. F. Meyer. 2019. 'ADP heptose, a novel pathogen-associated molecular pattern identified in Helicobacter pylori', *FASEB J*, 33: 9087-99.

Pfeffer, L. M. 2011. 'The role of nuclear factor kappaB in the interferon response', *J Interferon Cytokine Res*, 31: 553-9.

Piccolo, S., Y. Sasai, B. Lu, and E. M. De Robertis. 1996. 'Dorsoventral patterning in Xenopus: inhibition of ventral signals by direct binding of chordin to BMP-4', *Cell*, 86: 589-98.

Pinto, D., A. Gregorieff, H. Begthel, and H. Clevers. 2003. 'Canonical Wnt signals are essential for homeostasis of the intestinal epithelium', *Genes Dev*, 17: 1709-13.

Platanias, L. C., S. Uddin, E. Bruno, M. Korkmaz, S. Ahmad, Y. Alsayed, D. Van Den Berg, B. J. Druker, A. Wickrema, and R. Hoffman. 1999. 'CrkL and CrkII participate in the generation of the growth inhibitory effects of interferons on primary hematopoietic progenitors', *Exp Hematol*, 27: 1315-21.

Potten, C. S., J. W. Wilson, and C. Booth. 1997. 'Regulation and significance of apoptosis in the stem cells of the gastrointestinal epithelium', *Stem Cells*, 15: 82-93.

Pounder, R. E., and D. Ng. 1995. 'The prevalence of Helicobacter pylori infection in different countries', *Aliment Pharmacol Ther*, 9 Suppl 2: 33-9.

Powell, D. W., I. V. Pinchuk, J. I. Saada, X. Chen, and R. C. Mifflin. 2011. 'Mesenchymal cells of the intestinal lamina propria', *Annu Rev Physiol*, 73: 213-37.

Prosapio, J. G., and I. Jialal. 2019. 'Physiology, Gastrin.' in, *StatPearls* (Treasure Island (FL)).

Qi, Z., Y. Li, B. Zhao, C. Xu, Y. Liu, H. Li, B. Zhang, X. Wang, X. Yang, W. Xie, B. Li, J. J. Han, and Y. G. Chen. 2017. 'BMP restricts stemness of intestinal Lgr5(+) stem cells by directly suppressing their signature genes', *Nat Commun*, 8: 13824.

Qiao, X. T., J. W. Ziel, W. McKimpson, B. B. Madison, A. Todisco, J. L. Merchant, L. C. Samuelson, and D. L. Gumucio. 2007. 'Prospective identification of a multilineage progenitor in murine stomach epithelium', *Gastroenterology*, 133: 1989-98.

Reis, C. A., L. David, P. Correa, F. Carneiro, C. de Bolos, E. Garcia, U. Mandel, H. Clausen, and M. Sobrinho-Simoes. 1999. 'Intestinal metaplasia of human stomach displays distinct patterns of mucin (MUC1, MUC2, MUC5AC, and MUC6) expression', *Cancer Res*, 59: 1003-7.

Rider, C. C., and B. Mulloy. 2010. 'Bone morphogenetic protein and growth differentiation factor cytokine families and their protein antagonists', *Biochem J*, 429: 1-12.

Ring, A., Y. M. Kim, and M. Kahn. 2014. 'Wnt/catenin signaling in adult stem cell physiology and disease', *Stem Cell Rev Rep*, 10: 512-25.

Ritchie ME, Phipson B, Wu D, Hu Y, Law CW, Shi W, Smyth GK. 2015. 'limma powers differential expression analyses for RNA-sequencing and microarray studies', *Nucleic Acids Res.*, 43.

Roelen, B. A., O. S. Cohen, M. K. Raychowdhury, D. N. Chadee, Y. Zhang, J. M. Kyriakis, A. A. Alessandrini, and H. Y. Lin. 2003. 'Phosphorylation of threonine 276 in Smad4 is involved in transforming growth factor-beta-induced nuclear accumulation', *Am J Physiol Cell Physiol*, 285: C823-30.

Romieu-Mourez, R., M. Francois, M. N. Boivin, J. Stagg, and J. Galipeau. 2007. 'Regulation of MHC class II expression and antigen processing in murine and human mesenchymal stromal cells by IFN-gamma, TGF-beta, and cell density', *J Immunol*, 179: 1549-58.

Rothhammer, T., I. Poser, F. Soncin, F. Bataille, M. Moser, and A. K. Bosserhoff. 2005. 'Bone morphogenic proteins are overexpressed in malignant melanoma and promote cell invasion and migration', *Cancer Res*, 65: 448-56.

Roulis, M., and R. A. Flavell. 2016. 'Fibroblasts and myofibroblasts of the intestinal lamina propria in physiology and disease', *Differentiation*, 92: 116-31.

Roulis, M., C. Nikolaou, E. Kotsaki, E. Kaffe, N. Karagianni, V. Koliaraki, K. Salpea, J. Ragoussis, V. Aidinis, E. Martini, C. Becker, H. R. Herschman, S. Vetrano, S. Danese, and G. Kollias. 2014. 'Intestinal myofibroblast-specific Tpl2-Cox-2-PGE2 pathway links innate sensing to epithelial homeostasis', *Proc Natl Acad Sci U S A*, 111: E4658-67.

Roy, S. A. B., J. M. Allaire, C. Ouellet, F. Maloum-Rami, V. Pomerleau, E. Lemieux, J. P. Babeu, J. Rousseau, M. Paquet, P. Garde-Granger, F. Boudreau, and N. Perreault. 2016. 'Loss of mesenchymal bone morphogenetic protein signaling leads to development of reactive stroma and initiation of the gastric neoplastic cascade', *Sci Rep*, 6: 32759.

Rugge, M., P. Correa, M. F. Dixon, T. Hattori, G. Leandro, K. Lewin, R. H. Riddell, P. Sipponen, and H. Watanabe. 2000. 'Gastric dysplasia: the Padova international classification', *Am J Surg Pathol*, 24: 167-76.

Saenz, J. B., and J. C. Mills. 2018. 'Acid and the basis for cellular plasticity and reprogramming in gastric repair and cancer', *Nat Rev Gastroenterol Hepatol*, 15: 257-73.

Salomon, H. 1896. ' Uber das spirillum des saugetiermagens und sein verhalten zu den belegzellen', *Zentralbl Bakteriol*, 19: 433-41.

San Roman, A. K., and R. A. Shivdasani. 2011. 'Boundaries, junctions and transitions in the gastrointestinal tract', *Exp Cell Res*, 317: 2711-8.

Sato, T., J. H. van Es, H. J. Snippert, D. E. Stange, R. G. Vries, M. van den Born, N. Barker, N. F. Shroyer, M. van de Wetering, and H. Clevers. 2011. 'Paneth cells constitute the niche for Lgr5 stem cells in intestinal crypts', *Nature*, 469: 415-8.

Sato, T., R. G. Vries, H. J. Snippert, M. van de Wetering, N. Barker, D. E. Stange, J. H. van Es, A. Abo, P. Kujala, P. J. Peters, and H. Clevers. 2009. 'Single Lgr5 stem cells build crypt-villus structures in vitro without a mesenchymal niche', *Nature*, 459: 262-5.

Sawai, N., M. Kita, T. Kodama, T. Tanahashi, Y. Yamaoka, Y. Tagawa, Y. Iwakura, and J. Imanishi. 1999. 'Role of gamma interferon in Helicobacter pylori-induced gastric inflammatory responses in a mouse model', *Infect Immun*, 67: 279-85.

Sayi, A., E. Kohler, I. Hitzler, I. Arnold, R. Schwendener, H. Rehrauer, and A. Muller. 2009. 'The CD4+ T cell-mediated IFN-gamma response to Helicobacter infection is essential for clearance and determines gastric cancer risk', *J Immunol*, 182: 7085-101.

Scherner, O., S. K. Meurer, L. Tihaa, A. M. Gressner, and R. Weiskirchen. 2007. 'Endoglin differentially modulates antagonistic transforming growth factor-beta1 and BMP-7 signaling', *J Biol Chem*, 282: 13934-43.

Schlaermann, P., B. Toelle, H. Berger, S. C. Schmidt, M. Glanemann, J. Ordemann, S. Bartfeld, H. J. Mollenkopf, and T. F. Meyer. 2016. 'A novel human gastric primary cell culture system for modelling Helicobacter pylori infection in vitro', *Gut*, 65: 202-13.

Schmidt, P. H., J. R. Lee, V. Joshi, R. J. Playford, R. Poulsom, N. A. Wright, and J. R. Goldenring. 1999. 'Identification of a metaplastic cell lineage associated with human gastric adenocarcinoma', *Lab Invest*, 79: 639-46.

Schreiber, S., M. Konradt, C. Groll, P. Scheid, G. Hanauer, H. O. Werling, C. Josenhans, and S. Suerbaum. 2004. 'The spatial orientation of Helicobacter pylori in the gastric mucus', *Proc Natl Acad Sci U S A*, 101: 5024-9.

Schroder, K., P. J. Hertzog, T. Ravasi, and D. A. Hume. 2004. 'Interferon-gamma: an overview of signals, mechanisms and functions', *J Leukoc Biol*, 75: 163-89.

Schwarz, S., G. Morelli, B. Kusecek, A. Manica, F. Balloux, R. J. Owen, D. Y. Graham, S. van der Merwe, M. Achtman, and S. Suerbaum. 2008. 'Horizontal versus familial transmission of Helicobacter pylori', *PLoS Pathog*, 4: e1000180.

Schwitalla, S., A. A. Fingerle, P. Cammareri, T. Nebelsiek, S. I. Goktuna, P. K. Ziegler, O. Canli, J. Heijmans, D. J. Huels, G. Moreaux, R. A. Rupec, M. Gerhard, R. Schmid, N. Barker, H. Clevers, R. Lang, J. Neumann, T. Kirchner, M. M. Taketo, G. R. van den Brink, O. J. Sansom, M. C. Arkan, and F. R. Greten. 2013. 'Intestinal tumorigenesis initiated by dedifferentiation and acquisition of stem-cell-like properties', *Cell*, 152: 25-38.

Sergushichev, A. 2016. 'An algorithm for fast preranked gene ser enrichment analysis using cumulative statistic calculation', *bioRxiv*.

Sheu, S. M., B. S. Sheu, W. C. Chiang, C. Y. Kao, H. M. Wu, H. B. Yang, and J. J. Wu. 2012. 'H. pylori clinical isolates have diverse babAB genotype distributions over different topographic sites of stomach with correlation to clinical disease outcomes', *BMC Microbiol*, 12: 89.

Shi, Y. J., and X. T. Pan. 2016. 'BMP6 and BMP4 expression in patients with cancer-related anemia and its relationship with hepcidin and s-HJV', *Genet Mol Res*, 15.

Shinohara, M., M. Mao, T. M. Keeley, M. El-Zaatari, H. J. Lee, K. A. Eaton, L. C. Samuelson, J. L. Merchant, J. R. Goldenring, and A. Todisco. 2010. 'Bone morphogenetic protein signaling

regulates gastric epithelial cell development and proliferation in mice', *Gastroenterology*, 139: 2050-60 e2.

Sigal, M., C. Y. Logan, M. Kapalczynska, H. J. Mollenkopf, H. Berger, B. Wiedenmann, R. Nusse, M. R. Amieva, and T. F. Meyer. 2017. 'Stromal R-spondin orchestrates gastric epithelial stem cells and gland homeostasis', *Nature*, 548: 451-55.

Sigal, M., M. D. M. Reines, S. Mullerke, C. Fischer, M. Kapalczynska, H. Berger, E. R. M. Bakker, H. J. Mollenkopf, M. E. Rothenberg, B. Wiedenmann, S. Sauer, and T. F. Meyer. 2019. 'R-spondin-3 induces secretory, antimicrobial Lgr5(+) cells in the stomach', *Nat Cell Biol*.

Sigal, M., M. E. Rothenberg, C. Y. Logan, J. Y. Lee, R. W. Honaker, R. L. Cooper, B. Passarelli, M. Camorlinga, D. M. Bouley, G. Alvarez, R. Nusse, J. Torres, and M. R. Amieva. 2015. 'Helicobacter pylori Activates and Expands Lgr5(+) Stem Cells Through Direct Colonization of the Gastric Glands', *Gastroenterology*, 148: 1392-404 e21.

Simons, M., and M. Mlodzik. 2008. 'Planar cell polarity signaling: from fly development to human disease', *Annu Rev Genet*, 42: 517-40.

Smith, D. M., C. Nielsen, C. J. Tabin, and D. J. Roberts. 2000. 'Roles of BMP signaling and Nkx2.5 in patterning at the chick midgut-foregut boundary', *Development*, 127: 3671-81.

Smith, D. M., and C. J. Tabin. 1999. 'BMP signalling specifies the pyloric sphincter', *Nature*, 402: 748-9.

Smythies, L. E., K. B. Waites, J. R. Lindsey, P. R. Harris, P. Ghiara, and P. D. Smith. 2000. 'Helicobacter pylori-induced mucosal inflammation is Th1 mediated and exacerbated in IL-4, but not IFN-gamma, gene-deficient mice', *J Immunol*, 165: 1022-9.

Solnick, J. V., and P. Vandamme. 2001. 'Taxonomy of the Helicobacter Genus.' in H. L. T. Mobley, G. L. Mendz and S. L. Hazell (eds.), *Helicobacter pylori: Physiology and Genetics* (Washington (DC)).

Soshnikova, N., D. Zechner, J. Huelsken, Y. Mishina, R. R. Behringer, M. M. Taketo, E. B. Crenshaw, 3rd, and W. Birchmeier. 2003. 'Genetic interaction between Wnt/beta-catenin and BMP receptor signaling during formation of the AER and the dorsal-ventral axis in the limb', *Genes Dev*, 17: 1963-8.

Stange, D. E., B. K. Koo, M. Huch, G. Sibbel, O. Basak, A. Lyubimova, P. Kujala, S. Bartfeld, J. Koster, J. H. Geahlen, P. J. Peters, J. H. van Es, M. van de Wetering, J. C. Mills, and H. Clevers. 2013. 'Differentiated Troy+ chief cells act as reserve stem cells to generate all lineages of the stomach epithelium', *Cell*, 155: 357-68.

Stein, S. C., E. Faber, S. H. Bats, T. Murillo, Y. Speidel, N. Coombs, and C. Josenhans. 2017. 'Helicobacter pylori modulates host cell responses by CagT4SS-dependent translocation of an intermediate metabolite of LPS inner core heptose biosynthesis', *PLoS Pathog*, 13: e1006514.

Stevens, M. L., P. Chaturvedi, S. A. Rankin, M. Macdonald, S. Jagannathan, M. Yukawa, A. Barski, and A. M. Zorn. 2017. 'Genomic integration of Wnt/beta-catenin and BMP/Smad1 signaling coordinates foregut and hindgut transcriptional programs', *Development*, 144: 1283-95.

Stzepourginski, I., G. Nigro, J. M. Jacob, S. Dulauroy, P. J. Sansonetti, G. Eberl, and L. Peduto. 2017. 'CD34+ mesenchymal cells are a major component of the intestinal stem cells niche at homeostasis and after injury', *Proc Natl Acad Sci U S A*, 114: E506-E13.

Subramanian, A., P. Tamayo, V. K. Mootha, S. Mukherjee, B. L. Ebert, M. A. Gillette, A. Paulovich, S. L. Pomeroy, T. R. Golub, E. S. Lander, and J. P. Mesirov. 2005. 'Gene set enrichment analysis: a knowledge-based approach for interpreting genome-wide expression profiles', *Proc Natl Acad Sci U S A*, 102: 15545-50.

Suerbaum, S., and P. Michetti. 2002. 'Helicobacter pylori infection', *N Engl J Med*, 347: 1175-86.

Sycuro, L. K., Z. Pincus, K. D. Gutierrez, J. Biboy, C. A. Stern, W. Vollmer, and N. R. Salama. 2010. 'Peptidoglycan crosslinking relaxation promotes Helicobacter pylori's helical shape and stomach colonization', *Cell*, 141: 822-33.

Takabayashi, H., M. Shinohara, M. Mao, P. Phaosawasdi, M. El-Zaatari, M. Zhang, T. Ji, K. A. Eaton, D. Dang, J. Kao, and A. Todisco. 2014. 'Anti-inflammatory activity of bone morphogenetic protein signaling pathways in stomachs of mice', *Gastroenterology*, 147: 396-406 e7.

Takaoka, A., N. Tanaka, Y. Mitani, T. Miyazaki, H. Fujii, M. Sato, P. Kovarik, T. Decker, J. Schlessinger, and T. Taniguchi. 1999. 'Protein tyrosine kinase Pyk2 mediates the Jak-dependent activation of MAPK and Stat1 in IFN-gamma, but not IFN-alpha, signaling', *EMBO J*, 18: 2480-8.

Tan, D. W., and N. Barker. 2014. 'Intestinal stem cells and their defining niche', *Curr Top Dev Biol*, 107: 77-107.

Team, R Core. 2014. 'R: A Language and Environment for Statistical Computing ', *http://www.R-project.org/*.

Tennant, S. M., E. L. Hartland, T. Phumoonna, D. Lyras, J. I. Rood, R. M. Robins-Browne, and I. R. van Driel. 2008. 'Influence of gastric acid on susceptibility to infection with ingested bacterial pathogens', *Infect Immun*, 76: 639-45.

Tetteh, P. W., O. Basak, H. F. Farin, K. Wiebrands, K. Kretzschmar, H. Begthel, M. van den Born, J. Korving, F. de Sauvage, J. H. van Es, A. van Oudenaarden, and H. Clevers. 2016. 'Replacement of Lost Lgr5-Positive Stem Cells through Plasticity of Their Enterocyte-Lineage Daughters', *Cell Stem Cell*, 18: 203-13.

Todisco, A. 2017. 'Regulation of Gastric Metaplasia, Dysplasia, and Neoplasia by Bone Morphogenetic Protein Signaling', *Cell Mol Gastroenterol Hepatol*, 3: 339-47.

Todisco, A., M. Mao, T. M. Keeley, W. Ye, L. C. Samuelson, and K. A. Eaton. 2015. 'Regulation of gastric epithelial cell homeostasis by gastrin and bone morphogenetic protein signaling', *Physiol Rep*, 3.

Tomasek, J. J., G. Gabbiani, B. Hinz, C. Chaponnier, and R. A. Brown. 2002. 'Myofibroblasts and mechano-regulation of connective tissue remodelling', *Nat Rev Mol Cell Biol*, 3: 349-63.

Tong, Z., K. Martyn, A. Yang, X. Yin, B. E. Mead, N. Joshi, N. E. Sherman, R. S. Langer, and J. M. Karp. 2018. 'Towards a defined ECM and small molecule based monolayer culture system for the expansion of mouse and human intestinal stem cells', *Biomaterials*, 154: 60-73.

Uddin, S., D. A. Sher, Y. Alsayed, S. Pons, O. R. Colamonici, E. N. Fish, M. F. White, and L. C. Platanias. 1997. 'Interaction of p59fyn with interferon-activated Jak kinases', *Biochem Biophys Res Commun*, 235: 83-8.

Ulloa, L., J. Doody, and J. Massague. 1999. 'Inhibition of transforming growth factor-beta/SMAD signalling by the interferon-gamma/STAT pathway', *Nature*, 397: 710-3.

Urist, M. R. 1965. 'Bone: formation by autoinduction', *Science*, 150: 893-9.

van Amerongen, R., and R. Nusse. 2009. 'Towards an integrated view of Wnt signaling in development', *Development*, 136: 3205-14.

van Dop, W. A., A. Uhmann, M. Wijgerde, E. Sleddens-Linkels, J. Heijmans, G. J. Offerhaus, M. A. van den Bergh Weerman, G. E. Boeckxstaens, D. W. Hommes, J. C. Hardwick, H. Hahn, and G. R. van den Brink. 2009. 'Depletion of the colonic epithelial precursor cell compartment upon conditional activation of the hedgehog pathway', *Gastroenterology*, 136: 2195-203 e1-7.

Van Zanten, S. J., M. F. Dixon, and A. Lee. 1999. 'The gastric transitional zones: neglected links between gastroduodenal pathology and helicobacter ecology', *Gastroenterology*, 116: 1217-29.

Vandamme, P., E. Falsen, R. Rossau, B. Hoste, P. Segers, R. Tytgat, and J. De Ley. 1991. 'Revision of Campylobacter, Helicobacter, and Wolinella taxonomy: emendation of generic descriptions and proposal of Arcobacter gen. nov', *Int J Syst Bacteriol*, 41: 88-103.

Veeman, M. T., J. D. Axelrod, and R. T. Moon. 2003. 'A second canon. Functions and mechanisms of beta-catenin-independent Wnt signaling', *Dev Cell*, 5: 367-77.

Vishnubalaji, R., S. Yue, M. Alfayez, M. Kassem, F. F. Liu, A. Aldahmash, and N. M. Alajez. 2016. 'Bone morphogenetic protein 2 (BMP2) induces growth suppression and enhances chemosensitivity of human colon cancer cells', *Cancer Cell Int*, 16: 77.

Voorneveld, P. W., L. L. Kodach, R. J. Jacobs, C. J. van Noesel, M. P. Peppelenbosch, K. S. Korkmaz, I. Molendijk, E. Dekker, H. Morreau, G. W. van Pelt, R. A. Tollenaar, W. Mesker, L. J. Hawinkels, M. Paauwe, H. W. Verspaget, D. T. Geraets, D. W. Hommes, G. J. Offerhaus, G. R. van den Brink, P. Ten Dijke, and J. C. Hardwick. 2015. 'The BMP pathway either enhances or inhibits the Wnt pathway depending on the SMAD4 and p53 status in CRC', *Br J Cancer*, 112: 122-30.

Wagner, D. O., C. Sieber, R. Bhushan, J. H. Borgermann, D. Graf, and P. Knaus. 2010. 'BMPs: from bone to body morphogenetic proteins', *Sci Signal*, 3: mr1.

Wang, F., S. Zhang, R. Jeon, I. Vuckovic, X. Jiang, A. Lerman, C. D. Folmes, P. D. Dzeja, and J. Herrmann. 2018. 'Interferon Gamma Induces Reversible Metabolic Reprogramming of M1 Macrophages to Sustain Cell Viability and Pro-Inflammatory Activity', *EBioMedicine*, 30: 303-16.

Wang, R. N., J. Green, Z. Wang, Y. Deng, M. Qiao, M. Peabody, Q. Zhang, J. Ye, Z. Yan, S. Denduluri, O. Idowu, M. Li, C. Shen, A. Hu, R. C. Haydon, R. Kang, J. Mok, M. J. Lee, H. L. Luu, and L. L. Shi. 2014. 'Bone Morphogenetic Protein (BMP) signaling in development and human diseases', *Genes Dis*, 1: 87-105.

Wang, Y. C., C. L. Chen, B. S. Sheu, Y. J. Yang, P. C. Tseng, C. Y. Hsieh, and C. F. Lin. 2014. 'Helicobacter pylori infection activates Src homology-2 domain-containing phosphatase 2 to suppress IFN-gamma signaling', *J Immunol*, 193: 4149-58.

Weck, M. N., and H. Brenner. 2008. 'Association of Helicobacter pylori infection with chronic atrophic gastritis: Meta-analyses according to type of disease definition', *Int J Cancer*, 123: 874-81.

Wehrli, M., S. T. Dougan, K. Caldwell, L. O'Keefe, S. Schwartz, D. Vaizel-Ohayon, E. Schejter, A. Tomlinson, and S. DiNardo. 2000. 'arrow encodes an LDL-receptor-related protein essential for Wingless signalling', *Nature*, 407: 527-30.

Wei, J., W. Guo, H. Lian, Q. Yang, H. Lin, S. Li, and H. B. Shu. 2017. 'SNX8 mediates IFNgamma-triggered noncanonical signaling pathway and host defense against Listeria monocytogenes', *Proc Natl Acad Sci U S A*, 114: 13000-05.

Wheelock, E. F. 1965. 'Interferon-like virus-inhibitor induced in human leukocytes by phytohemagglutinin', *Science*, 149: 310-1.

Willet, S. G., and J. C. Mills. 2016. 'Stomach Organ and Cell Lineage Differentiation: from Embryogenesis to Adult Homeostasis', *Cell Mol Gastroenterol Hepatol*, 2: 546-59.

Wozney, J. M., V. Rosen, A. J. Celeste, L. M. Mitsock, M. J. Whitters, R. W. Kriz, R. M. Hewick, and E. A. Wang. 1988. 'Novel regulators of bone formation: molecular clones and activities', *Science*, 242: 1528-34.

Wroblewski, L. E., R. M. Peek, Jr., and K. T. Wilson. 2010. 'Helicobacter pylori and gastric cancer: factors that modulate disease risk', *Clin Microbiol Rev*, 23: 713-39.

Yahiro, K., Y. Akazawa, M. Nakano, H. Suzuki, J. Hisatune, H. Isomoto, J. Sap, M. Noda, J. Moss, and T. Hirayama. 2015. 'Helicobacter pylori VacA induces apoptosis by accumulation of connexin 43 in autophagic vesicles via a Rac1/ERK-dependent pathway', *Cell Death Discov*, 1: 15035.

Yamamoto, T., M. Kita, T. Ohno, Y. Iwakura, K. Sekikawa, and J. Imanishi. 2004. 'Role of tumor necrosis factor-alpha and interferon-gamma in Helicobacter pylori infection', *Microbiol Immunol*, 48: 647-54.

Yan, K. S., L. A. Chia, X. Li, A. Ootani, J. Su, J. Y. Lee, N. Su, Y. Luo, S. C. Heilshorn, M. R. Amieva, E. Sangiorgi, M. R. Capecchi, and C. J. Kuo. 2012. 'The intestinal stem cell markers Bmi1 and Lgr5 identify two functionally distinct populations', *Proc Natl Acad Sci U S A*, 109: 466-71.

Yang, J., L. Ye, T. Q. Hui, D. M. Yang, D. M. Huang, X. D. Zhou, J. J. Mao, and C. L. Wang. 2015. 'Bone morphogenetic protein 2-induced human dental pulp cell differentiation involves p38 mitogen-activated protein kinase-activated canonical WNT pathway', *Int J Oral Sci*, 7: 95-102.

Yang, K., X. Wang, H. Zhang, Z. Wang, G. Nan, Y. Li, F. Zhang, M. K. Mohammed, R. C. Haydon, H. H. Luu, Y. Bi, and T. C. He. 2016. 'The evolving roles of canonical WNT signaling in stem cells and tumorigenesis: implications in targeted cancer therapies', *Lab Invest*, 96: 116-36.

Yao, X., and J. G. Forte. 2003. 'Cell biology of acid secretion by the parietal cell', *Annu Rev Physiol*, 65: 103-31.

Ye, W., H. Takabayashi, Y. Yang, M. Mao, E. S. Hibdon, L. C. Samuelson, K. A. Eaton, and A. Todisco. 2018. 'Regulation of Gastric Lgr5+ve Cell Homeostasis by Bone Morphogenetic Protein (BMP) Signaling and Inflammatory Stimuli', *Cell Mol Gastroenterol Hepatol*, 5: 523-38.

Yokoyama, Y., T. Watanabe, Y. Tamura, Y. Hashizume, K. Miyazono, and S. Ehata. 2017. 'Autocrine BMP-4 Signaling Is a Therapeutic Target in Colorectal Cancer', *Cancer Res*, 77: 4026-38.

Young, H. A. 1996. 'Regulation of interferon-gamma gene expression', *J Interferon Cytokine Res*, 16: 563-8.

Yu, S., K. Tong, Y. Zhao, I. Balasubramanian, G. S. Yap, R. P. Ferraris, E. M. Bonder, M. P. Verzi, and N. Gao. 2018. 'Paneth Cell Multipotency Induced by Notch Activation following Injury', *Cell Stem Cell*, 23: 46-59 e5.

Zhang, J., Y. Ge, L. Sun, J. Cao, Q. Wu, L. Guo, and Z. Wang. 2012. 'Effect of bone morphogenetic protein-2 on proliferation and apoptosis of gastric cancer cells', *Int J Med Sci*, 9: 184-92.

Zhang, R., N. L. Banik, and S. K. Ray. 2007. 'Combination of all-trans retinoic acid and interferon-gamma suppressed PI3K/Akt survival pathway in glioblastoma T98G cells whereas NF-kappaB survival signaling in glioblastoma U87MG cells for induction of apoptosis', *Neurochem Res*, 32: 2194-202.

Zhang, R., B. O. Oyajobi, S. E. Harris, D. Chen, C. Tsao, H. W. Deng, and M. Zhao. 2013. 'Wnt/beta-catenin signaling activates bone morphogenetic protein 2 expression in osteoblasts', *Bone*, 52: 145-56.

Zhang, Y. E. 2009. 'Non-Smad pathways in TGF-beta signaling', *Cell Res*, 19: 128-39.

———. 2017. 'Non-Smad Signaling Pathways of the TGF-beta Family', *Cold Spring Harb Perspect Biol*, 9.

Zhang, Y., and J. Que. 2019. 'BMP Signaling in Development, Stem Cells, and Diseases of the Gastrointestinal Tract', *Annu Rev Physiol*.

Zhao, Y., Y. Zhou, Y. Sun, A. Yu, H. Yu, W. Li, Z. Liu, J. Zeng, X. Li, C. Chen, and J. Jia. 2011. 'Virulence factor cytotoxin-associated gene A in Helicobacter pylori is downregulated by interferon-gamma in vitro', *FEMS Immunol Med Microbiol*, 61: 76-83.

Zhao, Z., N. Hou, Y. Sun, Y. Teng, and X. Yang. 2010. 'Atp4b promoter directs the expression of Cre recombinase in gastric parietal cells of transgenic mice', *J Genet Genomics*, 37: 647-52.

Zheng, P. Y., and N. L. Jones. 2003. 'Helicobacter pylori strains expressing the vacuolating cytotoxin interrupt phagosome maturation in macrophages by recruiting and retaining TACO (coronin 1) protein', *Cell Microbiol*, 5: 25-40.

Zhu, Y., D. Song, Y. Song, and X. Wang. 2019. 'Interferon gamma induces inflammatory responses through the interaction of CEACAM1 and PI3K in airway epithelial cells', *J Transl Med*, 17: 147.

Zimmermann, S., L. Pfannkuch, M. A. Al-Zeer, S. Bartfeld, M. Koch, J. Liu, C. Rechner, M. Soerensen, O. Sokolova, A. Zamyatina, P. Kosma, A. P. Maurer, F. Glowinski, K. P. Pleissner, M. Schmid, V. Brinkmann, A. Karlas, M. Naumann, M. Rother, N. Machuy, and T. F. Meyer. 2017. 'ALPK1- and TIFA-Dependent Innate Immune Response Triggered by the Helicobacter pylori Type IV Secretion System', *Cell Rep*, 20: 2384-95.

Zorn, A. M., and J. M. Wells. 2009. 'Vertebrate endoderm development and organ formation', *Annu Rev Cell Dev Biol*, 25: 221-51.

Zuo, X., Y. Deguchi, W. Xu, Y. Liu, H. S. Li, D. Wei, R. Tian, W. Chen, M. Xu, Y. Yang, S. Gao, J. C. Jaoude, F. Liu, S. P. Chrieki, M. J. Moussalli, M. Gagea, M. M. Sebastian, X. Zheng, D. Tan, R. Broaddus, J. Wang, N. J. Ajami, A. G. Swennes, S. S. Watowich, and I. Shureiqi. 2019. 'PPARD and Interferon Gamma Promote Transformation of Gastric Progenitor Cells and Tumorigenesis in Mice', *Gastroenterology*, 157: 163-78.

List of abbreviations

Quantities and units were abbreviated according to the International System of Units.

2D	two-dimensional
3D	three-dimensional
4-OHT	4-hydroxytamoxifen
ACTR 1A/2A/2B	activin receptor type 1A/2A/2B
ADF	advanced DMEM/F12
ADP	adenozyno-5'-difosforan
ADP heptose	ADP-glycero-β-D-manno-heptose
AKT	protein kinase B
ALPK 1	alpha kinase 1
AMP 1/2/3/4/5/6	RNAscope amplification solution
AP1	activator protein 1
APC	antigen-presenting cells
ATP	adenosine triphosphate
ATP4b	ATPase H+/K+ transporting subunit beta
AXIN2	axis inhibition protein 2
BHI	brain heart infusion
BLAST	basic local alignment search tool
BMP	bone morphogenetic protein
BMPR 1A/1B/2	bone morphogenetic protein receptor type 1A/1B/2
bp	base pair
BSA	bovine serum albumin
Ca	calcium
Cag A/E/PAI	cytotoxin-associated gene A/E/pathogenicity island
CCKBR	cholecystokinin B receptor
CDK1	cyclin-dependent kinase 1
cDNA	complementary DNA
CFU	colony forming unit
CGT	cholesterol-a-glucosyltransferase
CHGA	chromogranin A
CHO	chinese hamster ovary
CHRD	chordin

CHRDL1	chordin like 1
CO2	carbon dioxide
COX 2	cyclooxygenase 2
CRC	colorectal cancer
CRE	cyclization recombinase
CRIM	cysteine rich transmembrane BMP regulator 1
cRNA	complementary RNA
CTL	cytotoxic T lymphocyte
CTRL	control
CXCR 4	C-X-C motif chemokine receptor 4
DAPI	4’,6-diamidino-2-phenylindole
DC	dendritic cells
DNA	deoxyribonucleic acid
dNTP	deoxynucleoside triphosphate
DPBS	dulbecco's phosphate-buffered saline
DTT	dithiothreitol
DVL	dishevelled segment polarity protein
EDTA	ethylenediaminetetraacetic acid
EdU	5-ethynyl-2'-deoxyuridine
EGF	epidermal growth factor
EMA	european medicines agency
EpCAM	epithelial cell adhesion molecule
ER1	estrogen receptor 1
FACS	fluorescence-activated cell sorting
FCS	fetal calf serum
FDA	american food and drug administration
FGF	fibroblast growth factor
FITC	fluorescein isothiocyanate
FSC	forward scatter
FZD	frizzled class receptor
GAS	gamma interferon activated site
GAST	gastrin
GFP	green fluorescence protein
GREM 1/2	cysteine knot superfamily 1, BMP antagonist 1/2

GS	glycine-serine
GS II	griffonia simplicifolia II
GSEA	gene set enrichment analysis
H. pylori	*Helicobacter pylori*
H+L	heavy and light chain
hBD3	human β-defensin 3
HBSS	hank's balanced salt solution
HCl	hydrochloric acid
HDACs	histone deacetylases
HOP	helicobacter outer porins
HOR	hop-related proteins
HSCs	hematopoietic stem cells
ID 1/2/3	inhibitor of differentiation 1/2/3
IFNGR 1/2	interferon-gamma receptor alpha/beta chain
IFNγ	interferon gamma
IgG	immunoglobulin G
IL-1/6/8	interleukin 1/6/8
iNOS	inducible nitric oxide synthase
ISH	single-molecule RNA *in situ* hybridization
ITLN1	intelectin 1
JAK 1/2	janus kinase 1/2
JNK	c-Jun N-terminal kinase
KO	knock-out
LE	low electroendosmosis
LEF	lymphoid enhancer binding factor
LGR5	leucine rich repeat containing G protein-coupled receptor 5
loxP	locus of X-over P1
LPS	lipopolysaccharides
LRIG1	leucine rich repeats and immunoglobulin like domains 1
LRP	low-density lipoprotein-related protein
MALT	mucosa associated lymphoid tissue
MAPK	mitogen-activated protein kinase
Mg	magnesium
MIP 2	macrophage-inflammatory protein 2

MIST1	muscle, intestine and stomach expression 1
MPIIB	Max Planck institute for infection biology
mRNA	messenger RNA
MSC	mesenchymal stem cells
MUC 2/5AC/6	mucin 2/5AC/6
MYH 11	myosin heavy chain 11
NAC	nicotinamid
NF-κB	nuclear factor κB
NK	natural killer cells
NKT	natural killer T cells
NOD 1	nucleotide binding oligomerization domain containing 1
NOG	noggin
OD	optical density
OMP	outer membrane proteins
P/KC	protein kinase C
P.I.	post infection
P53	protein 53
PBS	phosphate buffered saline
PCP	planar cell polarity
PEN/STREP	penicillin/streptomycin
PFA	paraformaldehyde
PI	propidium iodide
PI3K	phosphoinositide 3-kinase
PLC	phospholipase C
qRT-PCR	quantitative reverse transcription polymerase chain reaction
REG3 B/G	regenerating family member 3 beta/gamma
RH/M	recombinant human.mouse
RHOA	Ras homolog gene family member A
RNA	ribonucleic acid
RNAseq	RNA sequencing
RPM	revolutions per minute
RSPO	R-spondin
RT	reverse transcription
RUNX	runt-related transcription factor

SEM	standard error of the mean
SHP2	src homology-2 domain–containing phosphatase 2
SMAD 1/4/5/6/7/8	SMAD family member 1/4/5/6/7/8
SOX2	SRY-box transcription factor 2
SPEM	spasmolytic polypeptide-expressing metaplasia
SSC	side scatter
STAT 1	signal transducer and activator of transcription 1
T4SS	type IV secretion system
TCF	transcription factor
TFF2	trefoil factor 2
TGFβ	transforming growth factor beta
Th1	T helper type 1 cells
TIFA	TRAF-interacting protein with forkhead-associated domain
TL	low thermolysin
TNFα	tumor necrosis factor alpha
TPL 2	tumor progression locus-2
TROY	tumor necrosis factor receptor superfamily member 19
TWIST1	twist family BHLH transcription factor 1
VacA	vacuolating toxin A
VIM	vimentin
WHO	world health organization
WNT	wingless-type mmtv integration site family
WT	wild type
α-SMA	α smooth muscle actin

List of figures

List of tables